EVALUATION OF SELF CONSOLIDATING CONCRETE AND CLASS IV CONCRETE FLOW IN DRILLED SHAFTS – PART 1

BDV25 TWO977-25

Task 2a Deliverable – Exploratory Evaluation of Previously Cast Lab Shaft Specimens

Submitted to

The Florida Department of Transportation
Research Center
605 Suwannee Street, MS30
Tallahassee, FL 32399
Research.center@dot.state.fl.us

Submitted by

Sarah J. Mobley, P.E., Doctoral Student
Kelly Costello, E.I., Doctoral Candidate
and
Gray Mullins, Ph.D., P.E.
Professor
Principal Investigator
Department of Civil and Environmental Engineering
University of South Florida
4202 E. Fowler Avenue, ENB 118
Tampa, FL 33620
(813) 974-5845
gmullins@usf.edu

April, 2017

Preface

This deliverable is submitted in partial fulfillment of the requirements set forth and agreed upon at the onset of the project and indicates a degree of completion. It also serves as an interim report of the research progress and findings as they pertain to the individual task-based goals that comprise the overall project scope. Herein, the FDOT project manager's approval and guidance are sought regarding the applicability of the intermediate research findings and the subsequent research direction. The project tasks, as outlined in the scope of services, are presented below. The subject of the present report is highlighted in bold.

Task 1. Literature Review (pages 3-90)
Task 2a. Exploratory Evaluation of Previously Cast Lab Shaft Specimens (page 91-287)
Task 2b. Field Exploratory Evaluation of Existing Bridges with Drilled Shaft Foundations
Task 3. Corrosion Potential Evaluations
Task 4. Porosity and Hydration Products Determinations
Task 5. Rheology Modeling and Testing
Task 6. Effects of Construction Approach
Task 7. Reporting: Draft and Final Report

The proposed study will culminate with a comprehensive final report describing all aspects of the study. This interim report is also intended to serve as a living draft of what will ultimately be the final report. As such, all previously submitted interim reports to date will be included for completeness (in greyed-out font) but may contain changes based on any new findings; this is especially applicable to the *Literature Review* component.

Chapter Three: Exploratory Evaluation of Previously Cast Lab Shaft Specimens (Task 2a Deliverable)

When considering the importance of the concrete quality in a drilled shaft, it becomes apparent the cover region is the most important where it contributes far more to the bending moment of inertia than the core concrete within the cage, forms the mechanical/structural bond to the surrounding bearing strata, and provides a barrier from external chemical agents that promote corrosion (e.g. chlorides or sulfates). Until recently, this portion of drilled shaft concrete could not be adequately tested via non-destructive integrity methods and went largely unassessed. This implies that there may be shafts in service with flaws in the cover; Task 2b will entertain this possibility.

With regards to the focus of this study (and Task 2a), the ability or inability of drilled shaft concrete to freely flow into the annular cover region and maintain the desired concrete properties can have the most dire effects on durability / longevity of the structural integrity. While SCC alternatives are sought to enhance concrete cover performance, means and methods of assessing an as-built shaft must be identified.

The overall goal of this task was to create and implement methods that describe the electrochemical, physical and strength characteristics of 24 test shaft specimens tremie-placed in varied slurry conditions. This investigation was subdivided into four methods of assessing the as-built quality of the shafts: (1) side-of-shaft surface texture / void volume determination, (2) structured light 3D surface profiling (3) surface potential screening and (4) Coring with dynamic strength profiling and compressive strength testing.

3.1 Test Specimens

The specimens examined in this study were constructed during two previous University of South Florida research projects. Full details the shaft construction can be found elsewhere (Mullins, et al, 2014; Bowen 2013). The purpose of those studies was to define the current upper viscosity limit for mineral slurries and to identify the effects of slurry casting environments on rebar/concrete bond as well as geotechnical side shear development. During this research, 24 test shafts were prepared. Each shaft measured 42in in diameter and 24in in height. Shaft specifics are provided in Table 3.1. Slurry product data sheets are included in Appendix A.

Table 3.1. Summary of all 24 shaft specimens

Shaft #	Concrete Mix	Slurry Type	Viscosity	Average Pullout Strength (kips)	Average Concrete Compressive Strength (psi)
1	4KDS	PG Bentonite	44	57.234	6150
2	4KDS	PG Bentonite	105	49.704	6150
3	4KDS	PG Bentonite	40	36.894	4358
4	4KDS	PG Bentonite	55	32.697	4358
5	4KDS	PG Bentonite	90	38.094	4358
6	4KDS	Water	26	54.304	4358

Shaft #	Concrete Mix	Slurry Type	Viscosity	Average Pullout Strength (kips)	Average Concrete Compressive Strength (psi)
7	4KDS	PG Bentonite	30	28.754	4530
8	4KDS	PG Bentonite	40	24.212	4530
9	4KDS	PG Bentonite	50	20.524	4530
10	4KDS	PG Bentonite	90	23.139	4530
11	4KDS	SP Polymer	65	32.338	4530
12	4KDS	SP Polymer	66	33.941	4530
13	4KDS	PG Bentonite	30	25.636	4753
14	4KDS	PG Bentonite	30	27.641	4753
15	4KDS	PG Bentonite	56	19.804	4753
16	4KDS	SP Polymer	85	24.077	4753
17	4KDS	SP Polymer	85	26.247	4753
18	4KDS	Water	26	34.042	4753
19	4KDS	KBI Polymer	63	20.9	4100
20	4KDS	KBI Polymer	121	19.3	4100
21	4KDS	PG Bentonite	42	20.7	4100
22	4KDS	Water	26	21.8	4100
23	SCC	Water	26	Not Tested	Not Tested
24	SCC	PG Bentonite	40	Not Tested	Not Tested

PG Bentonite- CETCO Puregold Gel ©

SP Polymer – Shore Pac ®

KBI Polymer – SlurryPro® CDP ™

Specimens cast in polymer slurry and water shafts were tested as well. The following sections will discuss the qualities of mineral and polymer slurry and separate the data above by slurry type for comparison. It should be noted that while two self-consolidating concrete shafts were cast pull out tests have not yet been performed and the concrete compressive strength is also currently unknown. Therefore, they will be excluded for the remainder of this section.

Mineral Slurry

Mineral slurry is the combination of water and a dry clay powder (usually sodium or calcium montmorillonite). The most commonly used clay is known as bentonite, though attapulgite, sepiolite and other naturally occurring clay minerals are also used. Bentonite is the common name for packaged, processed, clay powder made primarily of sodium montmorillonite. Bentonite slurry works two-fold during the excavation/construction process: (1) with the slurry level higher than the ground water, the differential hydrostatic slurry pressure pushes against the excavation walls preventing cave-ins and (2) the gel strength of the clay suspends soil particles long enough to be transported out of the excavation during the concreting process.

When bentonite slurry is introduced into an excavation, the slurry permeates the walls of the excavation and deposits clay particles as they are filtered out of suspension. The resulting layer of clay on the side walls, called a filter cake, further stabilizes the soil matrix from fluctuations in

local slurry pressure that accompany the auger passing by the walls. Filter cake formation occurs relatively quickly where within 4 – 8hrs flow into the surrounding soil can completely cease. Though generally beneficial to stability, the filter cake can have negative effects on the side shear of the shaft.

Viscosity is the best measure of slurry quality and is monitored via the American Petroleum Institute (API) test method known as the Marsh funnel test. While the test does not measure viscosity in the traditional sense (shear stress / shear rate), it provides an indication of gel strength by measuring the time required for 1 quart of fluid to pass through a standard orifice at the base of a standard funnel. For bentonite slurry to function properly, state and federal specifications require the slurry to fall between 28 and 50 sec/qt depending on the state. In Florida, the range is 30 to 40sec/qt. As a point of reference, water has a Marsh funnel viscosity of 26 sec/qt. Table 3.2 organizes the data for specimens cast in bentonite from Table 3.1 sorted by Marsh funnel viscosity. A wide range of pull-out resistance (rebar development bond) was observed that was a function of bonded length, concrete strength, slurry type and viscosity. It should be noted that while shaft 10 has been included here for initial comparison purposes, during testing of these shafts for this Task it was considered to be unusable as coring had been performed through the rebar, thus leaving the interior of the shaft exposed.

Table 3.2 Bentonite shaft specimens (13 total)

Shaft #	Concrete Mix	Slurry Type	Viscosity (sec)	Average Pullout Strength (kips)	Average Concrete Compressive Strength (psi)
7	4KDS	PG Bentonite	30	28.754	4530
13	4KDS	PG Bentonite	30	25.636	4753
14	4KDS	PG Bentonite	30	27.641	4753
3	4KDS	PG Bentonite	40	36.894	4358
8	4KDS	PG Bentonite	40	24.212	4530
24	SCC	PG Bentonite	40	Not Tested	Not Tested
21	4KDS	PG Bentonite	42	20.7	4100
1	4KDS	PG Bentonite	44	57.234	6150
9	4KDS	PG Bentonite	50	20.524	4530
4	4KDS	PG Bentonite	55	32.697	4358
15	4KDS	PG Bentonite	56	19.804	4753
5	4KDS	PG Bentonite	90	38.094	4358
10	4KDS	PG Bentonite	90	23.139	4530
2	4KDS	PG Bentonite	105	49.704	6150

Polymer Slurry

Polymer slurry is the combination of water and a proprietary blend of polyacrylamides. These slurries form long, hair-like, chain molecules that have been negatively charged to promote molecular repulsion (Reese and O'Neill, 1999). Like bentonite, polymer slurry requires a head differential sufficient to overcome the force of the groundwater inflow. The molecular structure of polymer slurries prohibits the formation of a filter cake (no particulates) and continuous

filtration is required to maintain the stability of the excavation. This requires a higher head differential for polymer slurry than that needed for mineral slurry and more reserve volume.
Considering the original study focused primarily on mineral slurry fewer polymer slurry shafts were cast. The only observation that could be noted here regarding pullout strengths would be that of the shafts cast on the same date (e.g. 6/18/2013) the 60 second polymer slurry yielded higher pullout resistance than 40, 50, and 90 sec/qt bentonite. However, on 5/3/2015 the 60 second polymer had almost identical pullout strength as the 40 sec/qt bentonite. As a result, the study findings normalized the pullout resistance to the concrete strength to remove the effects of the various mix strengths.

Table 3.3 Polymer shaft specimens (6 total)

Shaft #	Concrete Mix	Slurry Type	Viscosity	Average Pullout Strength (kips)	Average Concrete Compressive Strength (psi)
11	4KDS	SP Polymer	65	32.338	4530
12	4KDS	SP Polymer	66	33.941	4530
19	4KDS	KBI Polymer	60	20.9	4100
16	4KDS	SP Polymer	85	24.077	4753
17	4KDS	SP Polymer	85	26.247	4753
20	4KDS	KBI Polymer	121	19.3	4100

Surface texture variations in specimens can be noted via Figures 3.1 – 3.24 which show each of the shafts both before and after 2 to 4 years of weathering exposure. Immediately apparent are the variations in the surface texture which was in part a by-product of trapped slurry between the outward flowing concrete and the simulated excavation walls. As a first level of assessment, each specimen was rated based on the surface texture and indications of reinforcing cage projections to the side walls of the shafts. The ratings range from smooth with no indication of creases to rough with well-defined creases. In each figure, the condition is shown immediately after removal from formwork and pressure washing (left) and the present condition several years later.

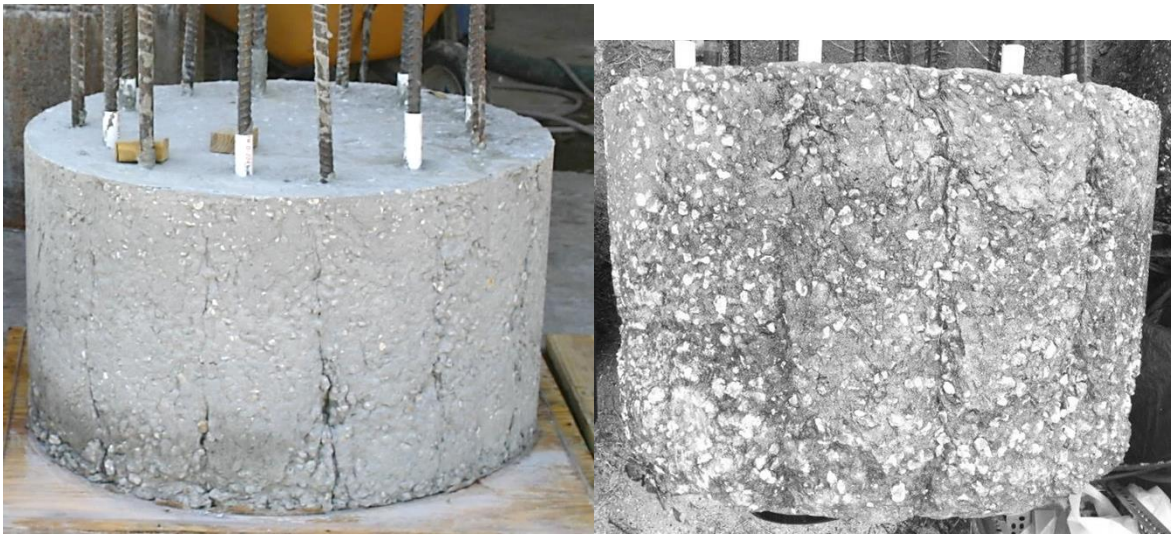

Figure 3.1 Shaft 1: f'c 6150psi; drilled shaft mix; 44 sec/qt bentonite; rough; well-defined creases.

Figure 3.2 Shaft 2: f'c 6150psi; drilled shaft mix; 105sec/qt bentonite; coarse; well-defined creases.

Figure 3.3 Shaft 3: f'c 4358 psi; drilled shaft mix; 40 sec/qt bentonite; coarse; well-defined creases.

Figure 3.4 Shaft 4: f'c 4358 psi; drilled shaft mix; 55 sec/qt bentonite; coarse; well-defined creases.

Figure 3.5 Shaft 5: f'c 4358 psi; drilled shaft mix; 90 sec/qt bentonite; coarse; well-defined creases.

Figure 3.6 Shaft 6: f'c 4358 psi; drilled shaft mix; water cast; smooth; faint channeling.

Figure 3.7 Shaft 7: f'c 4530 psi; drilled shaft mix; 30 sec/qt bentonite; rough; faint creases.

Figure 3.8 Shaft 8: f'c 4530 psi; drilled shaft mix; 40 sec/qt bentonite; coarse; faint creases.

Figure 3.9 Shaft 9: f'c 4530 psi; drilled shaft mix; 50 sec/qt bentonite; rough; with well-defined creases

Figure 3.10 Shaft 10: f'c 4530 psi; drilled shaft mix; 90 sec/qt bentonite; coarse; faint creases

Figure 3.11 Shaft 11: f'c 4530 psi; drilled shaft mix; 65 sec/qt polymer; smooth; no creases

Figure 3.12 Shaft 12: f'c 4530 psi; drilled shaft mix; 66 sec/qt polymer; coarse; no creases

Figure 3.13 Shaft 13: f'c 4753 psi; drilled shaft mix; 30 sec/qt bentonite; coarse; faint to no creases

Figure 3.14 Shaft 14: f'c 4753 psi; drilled shaft mix; 30 sec/qt bentonite; coarse; no creases

Figure 3.15 Shaft 15: f'c 4753 psi; drilled shaft mix; 56 sec/qt bentonite; coarse; well-defined vertical creases

Figure 3.16 Shaft 16: f'c 4753 psi; drilled shaft mix; 85 sec/qt polymer; smooth; faint to no creases

Figure 3.17 Shaft 17: f'c 4753 psi; drilled shaft mix; 85 sec/qt polymer; smooth; faint creases

Figure 3.18 Shaft 18: f'c 4753 psi; drilled shaft mix; water cast; smooth; faint channeling

Figure 3.19 Shaft 19: f'c 4100 psi; drilled shaft mix; 63 sec/qt polymer; smooth; no creases

Figure 3.20 Shaft 20: f'c 4100 psi; drilled shaft mix; 121 sec/qt polymer; smooth; faint creases.

Figure 3.21 Shaft 21: f'c 4100 psi; drilled shaft mix; 42 sec/qt bentonite; rough; well-defined creases

Figure 3.22 Shaft 22: f'c 4100 psi; drilled shaft mix; water cast; smooth; faint channeling

Figure 3.23 Shaft 23: Self consolidating concrete; water cast; smooth; faint channeling

Figure 3.24 Shaft 24: Self consolidating concrete; 40 sec/qt bentonite; rough; disintegrating; creases coincide with deteriorated regions.

3.2 Surface Anomalies and Corrosion Potential

An anomaly is a deviation from the perfect quality of the cast in-situ drilled shaft element. Anomalies can be, but are not necessarily defects. The marks left in the concrete surface during casing extraction is technically an anomaly, but should not be considered defects unless the structural integrity of the shaft is compromise. Most defects fall into three categories: inclusions, channeling, and quilting (DFI, 2016).

The term inclusion refers to any foreign material trapped within the concrete shaft outside of the design (Figure 3.25). It can be in-situ material, segregated concrete, or uncemented materials mixed with slurry. These can be detected during the construction process through indirect inspection methods such as cross-hole sonic logging or thermal integrity profiling.

Figure 3.25 Inclusions (DFI, 2016)

Channeling refers to systems of vertical narrow lanes with loose aggregates or lightly cemented material. They are customarily near the surface of the pile (Figure 3.26). This circumstance can be attributed to insufficient concrete stability. Channels are only considered defects if they are of significant depth and frequency to compromise the stability or durability of the shaft (DFI, 2016).

Figure 3.26 Channeling (DFI, 2016)

Quilting describes vertical or horizontal linear features emanating primarily from reinforcing bars. Concrete is always placed inside the cage such that flow must go outward through the reinforcement cage into the cover region. As the concrete flows around the reinforcement, a separation occurs whereby two separately contaminated faces, commonly referred to as laitance interfaces, must recombine outside the case by pressing these interfaces together. This creates visible or invisible pathways of altered concrete that may appear on the side of shaft surface as creases in the form of a quilted grid pattern (Figures 3.27, 3.28 and 3.29). The depth of the creases can extend to the reinforcing steel and presents significant durability issues as the openings facilitate the corrosion process through the access of environmental chlorides.

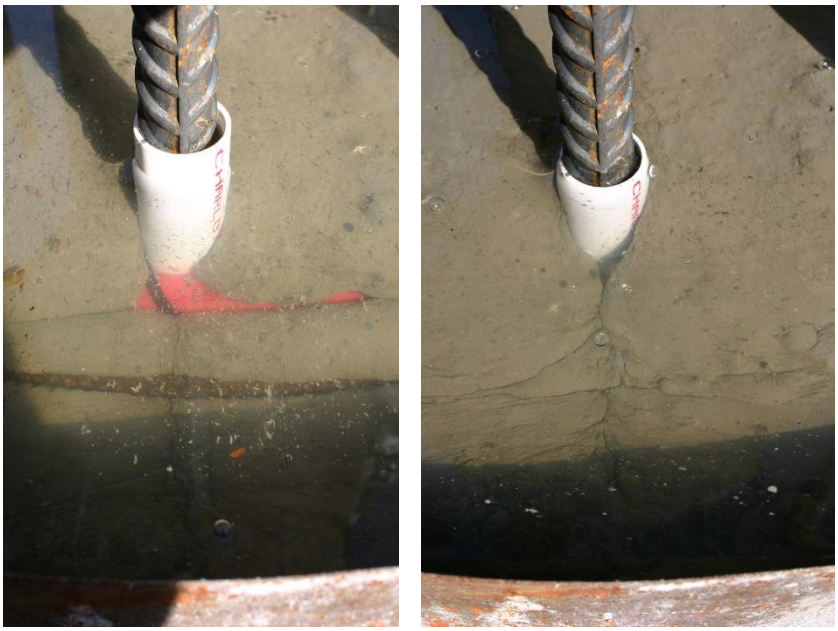

Figure 3.27 Laitance channel formation process

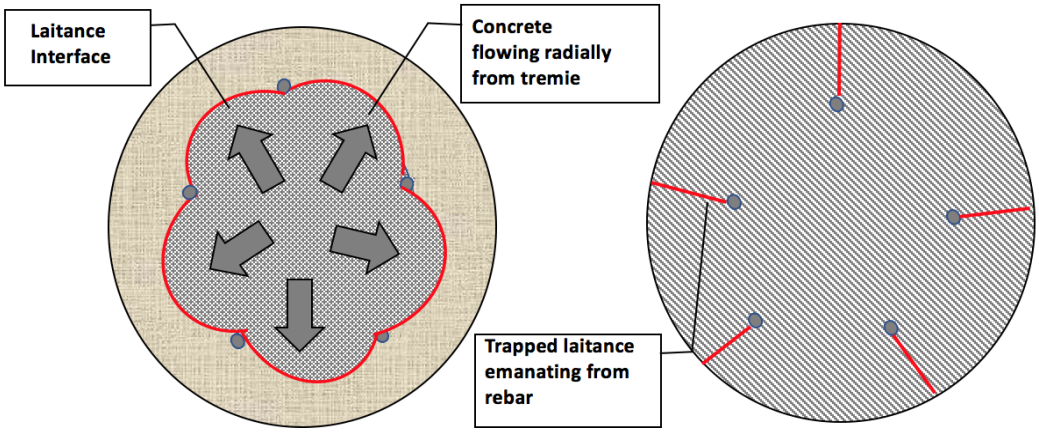

Figure 3.28 Laitance channel formation process

Figure 3.29 Quilting

Design lifespan computations assume a contiguous concrete cover. Field and laboratory observations have shown "quilting" in shaft specimens constructed in wet conditions, where concrete was placed into slurry using a tremie. The occurrence of quilting introduces the possibility of direct ground or sea water access to the reinforcing cage, thus negating the protection afforded and the life span computations presented in Chapter 2. This portion of the study focuses on diagnosing the condition of the concrete cover as it relates to the type of slurry used in construction in order to determine the suitability of standard corrosion lifespan calculations. Surface potential measurements are a quick way to assess the probability of active corrosion taking place within a reinforced or prestressed concrete element.

3.3 Testing Equipment and Procedures

Much of the focus of this task revolved around identifying physical surface features that may indicate concrete flow problems and potential adverse effects on the longevity of the structure. To this end, the surface condition of the shafts was an obvious variable for consideration. One method to classify the surface condition of the individual shafts was through approximate quantification of the surface void volume / roughness. This was accomplished by two means: physical and digital.

Note: Surface roughness was suspected to be an indication of concrete quality (cover protection) which would then make external physical assessment a direct link to the internal health of the structural steel reinforcement and the structure as a whole.

3.3.1 Physical Surface Void Volume Determination

The surface roughness was assessed by measuring the surface void volume through a procedure developed for this project wherein a representative area of the shaft surface was filled with a putty of a known density and finished in such a manner as to approximate a smooth shaft surface.

With the weight of the putty required a void volume was calculated and then extrapolated to approximate the void volume for the entire shaft surface. This assumed the original outer surface of the shaft was still in-part present and that severe radial reduction had not taken place.

Initially a testing area grid was created by cutting a 6 inch by 6 inch hole out of a sheet of thick plastic sheeting (Figure 3.30). This hole was used as a template for setting the limits of the testing area.

Figure 3.30 Template construction

Next a beaker with a known volume was filled with drywall putty and the density determined. Then all of the testing equipment was placed in a tray and the total equipment/material weight was recorded (Figure 3.31). The template was then placed on the surface of the shaft (Figure 3.32).

Figure 3.31 Weighing of testing equipment. Tray includes: plastic template, rubber gloves, two putty knives, beaker full of drywall putty

Figure 3.32 Testing template placed on shaft surface.

Figure 3.33 Testing template filled to approximate a void free surface

After putting on the rubber gloves, the putty knife was used to contour the concrete surface in the template area to approximate a smooth void free surface (Figures 3.33 and 3.34). Special care was taken to ensure that all putty stayed on the tools, the template, in the tray or on the concrete surface. The gloves, template, beaker with the remaining putty and all of the tools were then put back into the tray and reweighed (Figure 3.35). The difference in weight was then converted to a volume using the calculated density of the putty. This test was conducted two times on each

shaft, care was taken to place the template on an area representative of the overall surface condition.

Figure 3.34 Testing the second location on shaft 10

Figure 3.35 Weighing testing equipment after test is complete

Results

Void volume was computed for two test areas on each shaft, the results were then averaged and extrapolated over the entire shaft surface (Table 3.4). The values range from 38 cubic inches to 592 cubic inches. All raw data can be found in Appendix B.

Table 3.4 Physical Void Volume

	per 6"x6" square	per total surface area	total	avg per shaft
Shaft #	void volume (cm^3)(mL)	void volume (cm^3)	void volume (in^3)	(in^3)
1	68.7	6043.6	368.8	592.3
	151.9	13367.3	815.7	
2	127.0	11173.1	681.8	491.6
	56.1	4937.9	301.3	
3	32.9	2890.2	176.4	203.4
	42.9	3775.6	230.4	
4	62.6	5503.3	335.8	313.2
	54.1	4760.7	290.5	
5	44.2	3892.0	237.5	253.8
	50.3	4426.4	270.1	
6	6.9	610.1	37.2	41.9
	8.7	764.7	46.7	
7	89.9	7907.2	482.5	487.2
	91.6	8059.5	491.8	
8	47.9	4218.6	257.4	215.2
	32.2	2835.7	173.0	
9	41.7	3665.6	223.7	260.2
	55.3	4861.9	296.7	
10	90.9	8000.8	488.2	540.1
	110.3	9699.9	591.9	
11	17.2	1509.4	92.1	71.4
	9.5	831.6	50.7	
12	12.7	1120.9	68.4	59.4
	9.4	826.3	50.4	
13	34.4	3024.5	184.6	167.0
	28.6	2513.9	153.4	
14	54.8	4817.1	294.0	299.5
	56.8	4997.8	305.0	
15	48.6	4270.9	260.6	263.2
	49.5	4354.8	265.7	

	per 6"x6" square	per total surface area	total	avg per shaft
Shaft #	void volume (cm^3)(mL)	void volume (cm^3)	void volume (in^3)	(in^3)
16	14.5	1274.9	77.8	72.6
	12.5	1102.9	67.3	
17	6.4	564.5	34.5	38.2
	7.8	688.9	42.0	
18	9.8	865.4	52.8	47.4
	7.8	689.3	42.1	
19	8.0	706.0	43.1	43.3
	8.1	713.2	43.5	
20	6.4	567.2	34.6	32.7
	5.7	503.6	30.7	
21	125.3	11021.3	672.6	577.6
	89.9	7909.4	482.6	
22	6.7	585.1	35.7	29.6
	4.4	384.4	23.5	
23	8.3	732.5	44.7	48.1
	9.6	842.4	51.4	
24				

Note: Shaft 24 was not tested due to active surface degradation

3.3.2 Digital Surface Void Volume Determination

One side of each shaft was scanned using an Artec Eva 3D scanner (Figure 3.36). An Artec Eva is a structured light device that is used to make texture assessments and accurate 3D models of medium sized objects such as the selected portions of the shafts. The handheld scanner captures precise measurements in high resolution, and can be used for multiple applications.

Figure 3.36 Scanning shaft 20

A structured-light 3D scanner is a scanning device for measuring the three-dimensional shape or surface of an object using an established light pattern and camera system. Structured light is a method of projecting a known pattern of light on to a surface. The manner and extent in which this pattern of light is distorted or altered when it strikes a surface allows the system to calculate information about the depth and surface detail of the objects in the scan. Factory calibration ensures a minimum accuracy of 100 microns (0.1mm). Testing in a dark evening environment and the non-reflective surface of the samples enhanced the quality of the data collected. Figure 3.37 shows a sample of the data collected, this surface profile was generated using over 3 million data points.

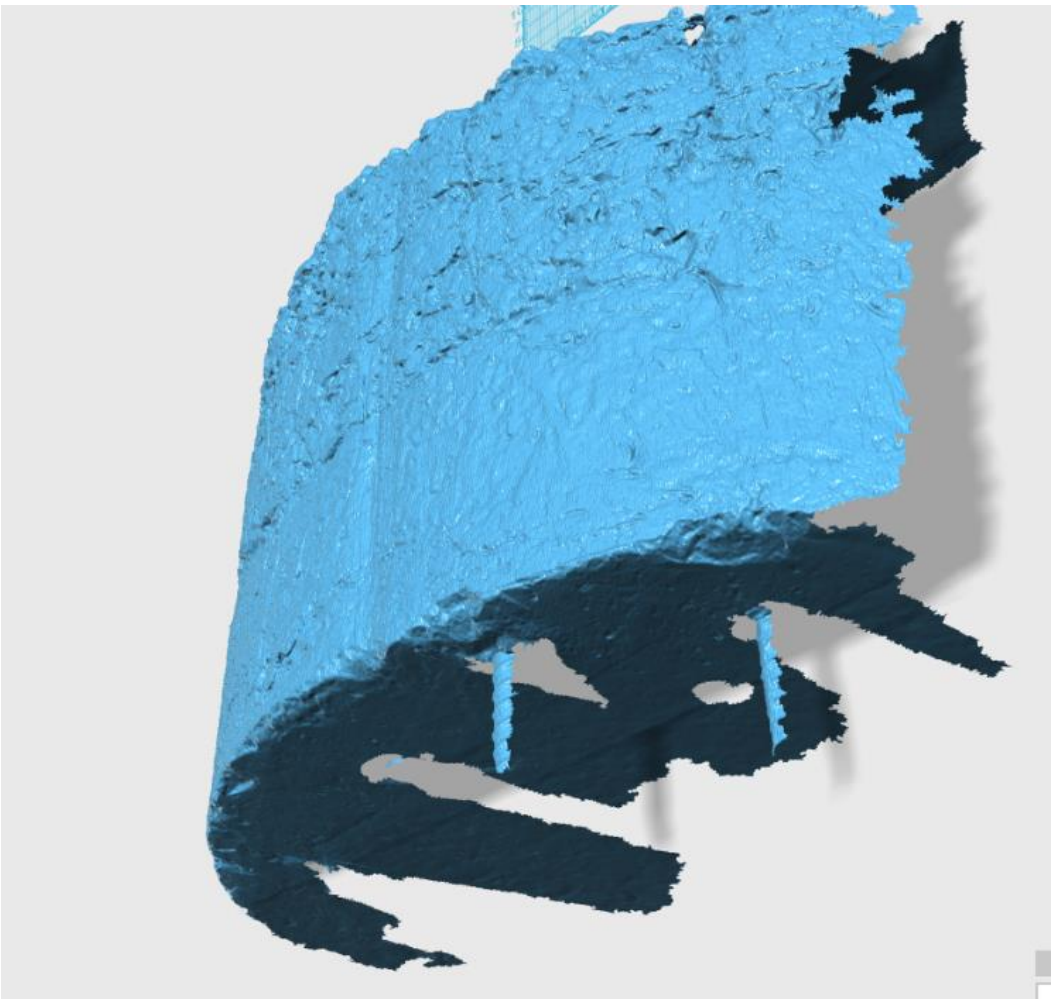

Figure 3.37 Scan data detail

Results

The analysis of the digital scans is a lengthy process that requires enormous computational capabilities. The files ranged in size from 3 million to 5 million data points and represented only a 24in by 48in surface area (Figures 3.38, 3.39, and 3.40). As a result, only shafts 6, 9 and 11 have been fully processed as shown (water, bentonite and polymer, respectively). The scan data for each shaft has been collected and stored for regression in an object file. A more robust computer system was purchased to complete the process for the remaining shafts. Complete results will be included in future reports. As the figures show, the data represents the surface condition of each shaft with a high degree of detail.

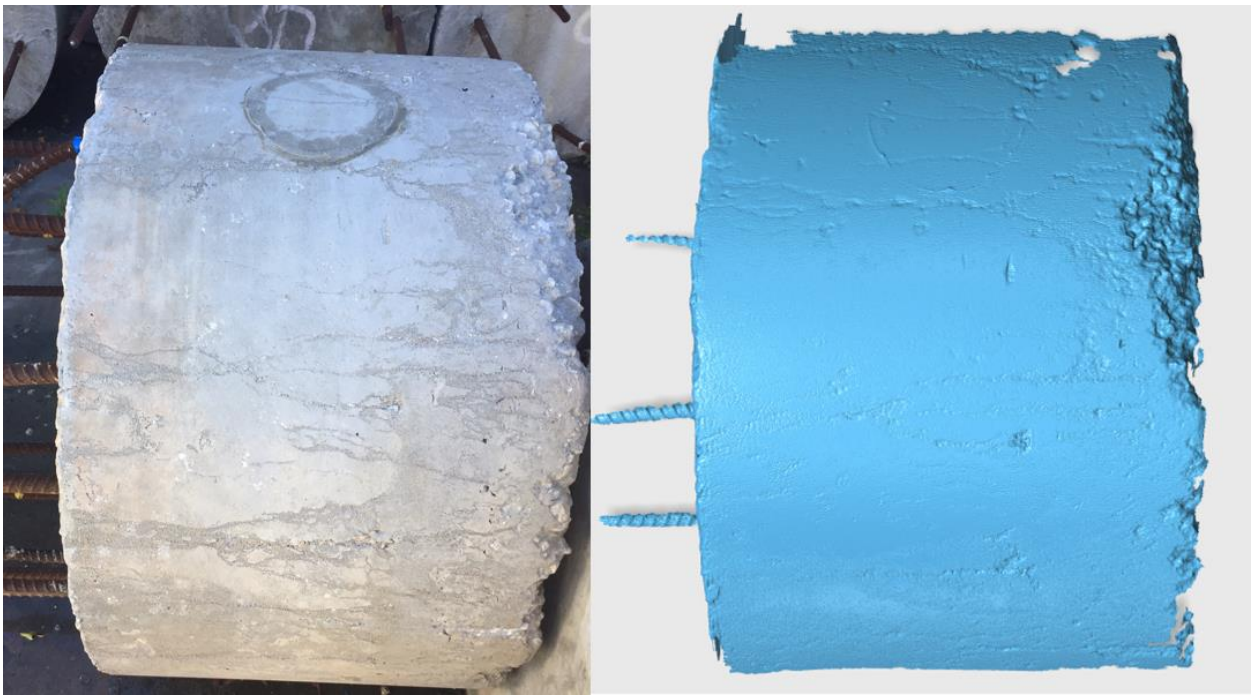

Figure 3.38 Shaft 6 (water) photo and scan comparison

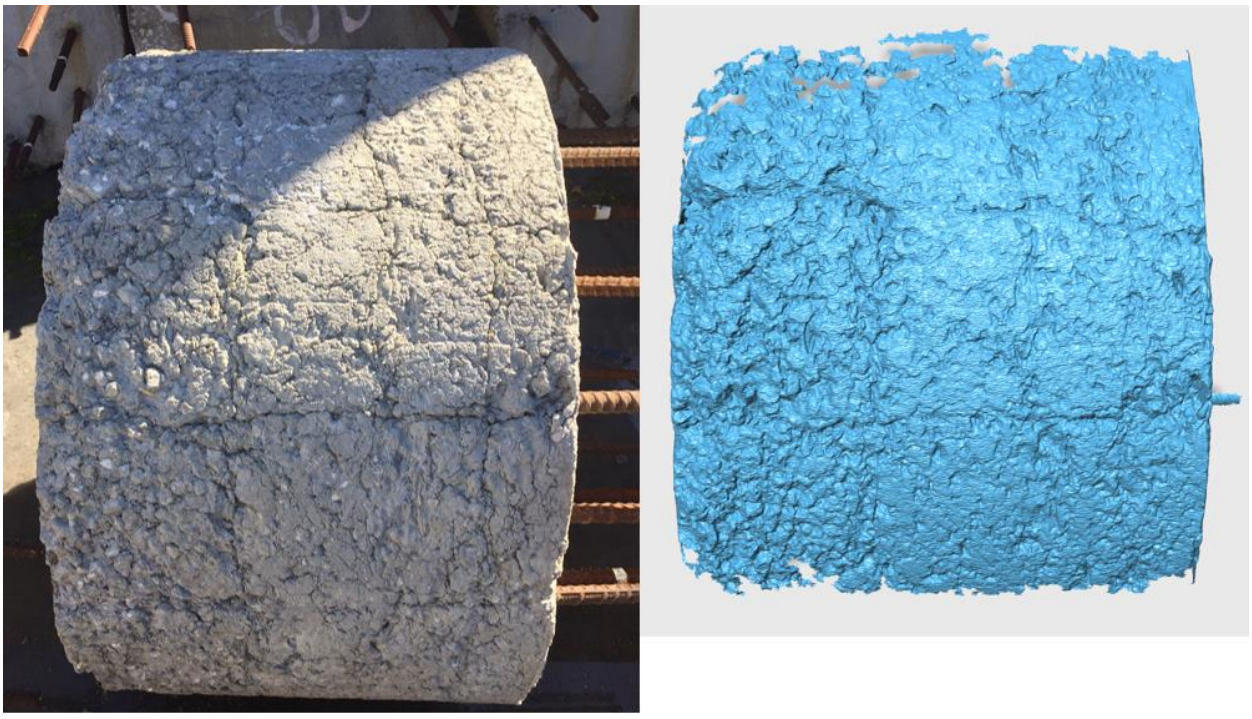

Figure 3.39 Shaft 9 (bentonite) photo and scan comparison

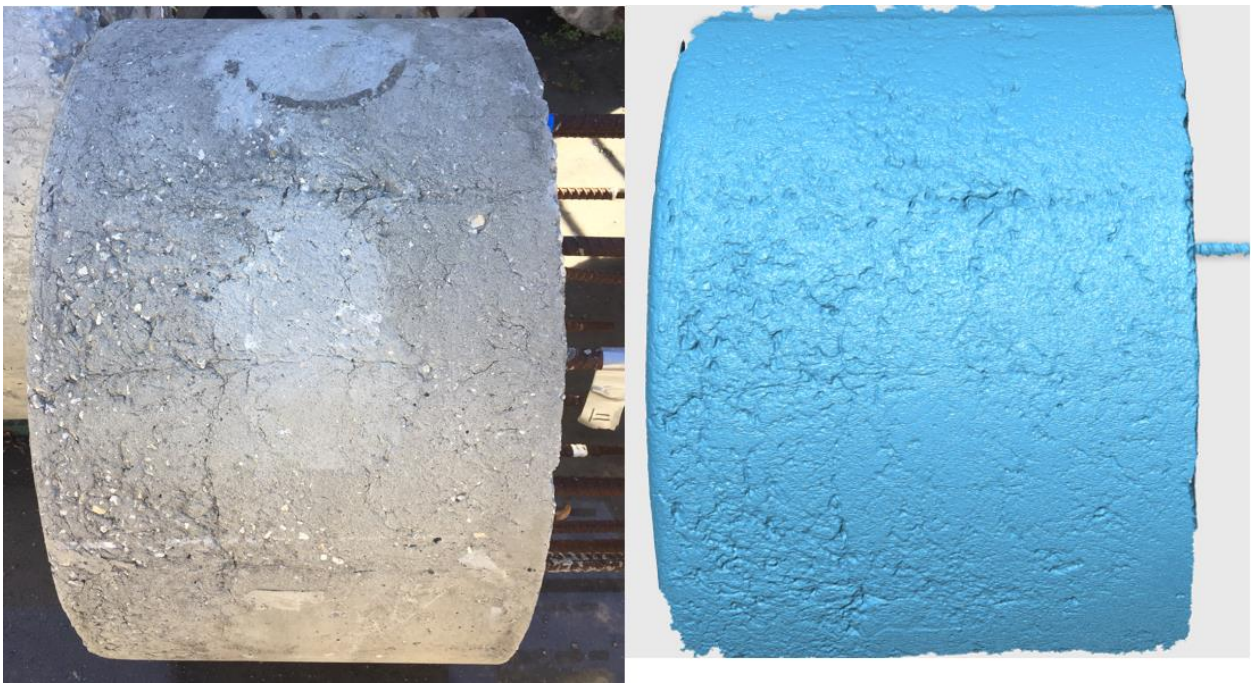

Figure 3.40 Shaft 11 (polymer) photo and scan comparison

As previously stated, the data was provided as an object file. Due to constraints in the AutoCAD software, the data had to be reduced prior to analysis. Each file was reduced from its original size of 3-5 million points to a manageable 300,000 points using a free, web-sourced, software called MeshLab and reducing by no more than 50% in each stage of the process. The surfaces were exported from MeshLab as ASCII files that could then be uploaded into AutoCAD Civil3D for analysis.

A surface was then generated for each shaft using the imported ASCII data file. Using the same general methodology as the physical void volume calculations, two six inch by six inch squares were chosen as test areas. If the surface showed signs of creasing then care was taken to represent those creases in the test areas. A profile was taken horizontally across the center of each test area to identify the surface shape and condition (a circumferential slice). The ideal surface profile was approximated using a tan-tan-radius curve in the profile creation tools menu (Figure 3.41). This function allowed for variation in the shaft radius due to the nature of construction and any distortion away from circular that may have been induced by the somewhat flexible forms. The ideal surface profile elevation was set to match the highest points in the region of interest (Figure 3.42). Using a flat assembly with perfectly vertical side slopes, the ideal surface profile was used to create a corridor and the surface from the corridor was compared with the existing surface using cut and fill tools to generate the digital surface void volume data.

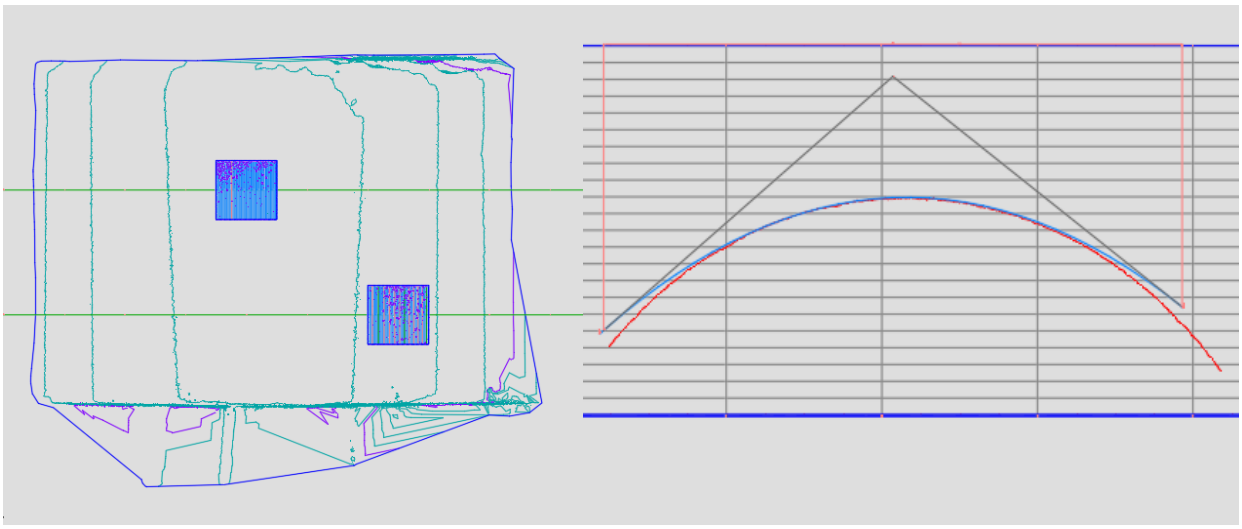

Figure 3.41 Shaft 6 surface data analysis plan and profile

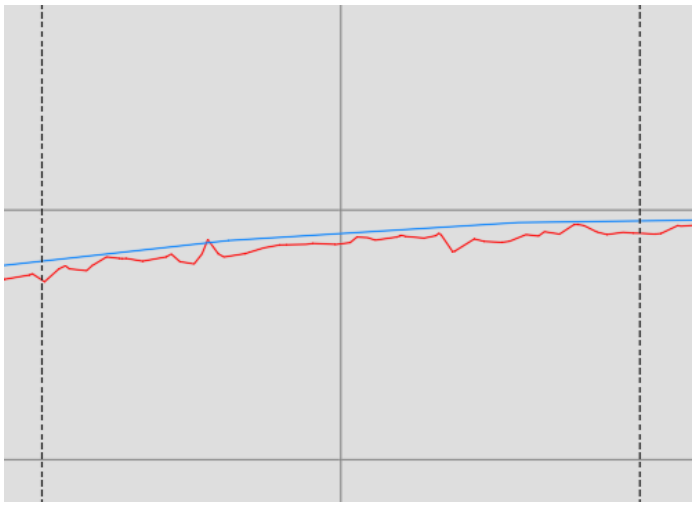

Figure 3.42 Shaft 6 existing and finished grade

Void volume was computed for two test areas on each shaft (Figures 3.43, 3.44 and 3.45) the results were then extrapolated over the entire shaft surface (Table 3.5). Digital void volume determination resulted in a higher value than physical void volume determination in all cases.

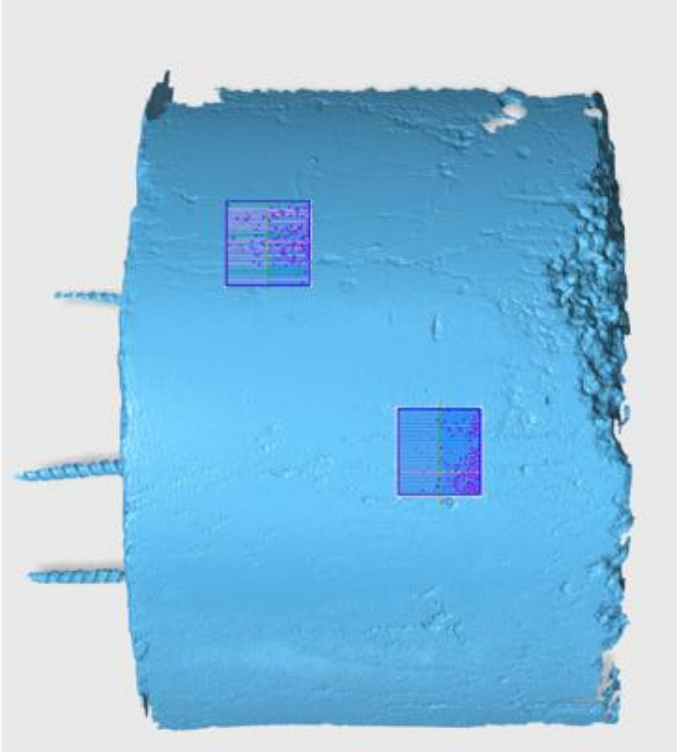

Figure 3.43 Shaft 6 Digital void volume determination

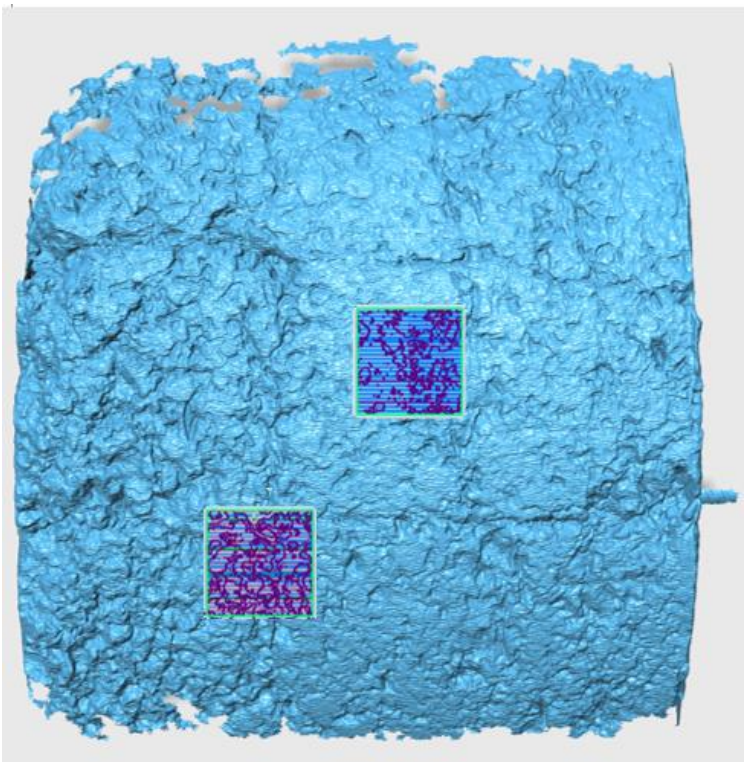

Figure 3.44 Shaft 9 Digital void volume determination

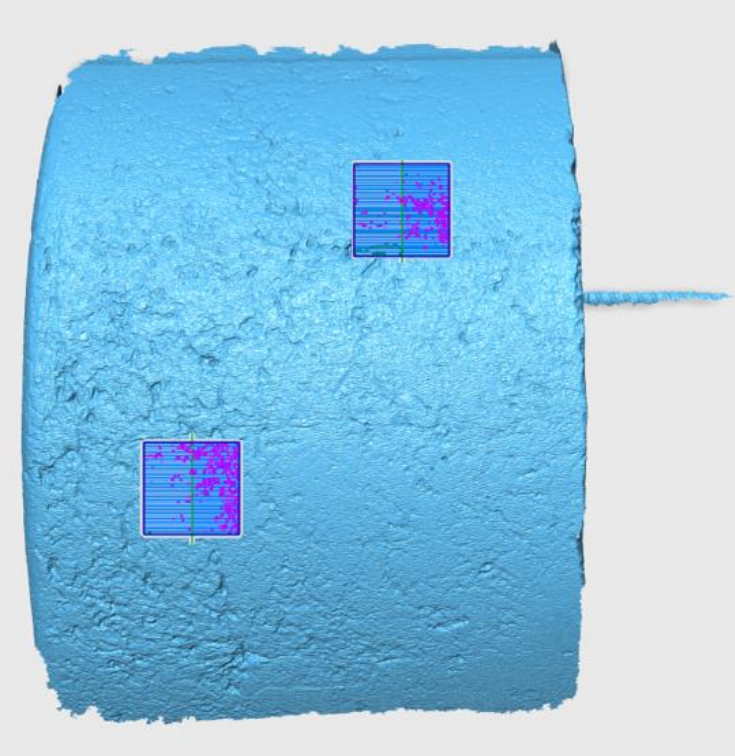

Figure 3.45 Shaft 11 Digital void volume determination

Table 3.5 Digital surface void volume data

Shaft #	Slurry type and viscosity (sec/qt)	Per 6"x6" square (in^3)	Digital Void Volume Per total surface area (in^3)	Physical Void Volume Per total surface area (in^3)	Percent increase from physical vol.
6	Water 26	0.608	53.55	42	22%
9	Bentonite 50	3.434	302.12	260	14%
11	Polymer 65	0.919	80.84	71	12%

Digital surface void volume determination resulted in a higher quantity than the physical surface void volume method used in all cases. The percent difference shown above illustrates the conservative nature of the physical method. This could be due to the reference ideal surface used in both cases as the datum. The physical void volume ideal surface is created without a template and as such is left to the judgement of the technician performing the test. The digital void volume uses the highest elevation along the selected profile to determine the ideal surface elevation. This method is also reliant on the judgement of the technician performing the analysis. Nevertheless, Figure 3.46 shows that the results of the two testing methods follow a linear relationship thus supporting the validity of either when reviewed against the other.

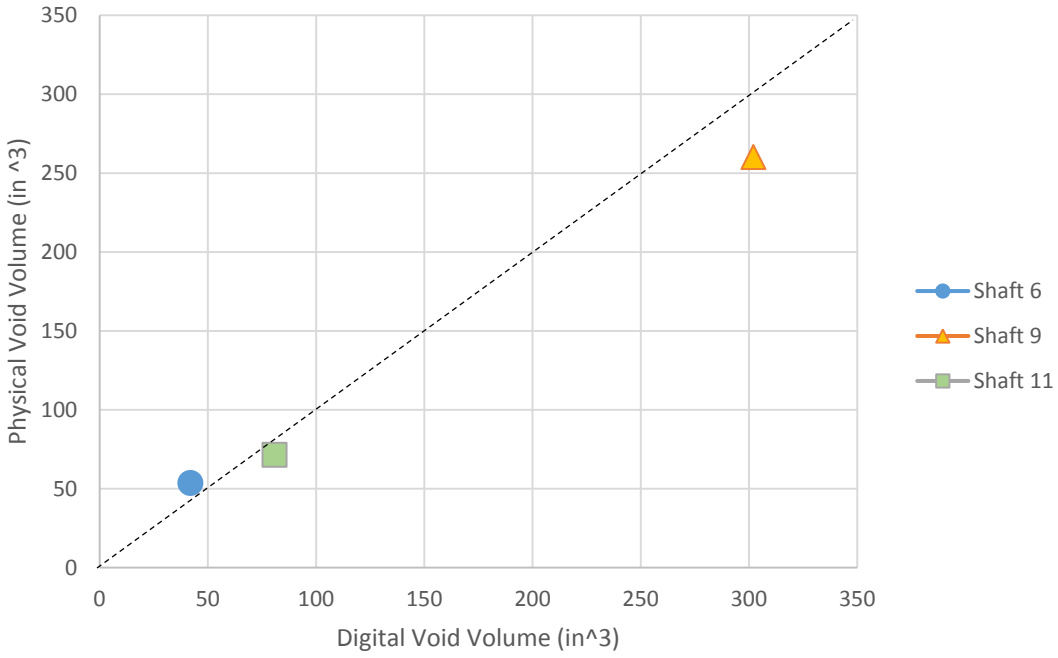

Figure 3.46 Digital void volume vs physical void volume with 1:1 line.

3.3.3 Multi-Point Surface Potential Mapping

Corrosion is most often defined as the destruction of a metallic material due to a reaction with its environment. Practically all environments are corrosive to some degree, but this research focuses on corrosion in wet environments. Corrosion in wet environments accounts for a large majority of all corrosion and usually involves aqueous solutions or electrolytes. Uniform corrosion is characterized by a chemical or electrochemical reaction that occurs over a large area. This reaction thins the metal to a point of eventual failure. Overall corrosion represents the greatest destruction of metal on a tonnage basis but this does not raise major industry concerns because uniform corrosion is both predictable and preventable in most instances (Fontana, 1967). However, this assumes the concrete barrier protecting the reinforcing steel is contiguous. In the case of quilting, no such assumption can be made.

Surface potential measurements are a strong indicator of active corrosion within a reinforced concrete structure. This is performed by measuring the relative voltage potential between the reinforcing steel and a copper-copper sulfate electrode in contact with the concrete surface several inches away from the reinforcing steel.

The surface potential of each shaft specimen was mapped evenly over the surface using a prescribed grid. A grid template was made out of single piece of 21-inch by 27-inch rubberized plastic sheeting. A sharpened 2-inch diameter pipe was used to punch holes through the plastic (Figure 3.47) in rows with a 3 inch CTC spacing in both directions (Figure 3.48). This resulted in 80 measurement locations for each shaft. Surface potential testing was then conducted per ASTM C876-09: *Standard Test Method for Corrosion Potentials of Uncoated Reinforcing Steel in Concrete*, using a copper-copper sulfate reference electrode and a standard multi-meter.

Figure 3.47 Template Preparation

Figure 3.48 Completed Template

The saturated copper-copper sulfate reference electrode was selected because it provides a stable and reproducible potential over a temperature range of 32º to 120ºF. A wet sponge was used to establish an electrical junction at the concrete surface by means of a low electrical resistance liquid bridge between the concrete surface and the porous tip of the reference electrode. The sponge was wrapped around the tip of the reference electrode and secured with a rubber band to ensure continuous electrical contact.

Having previously established secure electrical connection to the reinforcing steel, an alligator clip was used to connect the steel to the positive port on the multi-meter. Similarly, the negative or COM port was attached to the cap of the reference electrode (Figure 3.49).

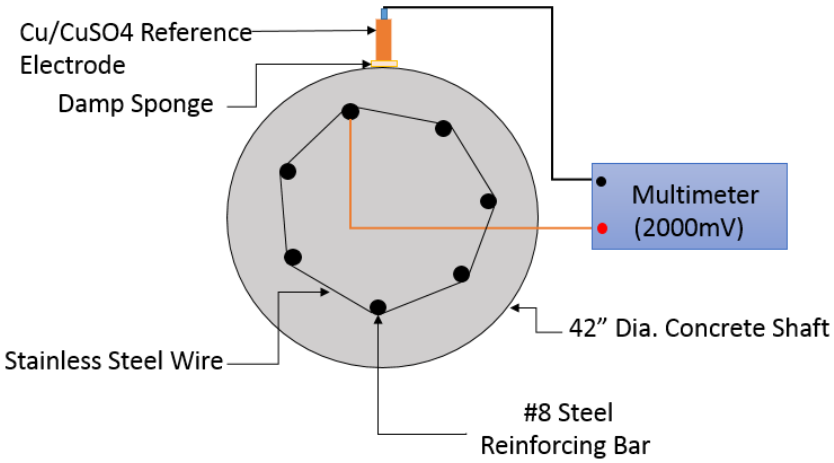

Figure 3.49 Surface Potential Mapping Wiring Diagram

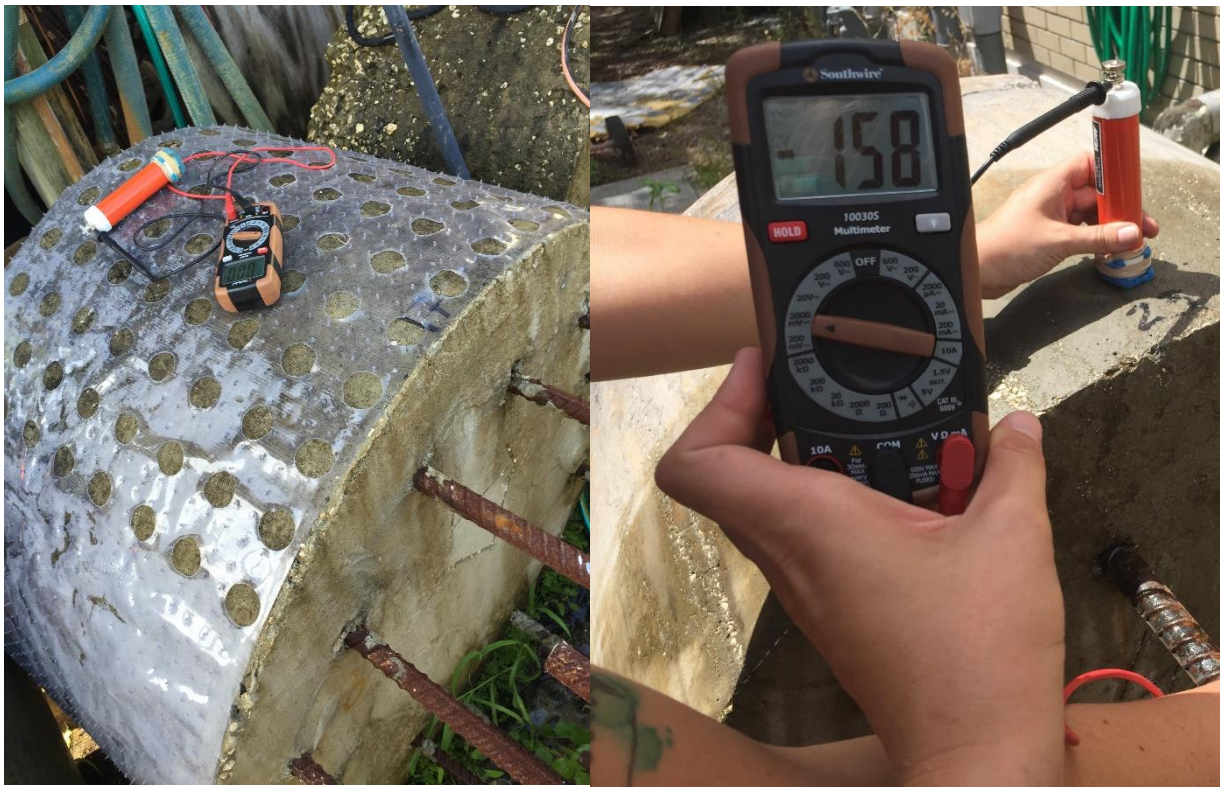

Figure 3.50 Surface potential testing

Prior to commencing testing, all shafts were saturated for 24 hours or until such time as a test measurement of corrosion potential revealed no change or fluctuation. Once saturated, measurements were taken systematically across the 80 grid positions with the multi-meter set to the ±2000 millivolt range. The readings were recorded to the nearest millivolt.

Results

The data from Shaft 1 is shown in Table 3.6 as an example; the complete data sets for all shafts are included in Appendix C.

Surface potential readings represent a potential difference of voltage in the system created during testing. A potential difference of zero signifies that no voltage is lost between the reference electrode and the reinforcement. The larger the magnitude of the potential difference, the larger the magnitude of voltage absorbed by the system. This is commonly used as an indicator of corrosion potential. For the purpose of this testing prescription, corrosion potential was used as a diagnostic indicator of concrete quality.

Using the copper-copper sulfate potential data, the 80 values for each shaft were plotted on a standard distribution (Figure 3.51) using a rank and percentage analysis. The median (potential at 50% ranking) or the E_{50} value was taken as the single point representative of each shaft for comparative plotting purposes. This is the preferred industry approach for such evaluations.

Table 3.6: Surface potential data collected from shaft 1 (all shaft data in Appendix C).

Circumferential position (in)	Vertical Position (in) Bottom to Top							
	0	3	6	9	12	15	18	21
0	-266	-289	-333	-337	-313	-298	-296	-289
3	-279	-292	-316	-317	-311	-301	-300	-293
6	-290	-302	-312	-312	-308	-306	-307	-303
9	-290	-308	-315	-312	-309	-310	-308	-307
12	-307	-316	-315	-318	-317	-314	-311	-302
15	-309	-317	-319	-325	-324	-322	-320	-311
18	-314	-323	-324	-332	-330	-328	-327	-320
21	-323	-330	-330	-338	-338	-342	-331	-322
24	-327	-330	-338	-344	-345	-348	-337	-329
27	-328	-333	-338	-344	-347	-349	-338	-337

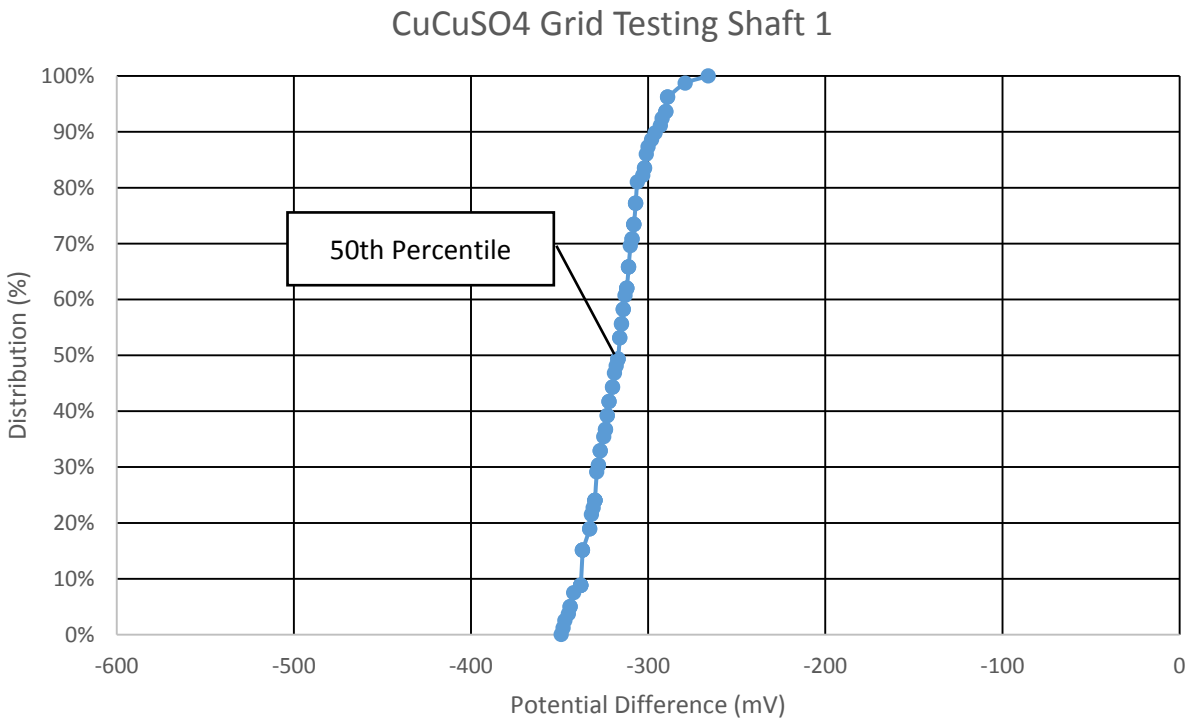

Figure 3.51 Surface potential mapping data distribution

E_{50} potential data for all shafts ranged from -508mV to -155mV with a standard deviation of 91mV. A total of 35% of the test shafts had an E_{50} potential below -350mV and all of that 35% were constructed using bentonite slurry (Table 3.7). All of the data was graphed topographically using three dimensional mapping software. Using a color coding system and standardized contour spacing, the topographic surface maps illustrate the corrosion potential of each shaft. (Figure 3.52-3.59). Lighter colors denote low corrosion probability; darker colors high.

Table 3.7 Comparison of all 24 shaft specimen E_{50} values.

Shaft #	Slurry	Mix	E_{50} (mV)	Shaft #	Slurry	Mix	E_{50} (mV)
1	B40 (44) 6K	4KDS	-317	14	B30	4KDS	-282
2	B90 (105)	4KDS	-449	15	B50 (56)	4KDS	-335
3	B40	4KDS	-373	16	P85	4KDS	-279
4	B50 (55)	4KDS	-443	17	P85	4KDS	-300
5	B90	4KDS	-447	18	water	4KDS	-293
6	Water	4KDS	-155	19	P60	4KDS	-243
7	B30	4KDS	-372	20	P130	4KDS	-242
8	B40	4KDS	-225	21	B40	4KDS	-508
9	B50	4KDS	-383	22	water	4KDS	-250
11	P60 (65)	4KDS	-285	23	water	SCC	-258
12	P60 (66)	4KDS	-190	24	B40	SCC	-425
13	B30	4KDS	-289				

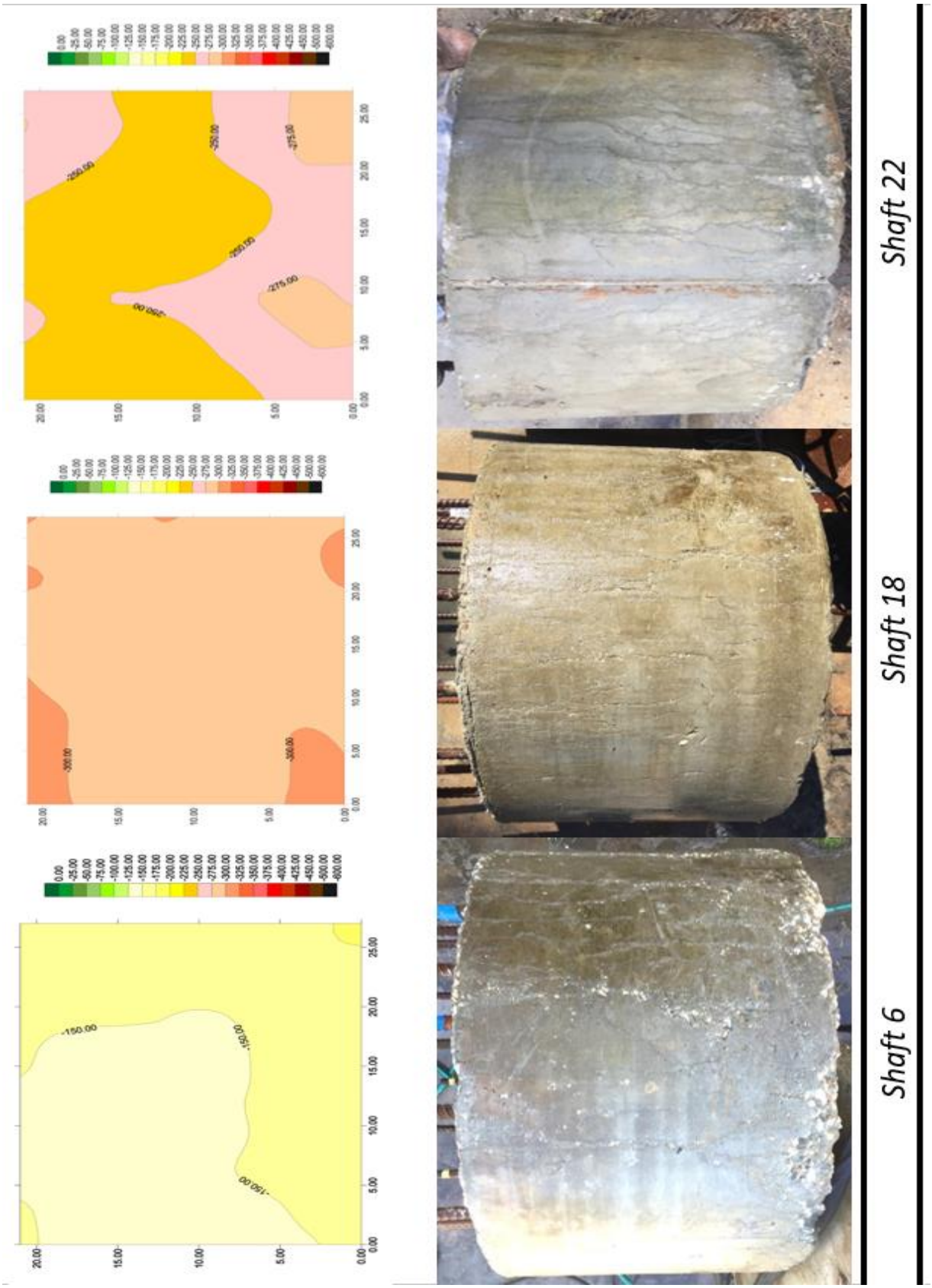

Figure 3.52 Surface potential maps, water cast shafts

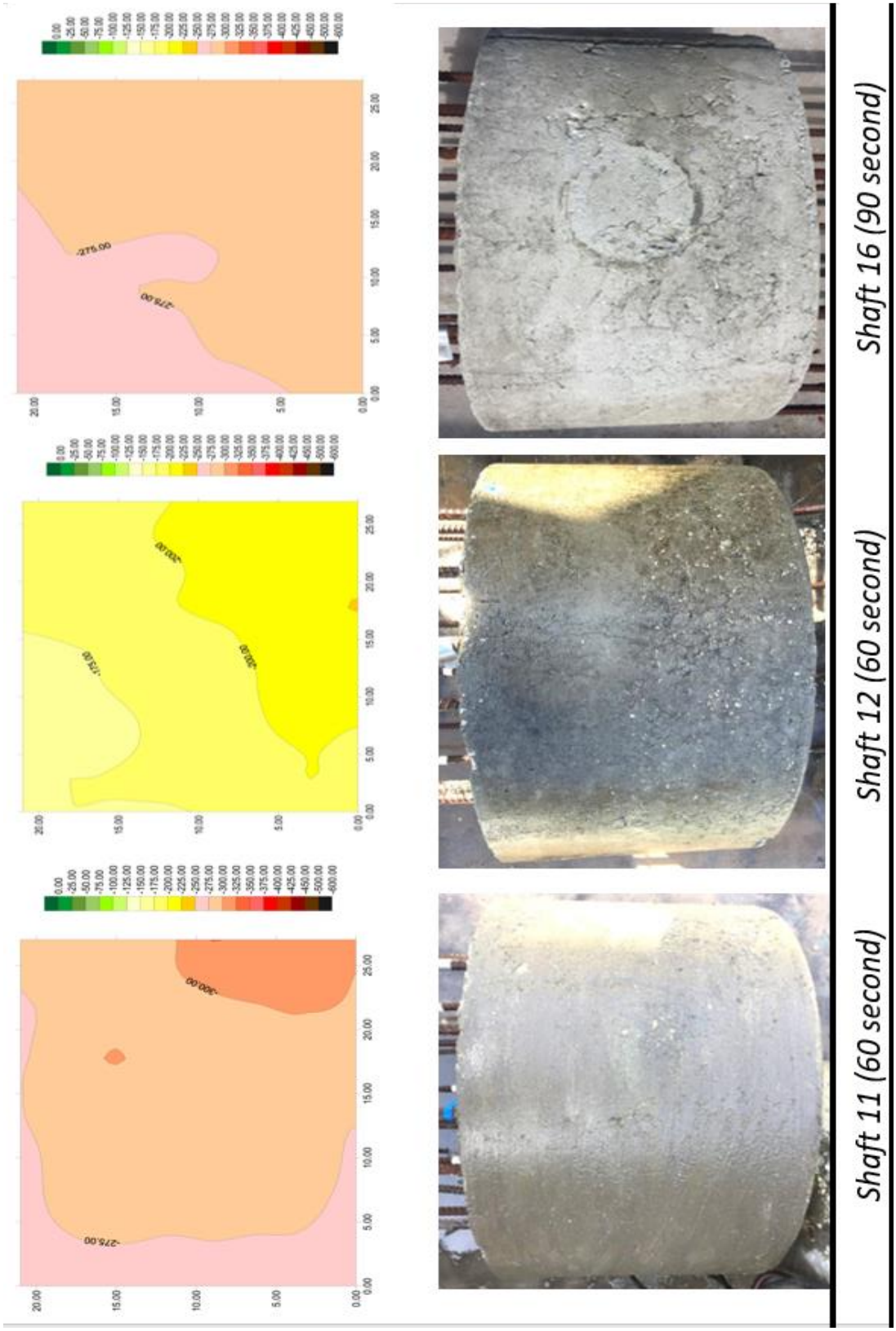

Figure 3.53 Surface potential maps, polymer cast shafts

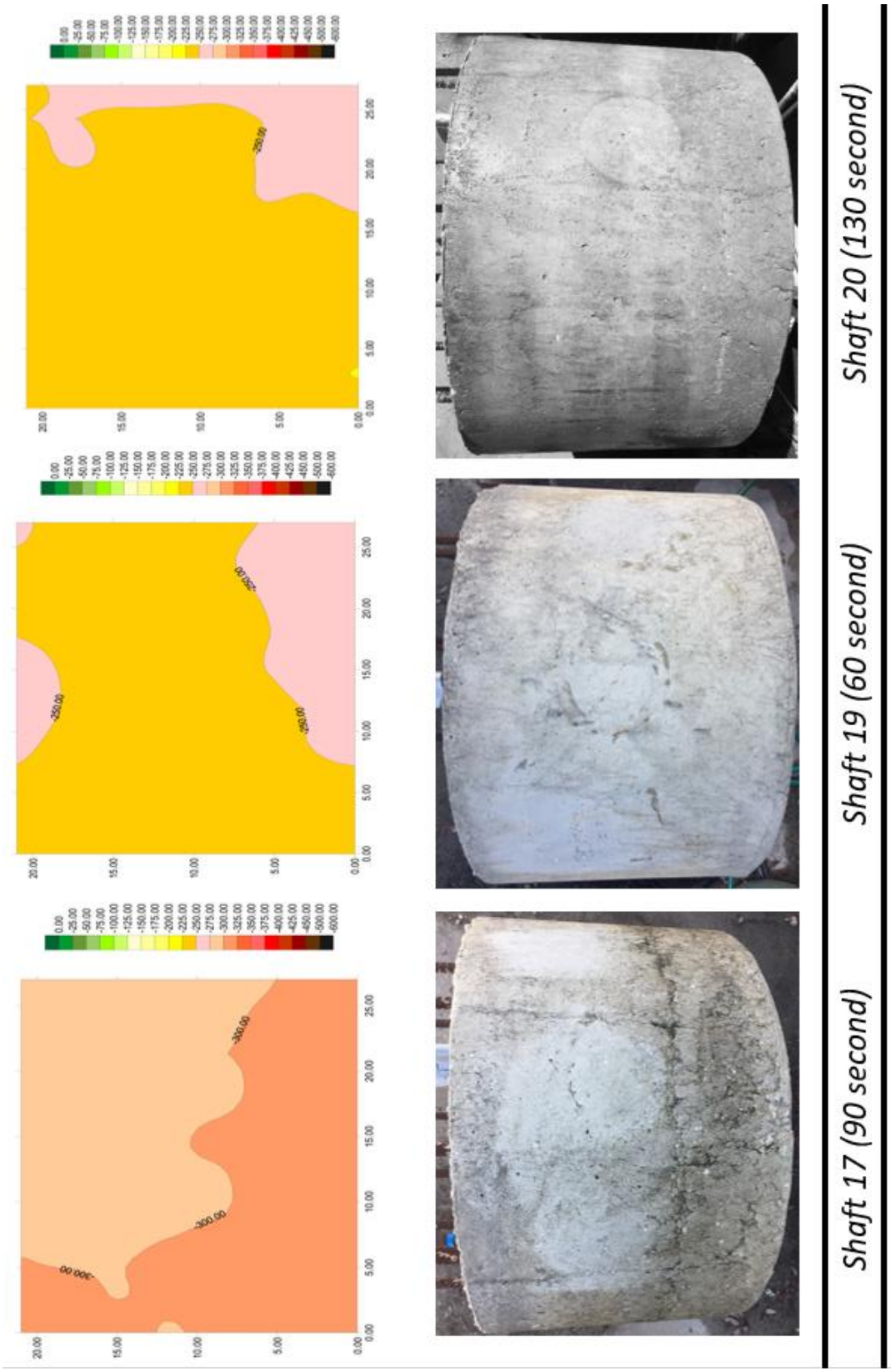

Figure 3.54 Surface potential maps, polymer cast shafts

Figure 3.55 Surface potential maps, bentonite cast shafts

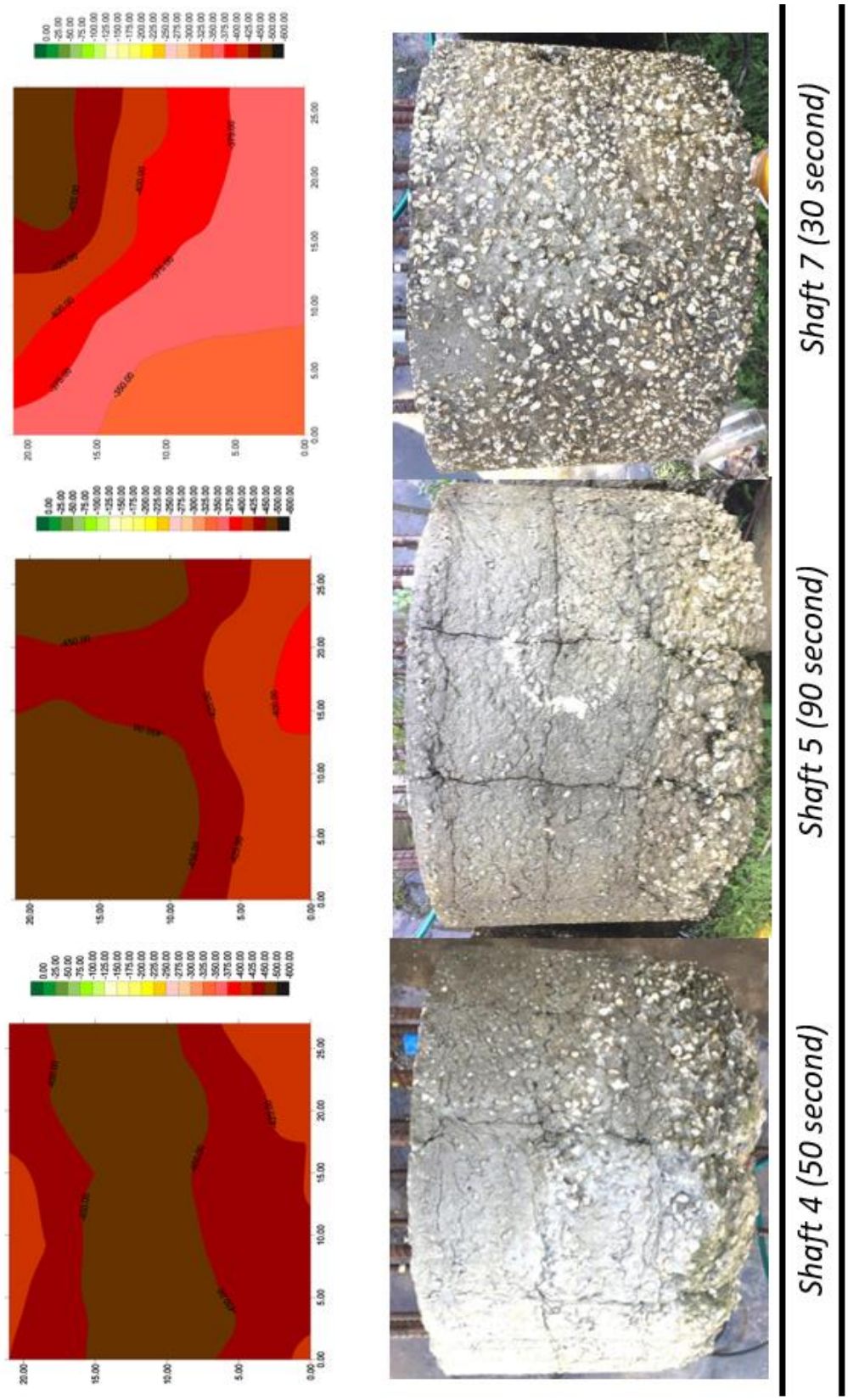

Figure 3.56 Surface potential maps, bentonite cast shafts

Figure 3.57 Surface potential maps, bentonite cast shafts

Figure 3.58 Surface potential maps, bentonite cast shafts

Figure 3.59 Surface potential maps, Self-consolidating concrete shafts

3.3.4 Concrete Core Compressive Strength Profiling

The goal of this subtask was to devise an instrument capable of providing a strength profile of concrete in real time. In concept, it is a concrete penetrometer which measures drilling resistance of the concrete via a fully instrumented concrete coring drill motor. This type of information would then serve as prescreening for regions of the shaft that would receive more in depth chemical analyses in future tasks (e.g. XRD and MIP). Figure 3.60 shows a line drawing schematic of the concept machine.

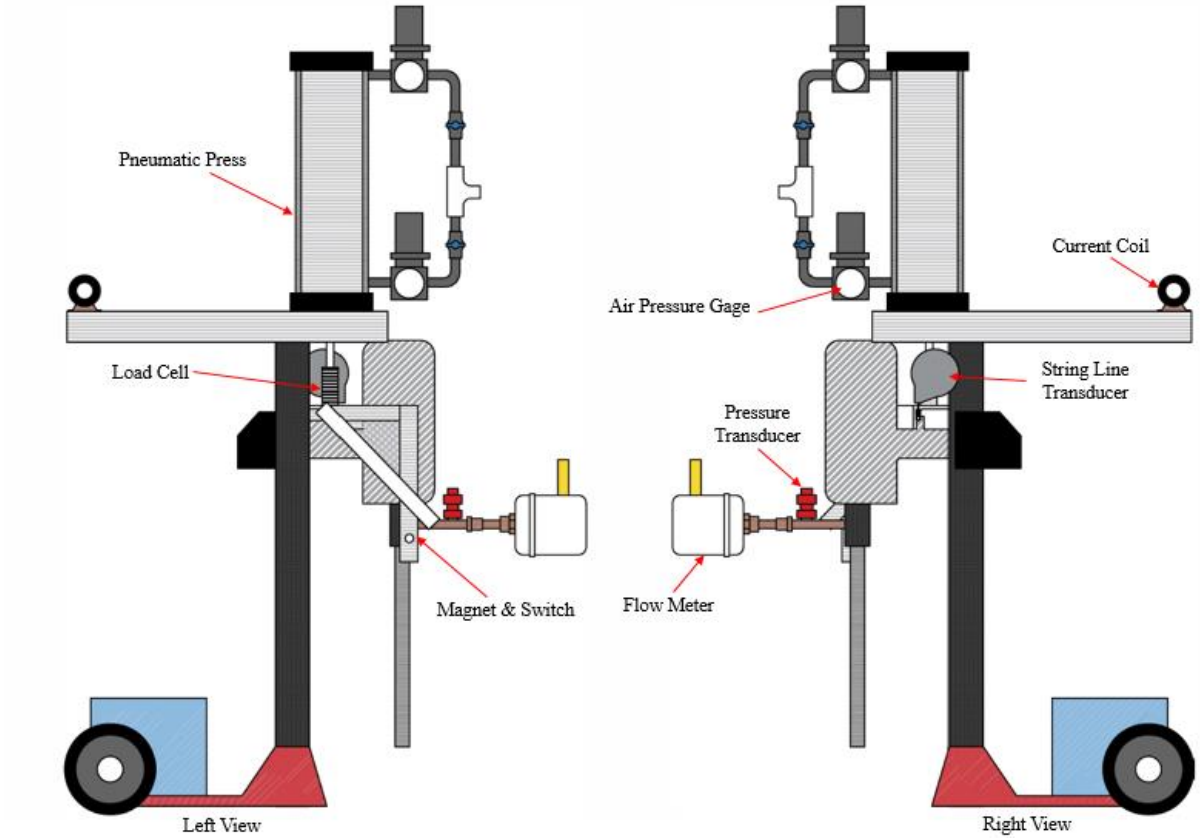

Figure 3.60 Coring machine schematic.

The platform of the machine was a Milwaukee 4049, 20 amp manually-operated coring machine fitted with a 1-inch inner diameter, diamond tip, core barrel. This is a wet core drill that lowers and lifts the core barrel with a linear gear / rack and pinion configuration, wherein turning the crank controls crowd and advances or retracts the drill with a manually-applied, variable force (Figure 3.61).

Figure 3.61 Standard manually operated core drill motor.

Producing usable and replicable data necessitated the isolation of variables that affect coring effectiveness including: force on core barrel, rotational velocity, torque, advancement rate, power consumption, fluid flow and pressure. Mechanically, the linear gear / crank assembly was removed and replaced with a Parker 4MA series, 18in stroke, 4in diameter, double acting, pneumatic cylinder (Figure 3.62). The pneumatic cylinder allowed for complete user control of applied force by using two air pressure regulators that controlled the downward crowd or upward extraction force independently. The exact force applied to the drill motor and core barrel was monitored using an Omega, LCCD-2K, 2000lb capacity load cell (Figure 3.63) connected between the pneumatic cylinder and coring drill motor.

A Celesco PT8101 string-line displacement transducer with a 20-inch range (Figure 3.64) was used to record the depth of coring and by recording the associated time, the vertical advancement rate could also be determined. The rotational velocity (rpm) was measured with a KEP, MRS-12 magnetic proximity switch (Figure 3.65) that was activated every revolution by a magnet attached to the spinning output shaft of the drill motor. As fluid was also used to flush cuttings from the annulus around the core barrel and in turn affects drilling performance, both the fluid flow rate and pressure were monitored with an Omega FMG80A low-flow magnetic flux flowmeter and a Honeywell Model AB/HP 6psi pressure transducer, respectively (Figure 3.66).

Figure 3.62- Pneumatic press

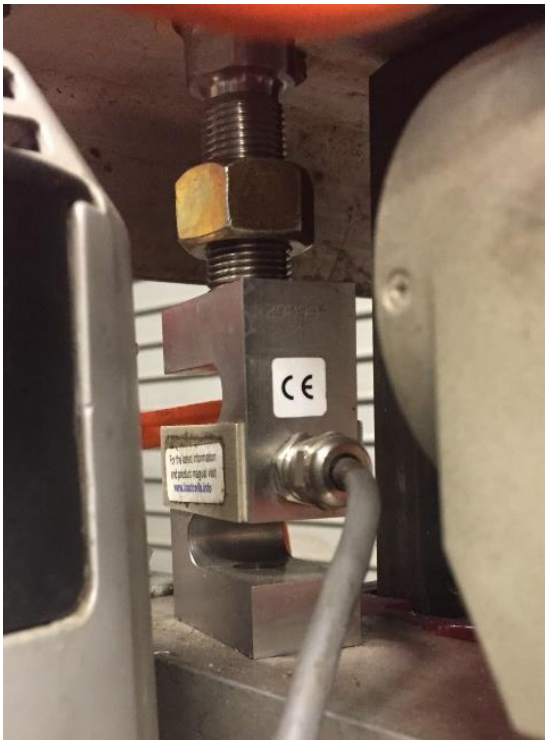

Figure 3.63 Load cell

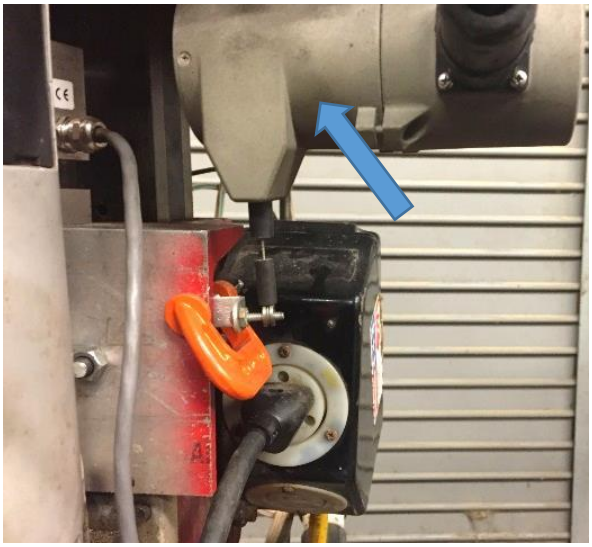

Figure 3.64- String-line transducer

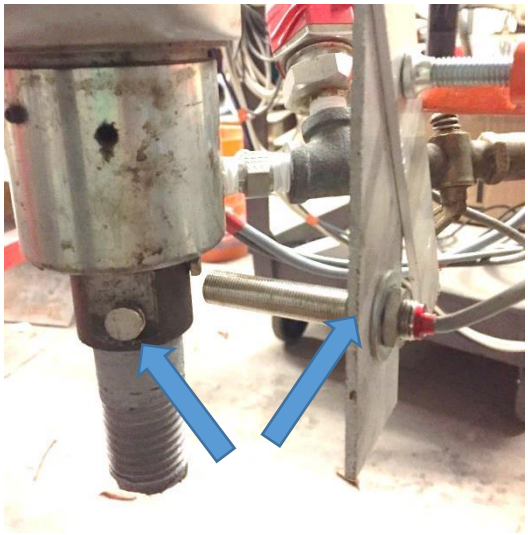

Figure 3.65- Magnet and switch

Similarly important, the torque that resulted from additional crowd and drilling resistance was monitored indirectly by measuring the amperage draw of the drill motor using an Omega, RCT151205A current coil (Figure 3.67) in conjunction with a DRF series AC to DC signal conditioner also from Omega. All data was monitored and recorded using a Model 3108 MEGADAC computerized data acquisition system from Optim Electronics. Data was collected at a 10Hz sampling rate.

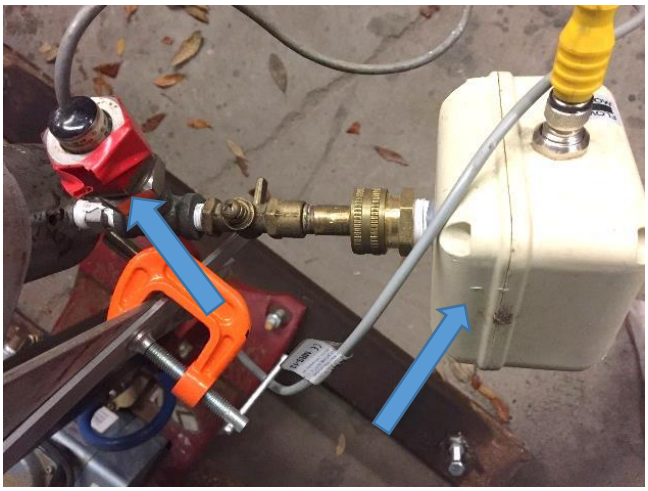

Figure 3.66-Pressure transducer and flow meter

Figure 3.67-Current coil

The result of this instrumentation was a drilling machine with the ability to provide dynamic force, velocity, pressure, current, and rpm data (Figure 3.68). In post-processing, this data could then be used to determine the resistive force and strength of the concrete. This data analysis process is outlined in the results section.

Figure 3.68- Instrumented, pneumatically controlled, core drill

Preliminary verification tests were conducted using the new coring system where each of the transducer outputs was checked.

Force. The upper chamber air pressure regulator was adjusted to a target pressure and the resulting force was compared to that expected for the 12.56in^2 cylinder area. Good agreement was noted. The lower chamber air pressure was also adjusted to provide uplift force that would just overcome the self-weight of the drill motor. The two regulators were never activated simultaneously and purge valves were added to completely negate the internal pressure and force from the inactive chamber.

Rotational velocity. The magnetic switch sensitivity and pulse duration was compared to the observed number of revolutions. This showed disagreement where the measured number of pulses was 3 to 5 times more than expected. A debounce circuit (Figure- 3.69) was then designed and implemented to account for switch closure intermittencies (known as switch bounce) which falsely cause multiple events when only a single switch closure had occurred. The switch closure in the circuit shown produced a pull-down effect on voltage (voltage source shorted to ground) whereas the original circuit that had problems was a voltage pull-up upon switch closure. Data collection was based on a totalizing counter of each switch closure. Rotational velocity was then a computed value using the timestamps associated with each data point.

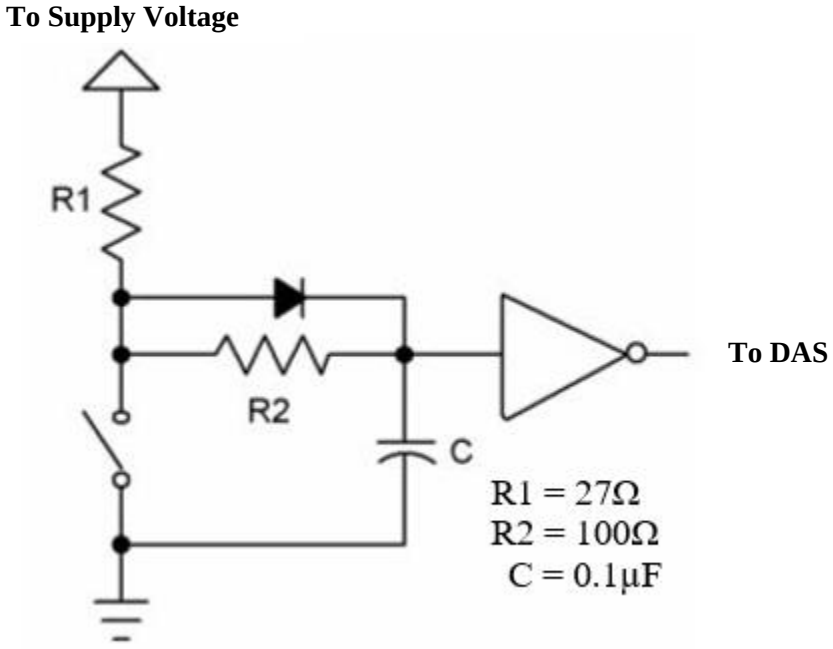

Figure 3.69- Debounce circuit diagram

Current. Voltage and current together are an accurate measure of the instantaneous power required. In this case, the current is also a strong indicator of motor torque, but even when not coring, the running drill motor has a baseline current draw. While the standard drill is equipped with an analog ammeter, the current loop chosen to automatically monitor the current was checked with two in-line ammeters for verification. Recorded values from the current loop were consistently low although linearly related to actual current draw. The system was then calibrated

to reflect the difference, but upon further discussions with the manufacturer, the current loop operates best when at least three wraps of one conductor pass through the coil which was not noted in the installation guide. Figure 3.45 shows only one pass going through the loop.

Displacement. While somewhat trivial compared to the other transducers, the string line transducer was confirmed to register the full 18in stroke of the pneumatic cylinder. Like rotational velocity, the advancement rate was then computed using the timestamps associated with each data point.

Pressure. Pressure of the drilling fluid, if appreciable, could reduce the net force on the cutting edge of the core barrel. However, the anticipated pressure range was small and the 6psi transducer range made simple calibration checks possible by using a simple column of water and comparing the hydrostatic pressure with that registered. Good agreement was noted.

Flow rate. Computationally, flow rate has no influence on the predicted concrete strength but can affect drilling effectiveness. If too slow, cuttings become trapped in the annular space around the core barrel and can cause an increase in torque from binding. If too fast, needless washing/scouring of the core sample can result. Flow rate was set to always show unaltered return flow and the transducer was simply tested by measuring the time required to fill a container of known volume. Good agreement was noted.

The process of coring was standardized to provide baseline measurements of crowd, flow, displacement, rpm, current and flow rate prior to making contact with the concrete surface. The core rig was equipped with a vacuum activated base plate but given the presence of rebar, a steel beam was secured to the rebar and the base plate was adjusted until level and coring was performed from a vertical/plumb orientation (Figure 3.70).

Figure 3.70- In position, prior to coring with 14in starter core barrel.

Steps used to perform the coring were as follows:

1. Initiate data acquisition
2. turn on the water
3. start the drill motor
4. de-activate uplift pressure regulator by closing air source and venting internal pressure on lower cylinder chamber

5. activate downward/crowd pressure regulator (to preset force) by opening air source to upper cylinder chamber that pushes down (Figure 3.71).
6. terminate first stage of coring when displacement reached 14in by de-activating downward pushing chamber
7. disconnect core barrel from drill motor (while core still in-hole)
8. activate uplift chamber and raise drill motor until 12in core barrel extension could be added.
9. Repeat steps 3 – 5 until core barrel penetrates bottom of sample.
10. Terminate data collection
11. Disconnect core barrel (and extension) from drill motor
12. Activate uplift chamber
13. Remove entire drill system to allow the full 24in core barrel to be removed with sample inside.
14. Carefully, disconnect core barrel from extension and remove core sample taking care to maintain orientation and order if sample is in multiple pieces.

Figure 3.71-Coring inside (left); outside cage (rt), both show coring after extension was added.

Figure 3.72 shows the core samples retrieved from shafts 6, 9 and 11. These three shafts were chosen for initial coring because they represent all three examined slurry types and were all cast from the same batch of concrete. Four cores were taken from each shaft: two inside the reinforcement cage and two outside of the reinforcement cage in the cover region. The collected cores were cataloged and then cut into sections for compression testing (Figure 3.73). An example core log overview and single core log are shown in Figures 3.74 and 3.75. Logs for all coring completed to date can be found in Appendix D.

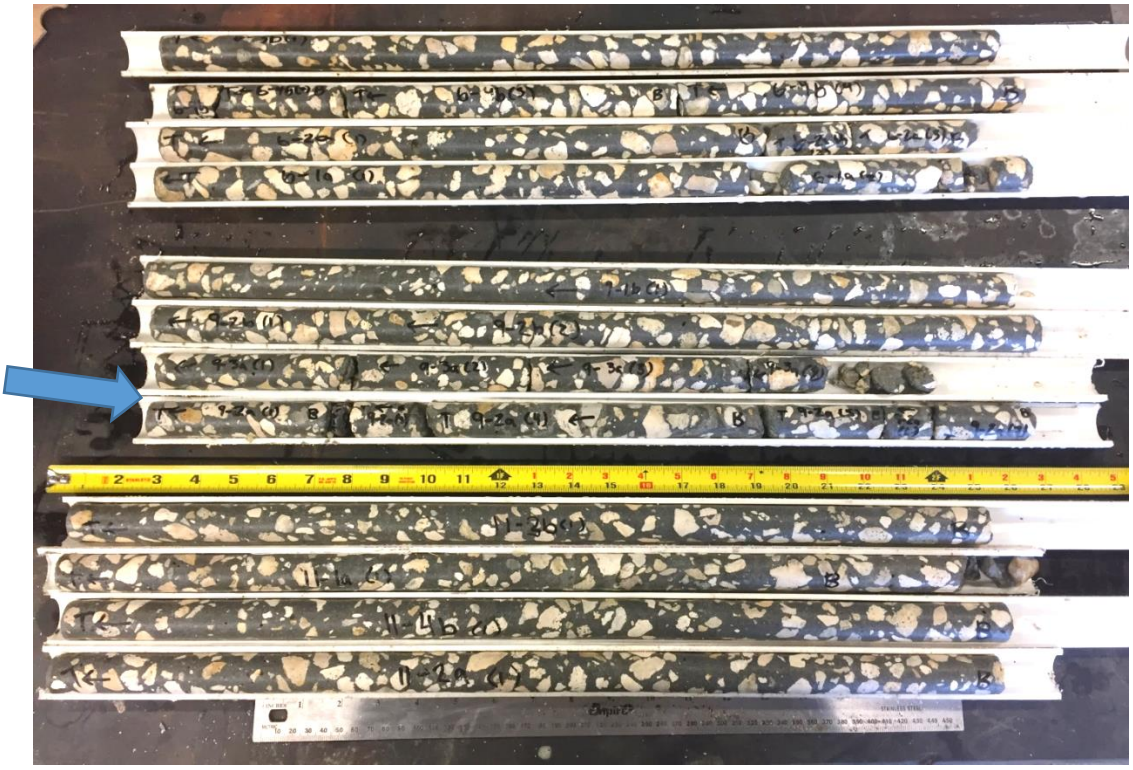

Figure 3.72 Core samples from shaft 11 (polymer), shaft 9 (bentonite), and shaft 6 (water)- (top to bottom).

The shaft 9 cores taken in the cover region were removed from the core barrel in 4 inch to 6 inch segments (the two cores indicated by the blue arrow in Figure 3.72. The spacing of the breaks in the core closely aligned with the spacing of the horizontal reinforcement creases. This could serve as further confirmation of the cover discontinuity introduced through laitance channel formation.

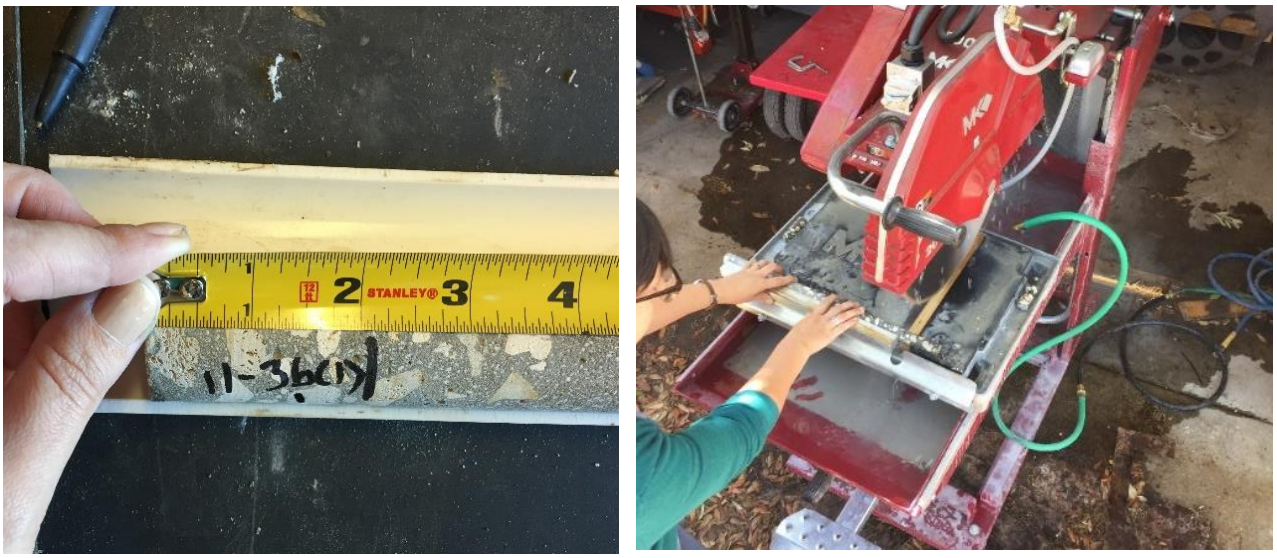

Figure 3.73 Core measuring, labeling and cutting.

Shaft 9	
Slurry	Bentonite
Viscosity	50 sec
Concrete Mix	Type IV
Concrete Compressive Strength	4530 psi

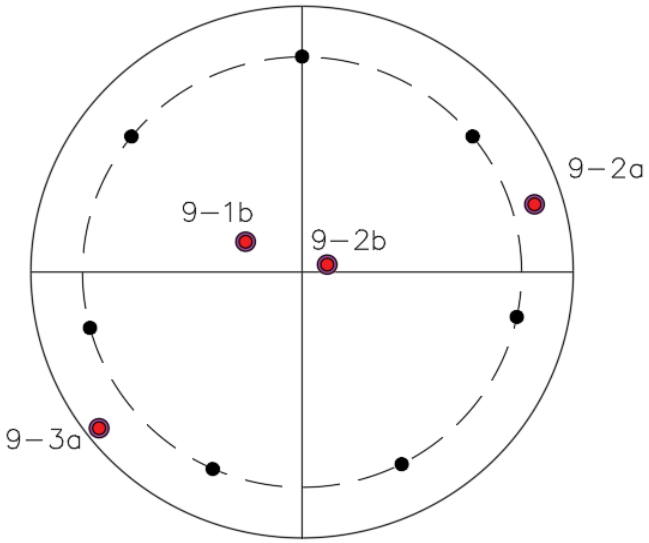

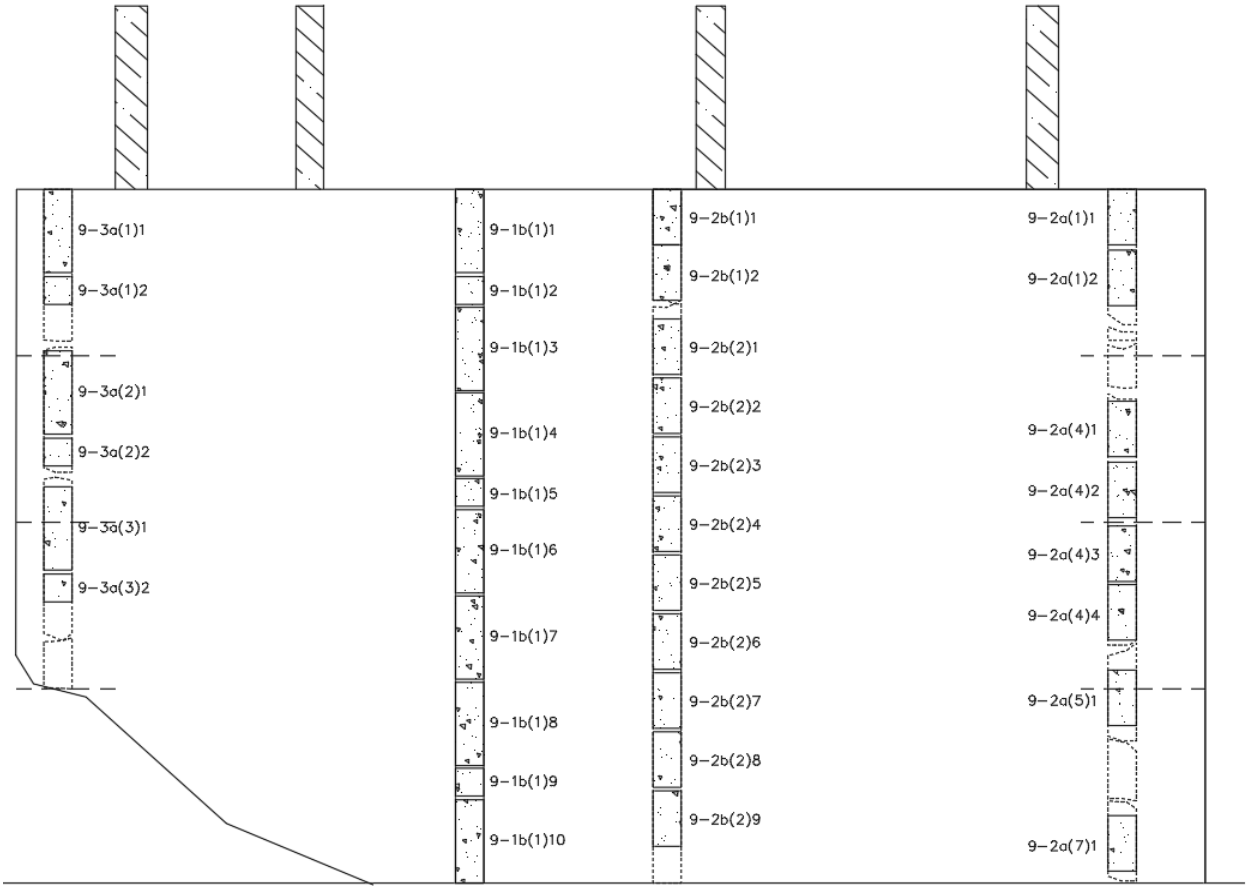

Figure 3.74 Shaft 9 coring overview

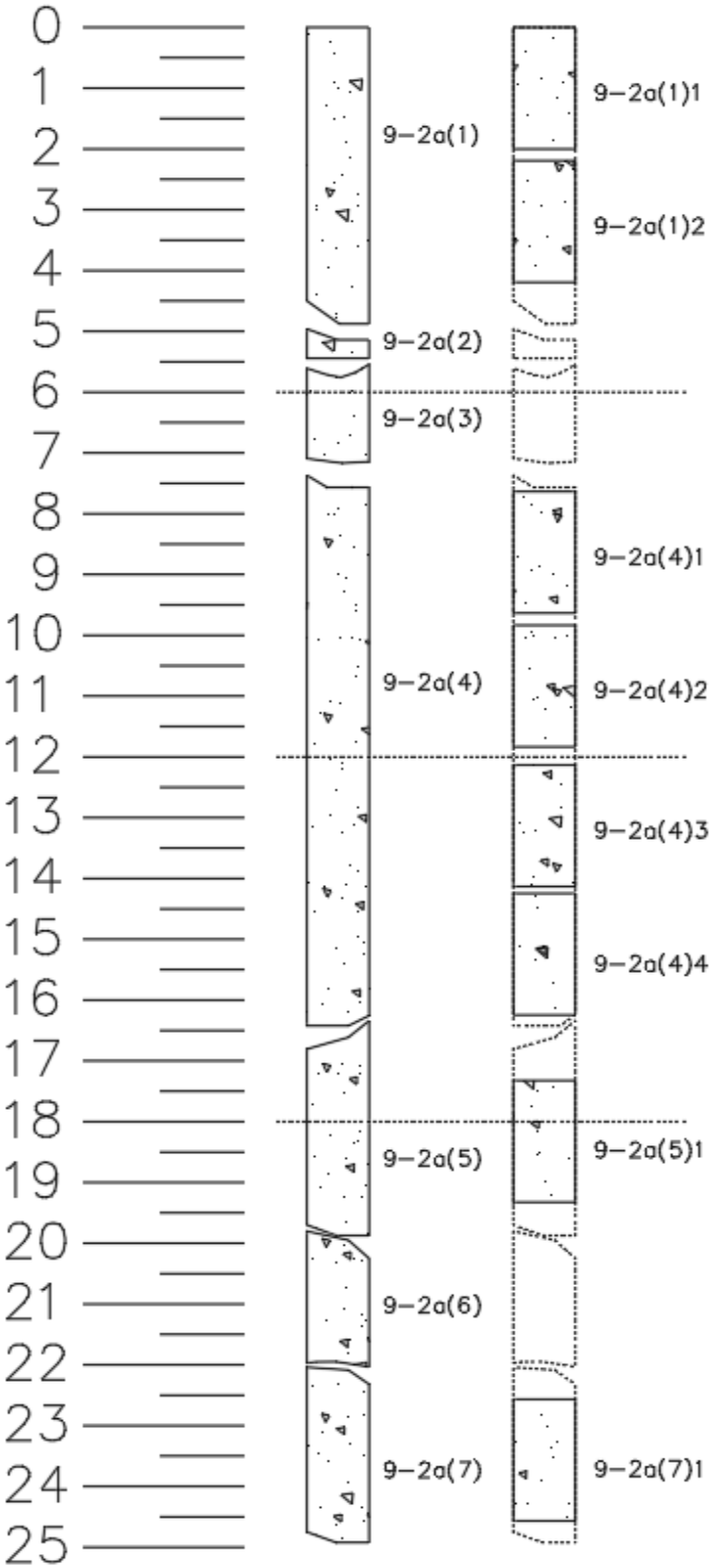

Figure 3.75 9-2a core log

Results

After trimming any data taken while the machine was not actively drilling, the current, displacement and flow were all plotted against time (Figures 3.76, 3.77 and 3.78). The complete set of graphs can be found in Appendix E. The gap in the data between 300 and 400 seconds represents the time taken to attach the core barrel extension.

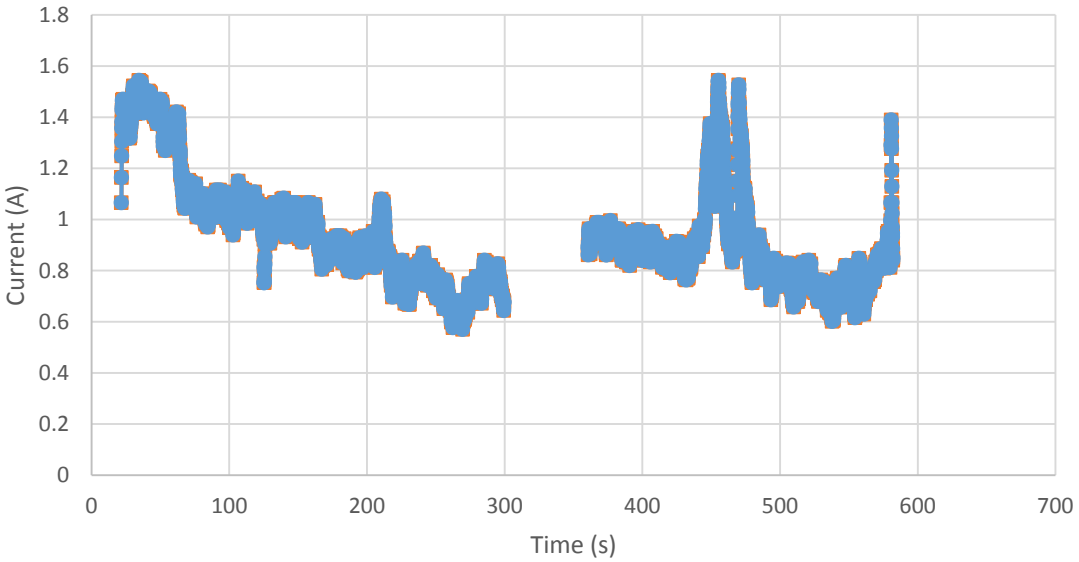

Figure 3.76 Core 6-1a, plot of current vs time

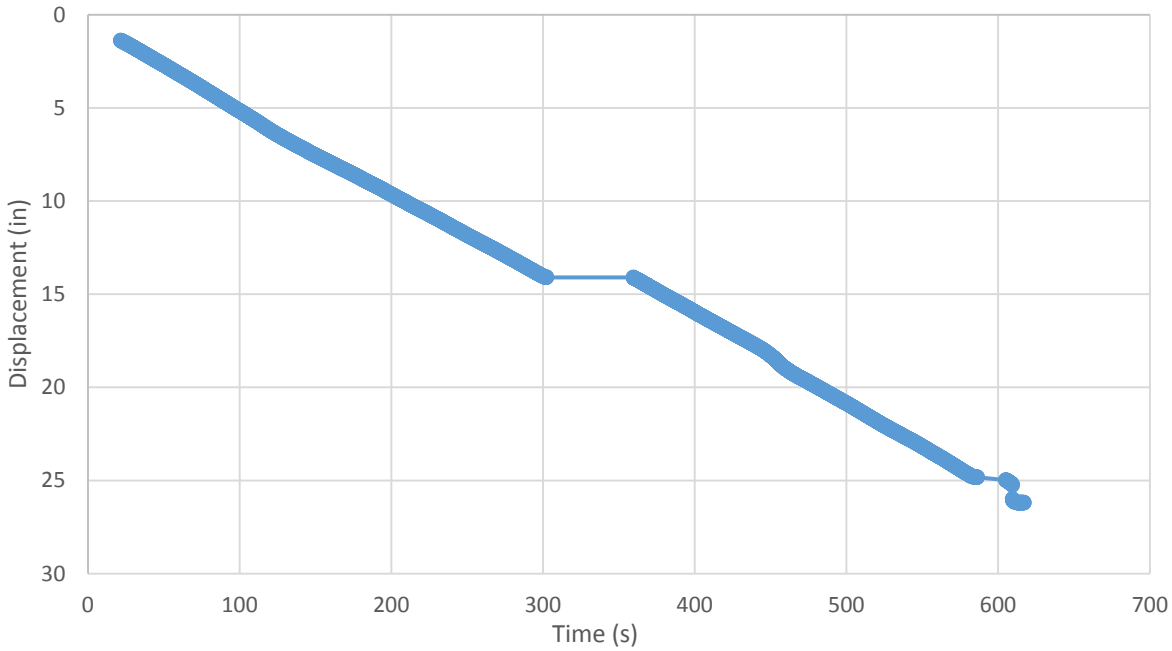

Figure 3.77 Core 6-1a, plot of displacement vs time

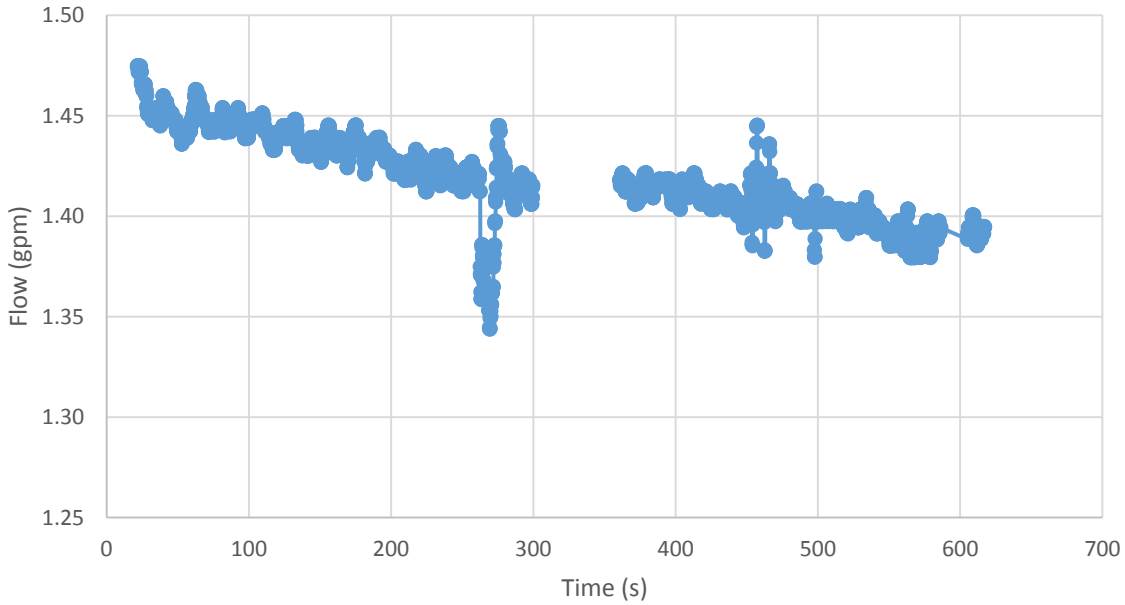

Figure 3.78 Core 6-1a, plot of flow vs time

The goal of the core drill instrumentation was to eliminate variables in two torque equations: mechanical and electrical. Electrical torque (not physical torque) or Power can be calculated through use of Kirchoff's laws:

$$P = IV$$

Wherein: P = Power
I= Current (A)
V = Voltage (V)

This result is made equate-able to mechanical torque and the resistive force of the concrete is thusly calculated by dividing the torque by the rate of advancement:

$$\tau_m / v = F$$

Wherein: τ_m = Electrical torque at unit of power (lb-in/sec)
F= Force (lbs)
v = Velocity (in/sec)

This resistive force is then converted to pounds per square inch through application of the drilling surface area and normalized to the expected concrete strength based of compression testing results. The force was then averaged per inch and graphed against depth (Figures 3.79, 3.80 and 3.81). To date this analysis has been completed for twelve cores. Those cores were taken from shafts 6, 9 and 11. Data for all 24 existing shafts and any future shafts will be included in future reports. For each figure, any sample with an 'a' suffix is a core taken outside the reinforcement cage (cover region), and any ending in 'b' is a core taken inside the reinforcement cage (interior concrete).

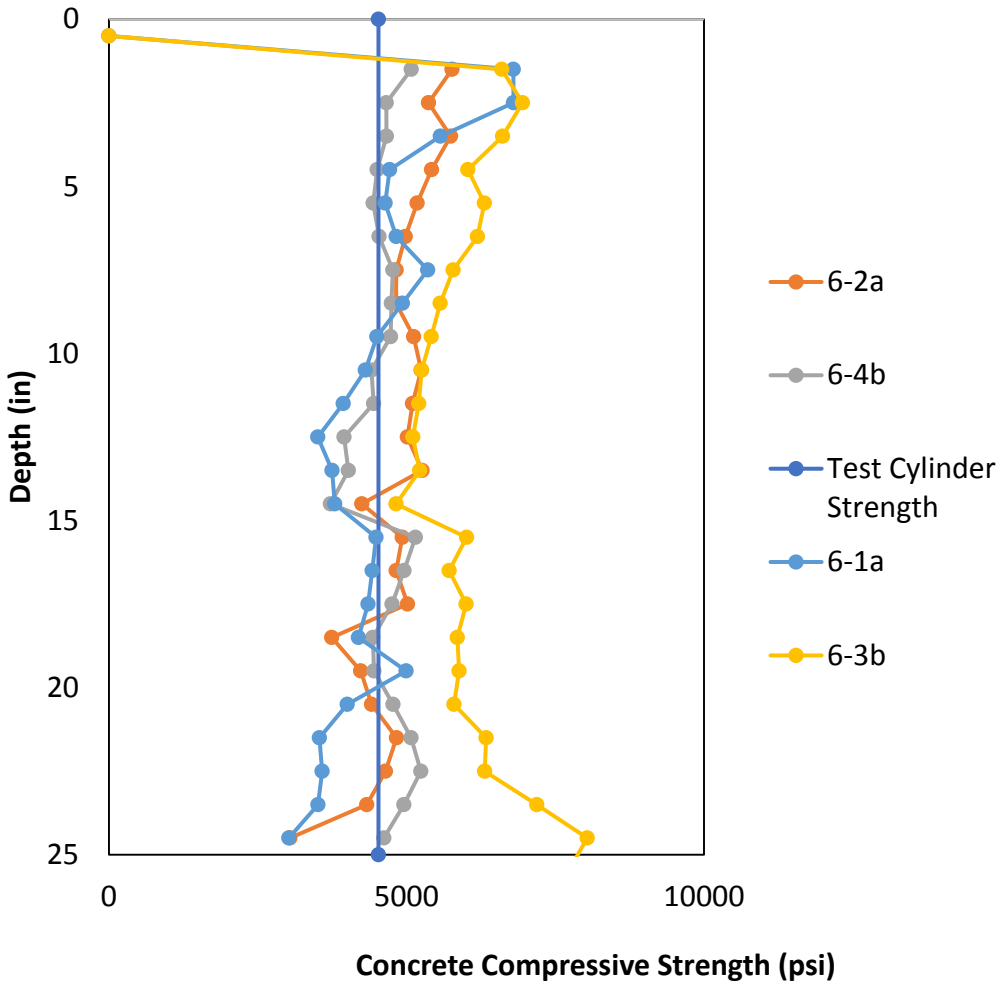

Figure 3.79 Shaft 6 core strength profiles

Shaft 6 (Figure 3.79) demonstrates a generally uniform profile between samples. Shaft six was cast in water and as such is being used as a control. A drilling effective constant was established using this sample and was used consistently for all remaining analyses. This constant was calculated using a ratio of calculated concrete strength to compressive strength tested at the time of construction. This value was used to normalize all data for comparative purposes. By design, the shaft 6 data averages on or near the compressive strength line. The close grouping of the data shows consistency in the concrete strength profile that is expected in the control samples.

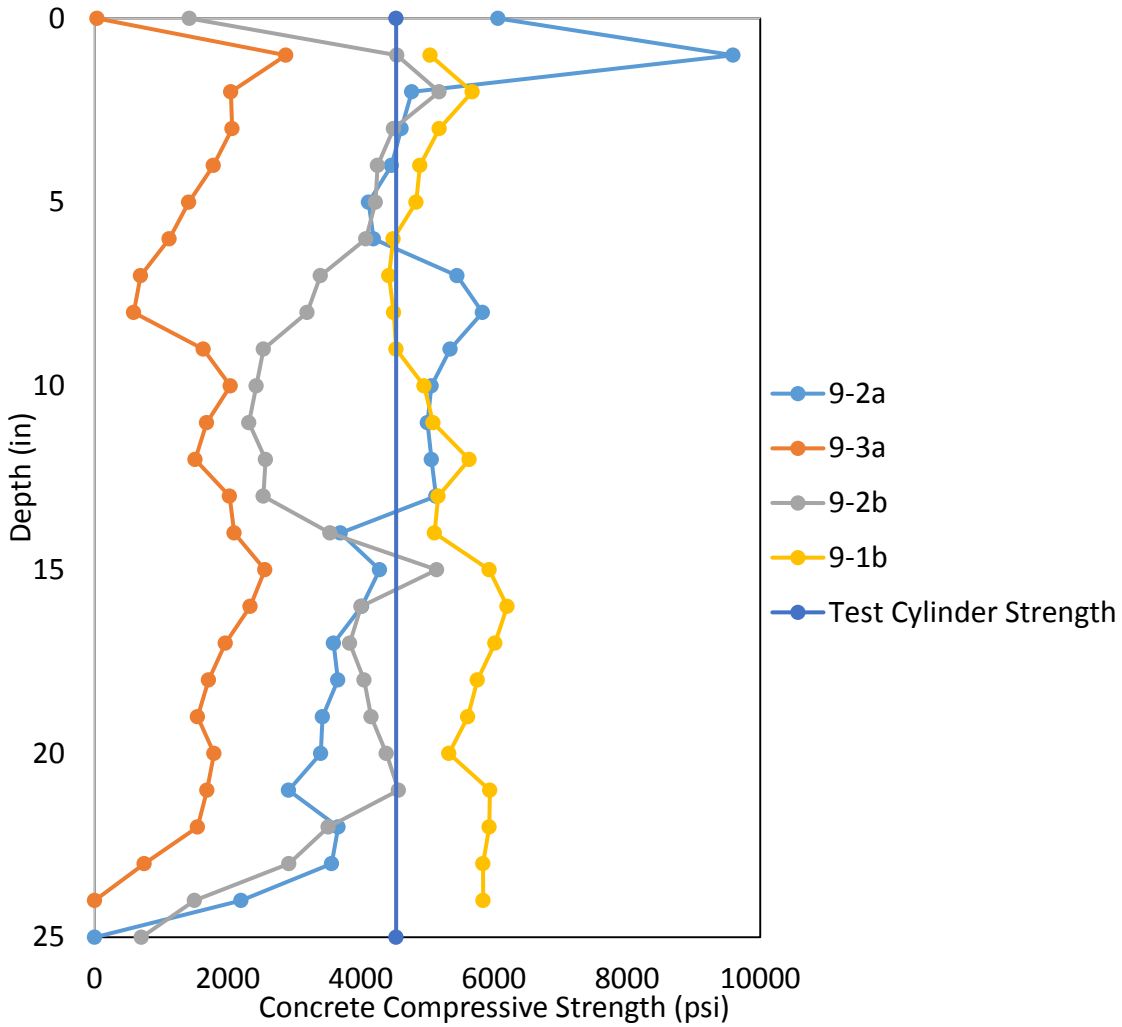

Figure 3.80 Shaft 9 core profiles

Shaft 9 (bentonite, Figure 3.80) shows four strength profiles with values that spread from 1000psi to 6000psi. While more samples need to be cored to corroborate the noted trends, the conclusion currently drawn is that bentonite does not yield a uniform strength profile. Additionally in three of the four cores the strength drops of significantly in the last four inches of the shaft. This trend could be attributed to localized deterioration and could be visually verified.

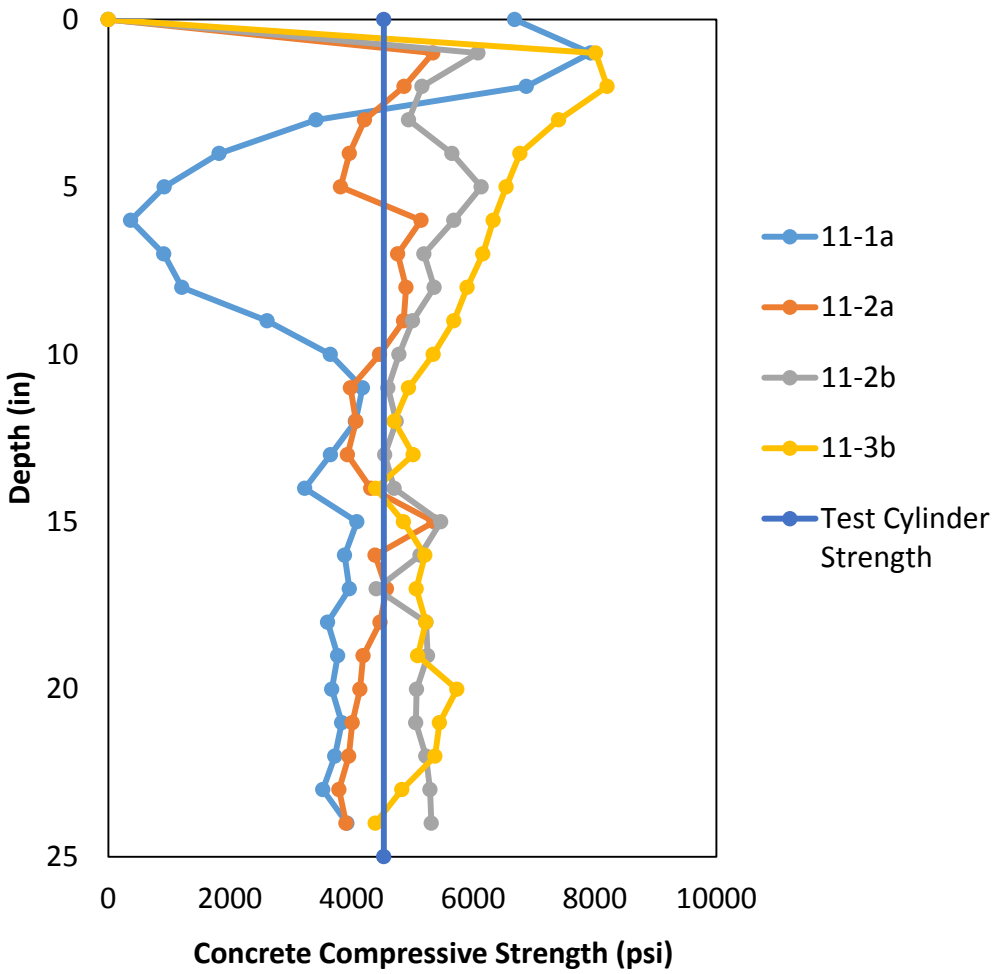

Figure 3.81 Shaft 11 core profiles

Shaft 11 (polymer, Figure 3.80) shows a similar trend, however a dip in strength is demonstrated on the first half of sample 11-1a. This is potentially a technical error caused by assuming voltage remains relatively constant (120VAC) with minor variations computed from known losses (i.e. wire length, size and current), it will have to be investigated further. In this case, only a voltage surge/increase could have caused the effect. Regardless, this uncertainty will be removed by adding a supply voltage monitoring sensor. From a depth of 12 inches to the bottom of the shaft, the cores show a behavior similar to the water cast control shaft. This is consistent with previous results from other testing procedures.

Core samples are currently being tested as a means to correlate compressive strength to the profiles calculated using the core drill data. Two core samples from each shaft were cut into 2in sections for testing (Figure 3.82). Custom compression testing caps and pads were constructed and then the samples were crushed at a loading rate of 30psi/sec (50lb/s) using force controlled loading with a 220 kip capacity MTS machine (Figure 3.83). The unconfined compressive strength was collected and then converted to pound per square inch using the cross sectional area of the cores.

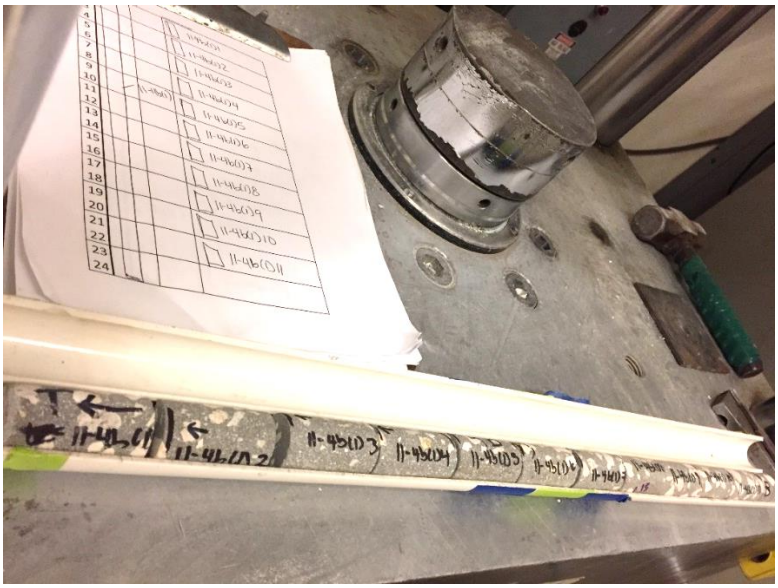

Figure 3.82-Core samples cut to 2:1 length to diameter ratio for compression testing.

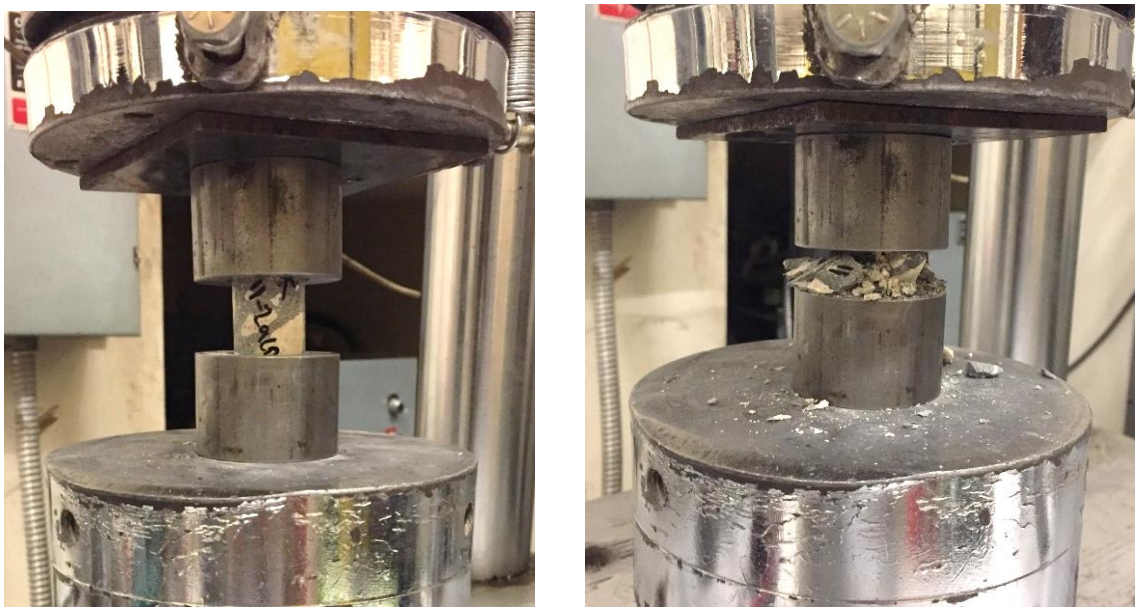

Figure 3.83 Core sample undergoing compressive strength testing

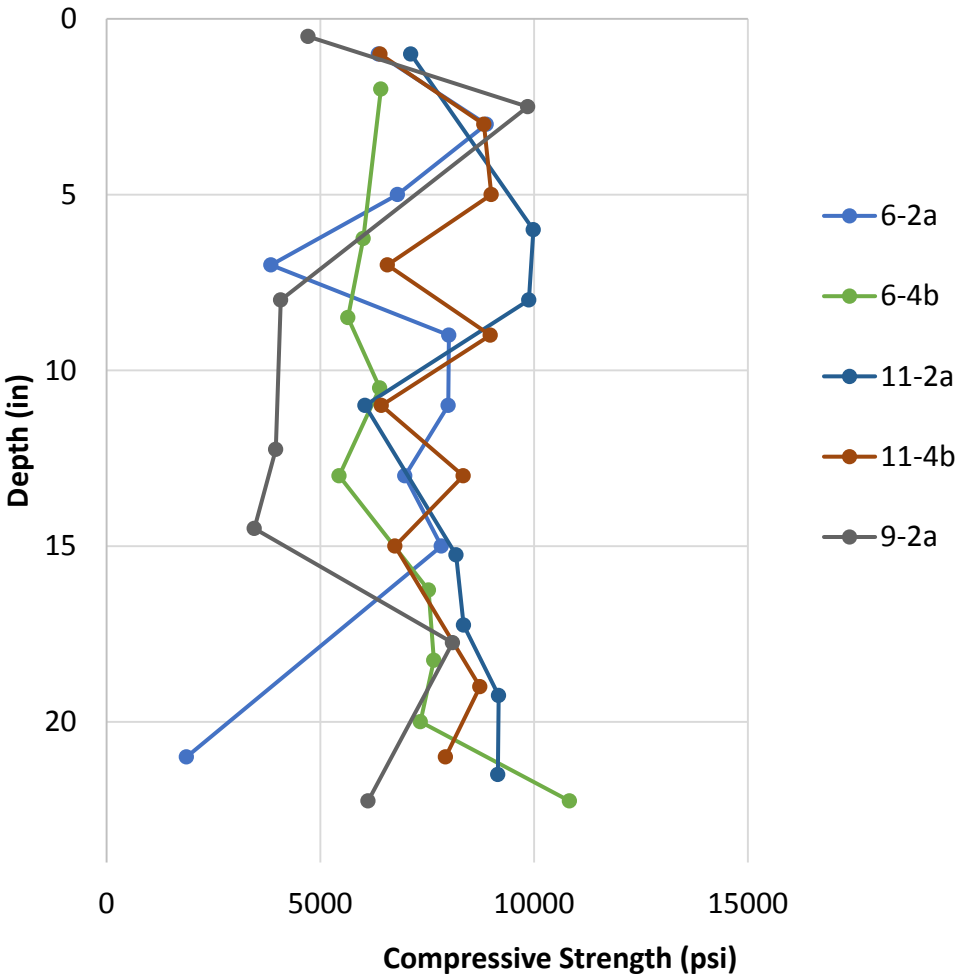

Figure 3.84 Core sample compressive strength profiles

The compressive strength data was plotted as a function of depth for each core (Figure 3.84). A correlation between the compressive strength profiles and core drill profiles is currently in progress but further testing is required. As soon as this correlation is refined, the core compressive strength data will be used to normalize the drill data as opposed to using the compressive strength determined during construction. Recall, the present calibration constant for the concrete penetrometer is based on 4yr old strength tests.

3.4 Chapter Summary

The Task 2a efforts focused on defining correlations between surface condition (observable) and the actual state of health of the reinforcing steel. The testing performed was both qualitative and quantitative. Table 3.8 summarizes the results of visual observations, physical and digital surface void volume measurements and the differences in electrochemical surface potential.

Table 3.8 Summary of shaft specimens and conditions

Shaft ID	f'c (psi) mix	Age (yrs)	Slurry	Roughness	Viscosity (sec/qt)	Crease/ Channel	Surface Volume		E_{50} (mV)
							Physical (in^3)	Digital (in^3)	
1	6150-DS	4	Bentonite	Rough	44	Well-Defined Creases	592		-317
2	6150-DS	4	Bentonite	Coarse	105	Well-Defined Creases	492		-449
3	4358-DS	4	Bentonite	Coarse	40	Well-Defined Creases	203		-373
4	4358-DS	4	Bentonite	Coarse	55	Well-Defined Creases	313		-443
5	4358-DC	4	Bentonite	Coarse	90	Well-Defined Creases	254		-447
6	4358-DC	4	Water	Smooth	26	Faint Channeling	42	54	-155
7	4350-DS	4	Bentonite	Rough	30	Faint Creases	487		-373
8	4350-DS	4	Bentonite	Coarse	40	Faint Creases	215		-225
9	4350-DS	4	Bentonite	Rough	50	Well-Defined Creases	260	302	-383
10	4530-DS	4	Bentonite	Coarse	90	Faint Creases	540		n/a
11	4530-DS	4	Polymer	Smooth	65	No Creases	71	81	-285
12	4530-DS	4	Polymer	Coarse	66	No Creases	59		-190
13	4753-DS	4	Bentonite	Coarse	30	Faint to No Creases	169		-289
14	4753-DS	4	Bentonite	Coarse	30	No Creases	299		-282
15	4753-DS	4	Bentonite	Coarse	56	Well-Defined	263		-335

						Vertical Creases			
16	4753-DS	4	Polymer	Smooth	85	Faint to No Creases	73		-279
17	4753-DS	4	Polymer	Smooth	85	Faint Creases	38		-300
18	4753-DS	4	Water	Smooth	26	Faint Channeling	47		-293
19	4100-DS	2	Polymer	Smooth	63	No Creases	43		-243
20	4100-DS	2	Polymer	Smooth	121	Faint Creases	33		-242
21	4100-DS	2	Bentonite	Rough	42	Well-Defined Creases	578		-508
22	4100-DS	2	Water	Smooth	26	Faint Channeling	30		-250
23	SCC	2	Water	Smooth	26	Faint Channeling	48		-258
24	SCC	2	Bentonite	Rough-Disintegrating	40	Creases coincide with deteriorated regions	N/A		-425

The ability or inability of drilled shaft concrete to freely flow into the annular cover region and maintain the desired concrete properties can have the most dire effects on durability / longevity of the structural integrity. While SCC alternatives are sought to enhance concrete cover performance, means and methods of assessing an as-built shaft must be identified.

Durability describes the ability of a material to resist wear and decay. One way to quantify durability in concrete in drilled shafts is to assess the quality of protection that the concrete is providing to the encased reinforcement. Certain materials used to stabilize the excavation during drilled shaft construction have been shown to cause a surface anomaly known as quilting (Figure 3.29). Quilting can create direct pathways for the transmission of environmental chlorides into the network of reinforcing steel, negating the protective qualities of the concrete cover. Final quantification of durability is achieved by correlating the stabilization material used with the corrosion potential of the encased steel.

Quilting is a phenomenon associated with concrete flow, but it is most readily quantified at the surface of the shaft. Through determining the volume of voids in the shaft surface, it is possible to ascertain the severity of the quilting or surface deterioration. The void volume was determined two ways: physically and digitally both of which were detailed previously. The digital void volume is being used to provide validation for the physical void volume technique. Though more accurate, the digital scanning equipment is costly the training required to operate it makes that system unreasonable for widespread field use. As shown in previous sections, the results from

both tests follow a linear relationship, so far validating the physical testing system. Further, most shafts are not exposed, in a state that can be assessed except for those exposed supporting over-water bridges. In these cases, the structured light system is not possible, but laser-based systems are well-suited for such environments. The knowledge obtained via the Task 2a efforts will serve as a basis for evaluation methods using other technologies.

Graphing the surface void volume against the slurry viscosity (Figure 3.85) reveals that polymer cast shafts have a low surface void volume across the full range of viscosity, in the same range as the water cast shafts. It also becomes apparent that bentonite shafts are overall more prone to high surface void volume and that this high volume is independent of slurry viscosity. Therefore, there is no safe threshold below which bentonite cast shafts were found to be unaffected.

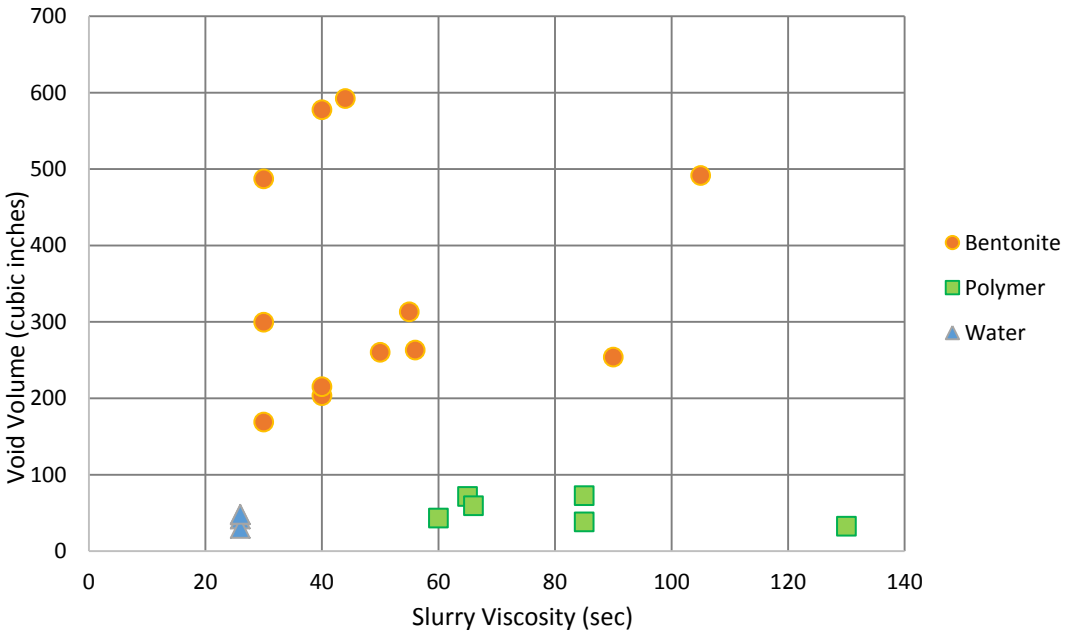

Figure 3.85 Slurry viscosity vs void volume plot

Corrosion potential data was collected using electro-chemical testing methods. A copper-copper sulfate reference electrode was used to collect potential difference data on an eighty-point grid in order to map changes in potential across a portion of the surface. The corrosion potential surface mapping data was analyzed for each specimen individually. Statistical methods were used to plot a distribution curve and determine the 50th percentile corrosion potential (E_{50}) for every shaft. The E_{50} values vs slurry viscosity are shown in Figure 3.86.

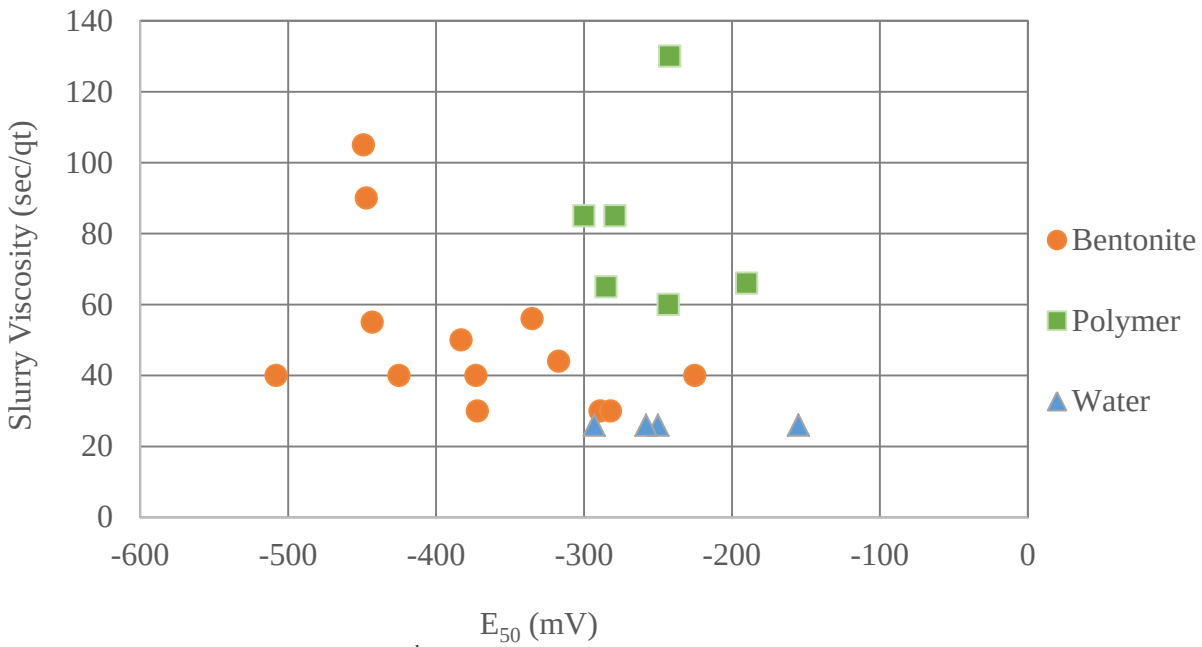

Figure 3.86 Slurry viscosity vs 50th percentile corrosion potential for Class IV shaft specimens.

ASTM C876 states that a potential reading below -350mV indicates a 90% chance of corrosion so it is generally used as the threshold for corrosion activity. When the 50th percentile corrosion potential is plotted against the slurry viscosity distinct divisions become apparent (Figure 3.86); seven of the 13 shafts cast with bentonite slurry fell below the -350mV threshold. Polymer shafts did not show indications of corrosion. This is a clear indicator that shafts cast using bentonite slurry are more prone to corrosion than shafts casts using the subject polymer. Recall that the surface potential measurements were taken with a freshwater wetted surface and where no chlorides had been introduced. It is likely that in the presence of chlorides more of the shafts would have crossed the -350mV threshold.

Core samples were taken from three of the 24 shafts using an instrumented, pneumatically controlled core drill coined as a concrete penetrometer. The preliminary results show a consistent strength profile in the water cast shaft, a non-uniform profile in the bentonite cast shaft, and a profile that was irregular in the top 12 inches and then consistent in the bottom 12 inches in the polymer cast shaft. When considering the initial segregation of shaft concrete as it leaves the tremie, these were unusual findings. The variations in these profiles could be loosely attributed to concrete properties but this early in the process, the data is still being refined and further testing is required to produce results with quantitative weight. That being said, when the coring data is plotted with the compressive strength data some similarities become apparent that shed light on future refinements of the system.

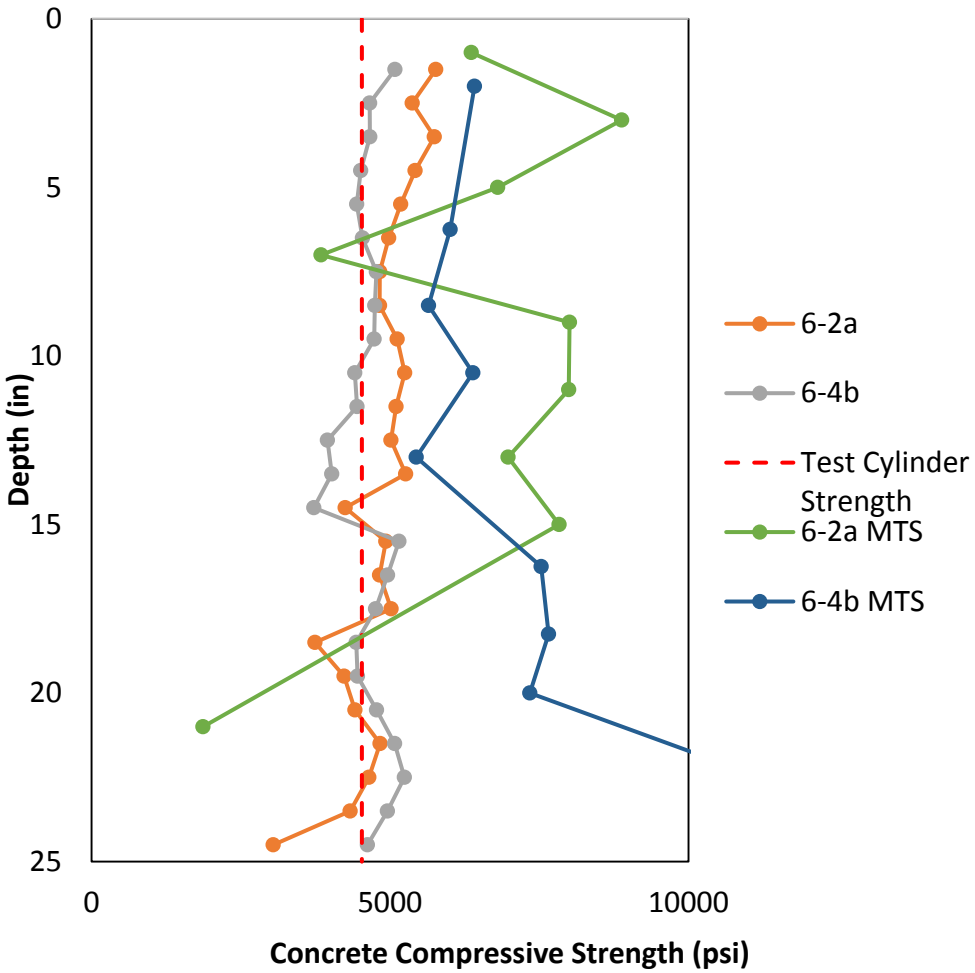

Figure 3.87 Shaft 6 Coring machine and MTS compressive strength profiles

Shaft 6 was used as the control for this data analysis because it was cast in water and showed little to no signs of cage effects. That means that all coring data was normalized to match the compressive strength of the concrete at the time of construction. This was the seven-day compressive strength taken four years ago so theoretically it is only 70% of the final compressive strength. If the data had been normalized to a 100% projected compressive strength then the drilling profile would more closely align with the core compressive strength profile shown in Figure 3.87. Further testing is required to establish a true baseline compressive strength for each shaft at which time the data for all cores will be refined and properly normalized. Graphs showing the core strength along with the calculated drilling strength for shafts 9 and 11 can be seen in Figures 3.88 and 3.89. However, as some variation is noted within each shaft, the true strength will require multiple samples. In newly constructed samples (Task 3 and 4), concrete cylinders will be available for comparison on the exact day of coring.

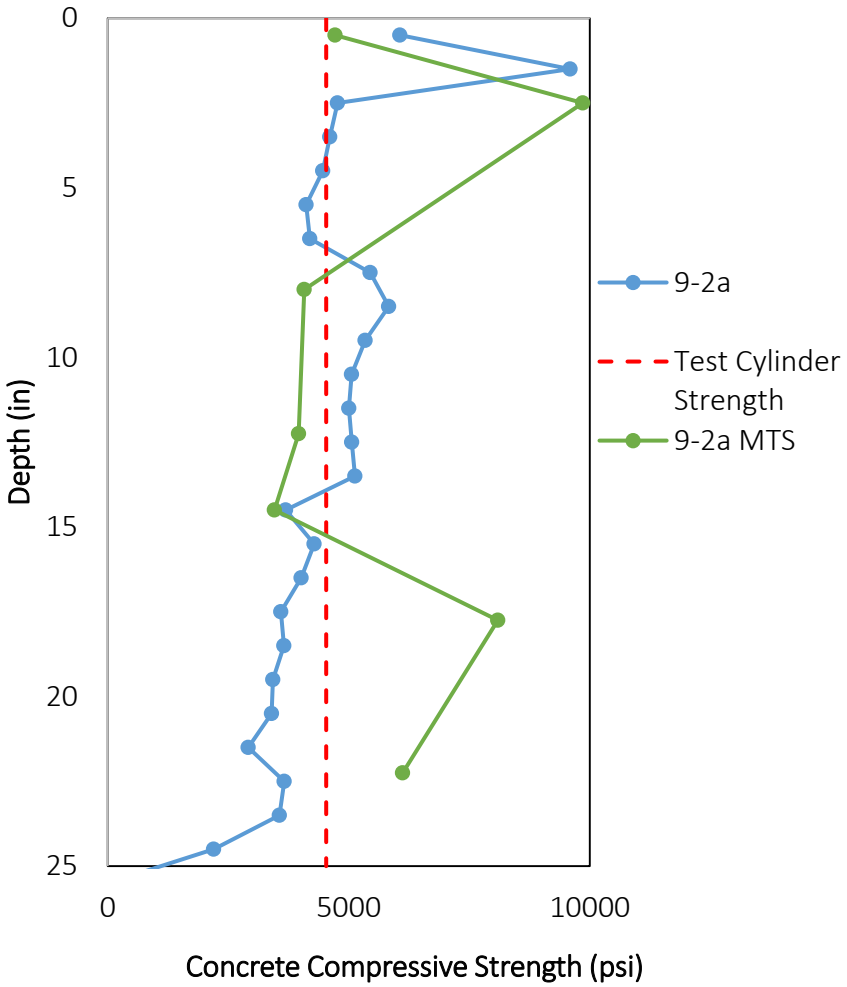

Figure 3.88 Shaft 9 Coring machine and MTS compressive strength profiles

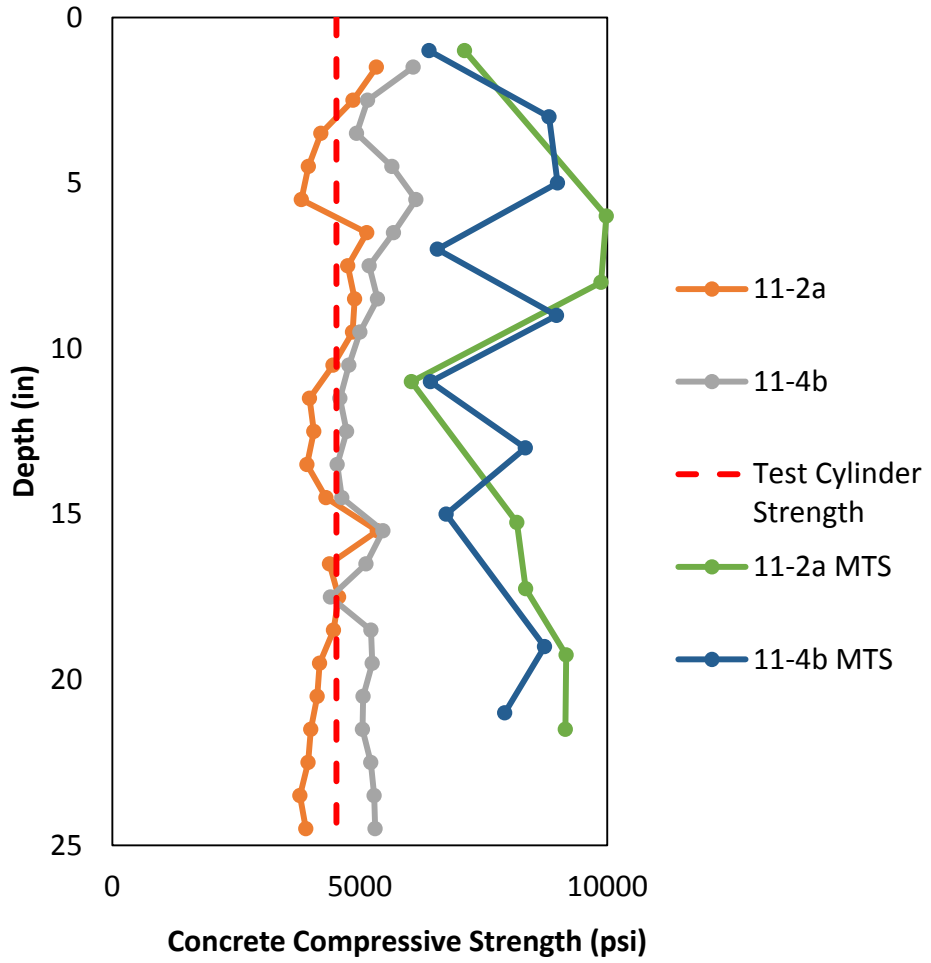

Figure 3.89 Shaft 11 Coring machine and MTS compressive strength profiles.

Conclusions

- 100% of tests shafts constructed using bentonite slurry had a surface void volume greater than 100 in^3, whereas 0% of test shafts cast using polymer slurry or water crossed the 100 in^3 threshold. Both sets of results were independent of slurry viscosity.

- When the 50^{th} percentile corrosion potential is plotted against the slurry viscosity distinct divisions become apparent. Seven of the 13 shafts cast with bentonite slurry fall below the -350mV line in a freshwater environment where none of the shafts cast with polymer do. This is a clear indicator that shafts cast using bentonite slurry are more prone to corrosion than shafts casts using the subject polymer.

- Coring test data shows distinct differences in concrete strength patterns for each slurry type. Further testing and data analysis refinement is necessary to confirm those trends.

3.5 Future and On-going Work

Close coordination with District VII maintenance engineers has provided construction, maintenance, and inspection records for over-water bridges along the west coast of Florida. Focusing on more-local bridges, the Gandy Bridge (westbound) inspection records were scrutinized for shafts with possible problems. This preliminary screening has been used to prioritize and schedule on-site visits and underwater inspections. Figure 3.90 shows the existing condition of one shaft before and after cleaning.

Figure 3.90 As-found and cleaned surface of shafts from Pier 95.

Figures 3.91 and 3.92 show close-up images of the concrete surface on the exterior side exposed to tidal flow and the interior side somewhat protected from tidal flow. After cleaning the crease noted in Figure 3.90 (top-right) revealed a 2-3in deep recess, but the entire exterior face was noticeably rougher.

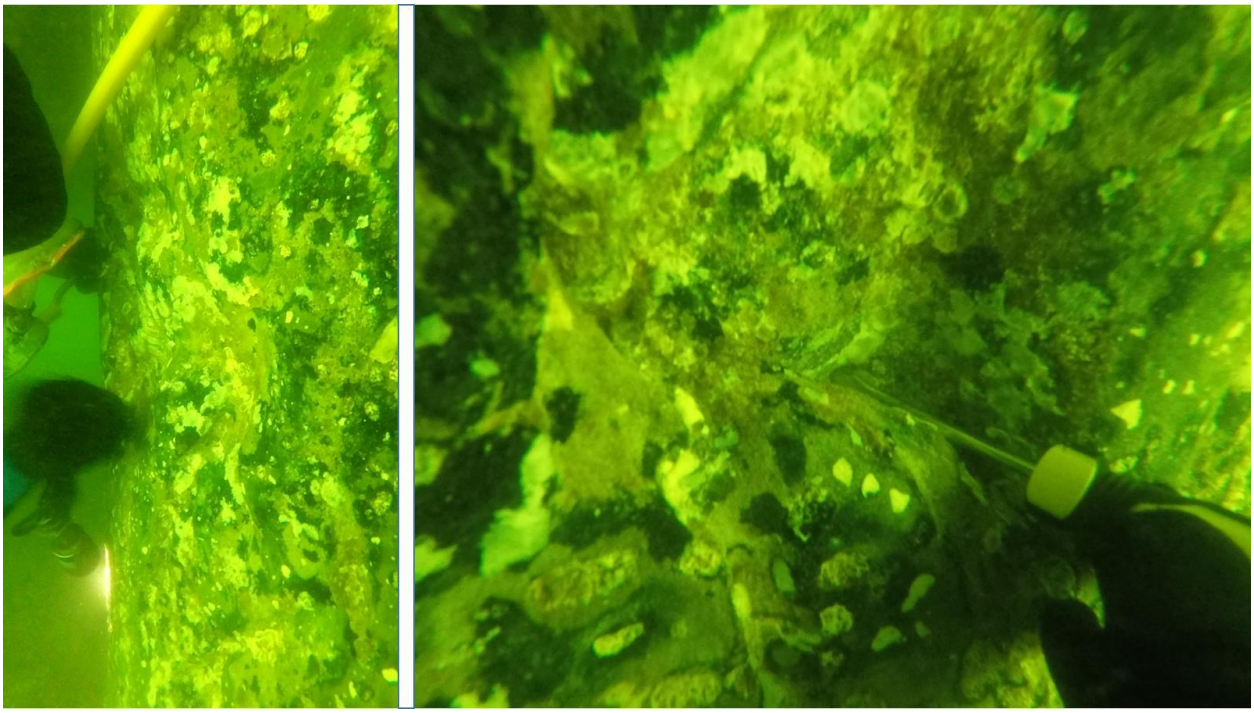

Figure 3.91 Visibly rough/voided side of shaft (unprotected from tidal flow).

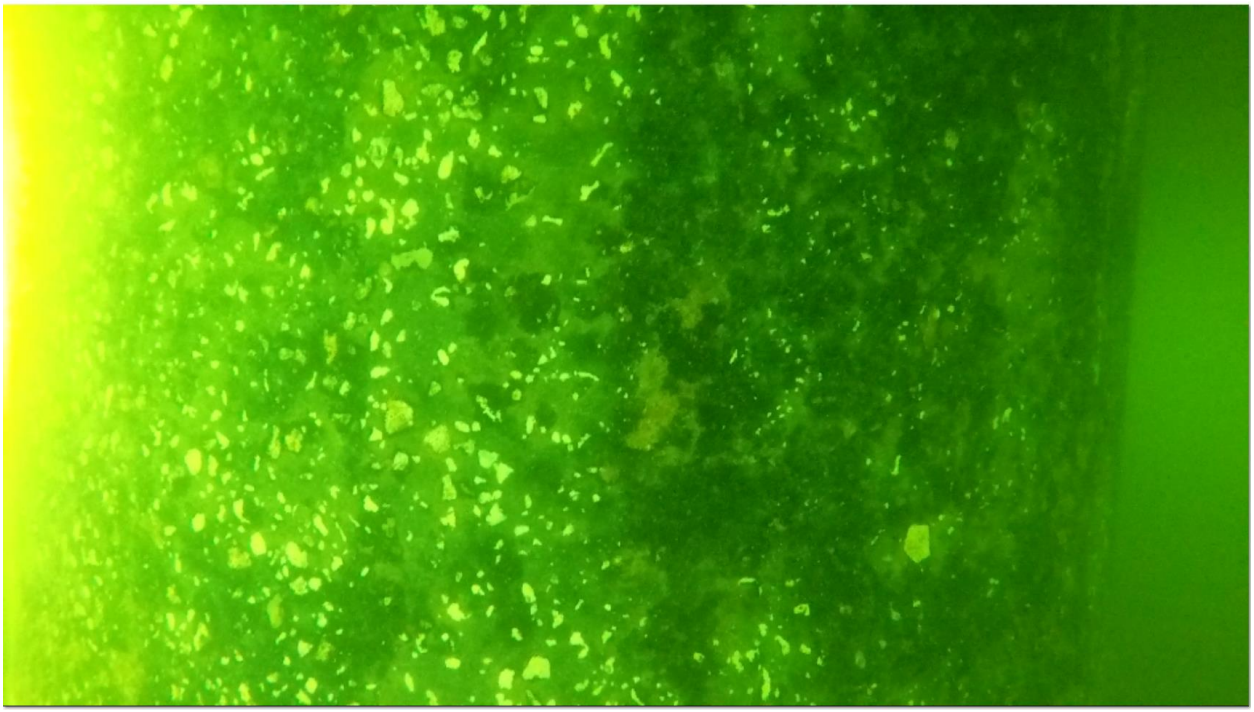

Figure 3.92 Visibly smooth side of shaft (protected from tidal flow).

Additionally, work will continue on the concrete penetration tests, to both refine the system and produce specimens for XRD and MIP testing. Cores are also need for electrochemical resistivity testing. Algorithms to automate the digital surface void volume will also continue to be developed so that all shaft specimens will ultimately be tested with this new technology.

In cooperation with the USF Department of Anthropology, underwater laser scanning of the shaft surface is being entertained to circumvent poor lighting and water clarity when attempting to quantify surface condition. This technology is routinely used to assess underwater pipelines that may have been damages by mooring anchors and in some instances for archeological explorations. The advantage over sonar based systems is the degree of precision which is down to sub-millimeter levels where sonar systems are limited to above 1cm. If successful, scans with detail like that shown in Figures 3.43-45 would better define the Figure 3.91 anomalies.

APPENDIX B
PHYSICAL VOID VOLUME RAW DATA

Table B.1 Physical void volume data

									per 6"x6" square	per total surface area	total	avg per shaft
Shaft #	tester	beaker tare (g)	beaker volume (mL)	full beaker (g)	Before weight (g)	After weight (g)	putty density (g/mL)	putty used (g)	void volume (cm^3)(mL)	void volume (cm^3)	void volume (in^3)	
1	s	38.7	350	490.07	1394.56	1298.36	1.4002	96.2	68.70447079	6043.5609	368.8004	592
		38.7	350	494.66	1396.81	1182.04	1.413314286	214.77	151.9619537	13367.2716	815.7204	
2	k	38.77	350	495.11	1344.03	1164.35	1.4146	179.68	127.0182384	11173.10781	681.8244	492
		38.77	350	497.79	1347.13	1267.29	1.422257143	79.84	56.13612166	4937.991167	301.3345	
3	s	38.7	350	493.31	1394.5	1348.19	1.409457143	46.31	32.8566216	2890.219389	176.3719	203
		38.7	350	492.61	1398.85	1338.44	1.407457143	60.41	42.92137797	3775.5616	230.3987	
4	k	38.77	350	489.96	1339.53	1251.95	1.399885714	87.58	62.56224998	5503.262938	335.8295	313
		38.77	350	485.93	1339.22	1264.08	1.388371429	75.14	54.12096392	4760.728635	290.5173	
5	s	38.7	350	482.22	1388.47	1327.51	1.377771429	60.96	44.24536519	3892.025598	237.5058	254
		38.7	350	491.82	1399.09	1328.38	1.4052	70.71	50.32023911	4426.399419	270.1153	
6	k	38.77	350	489.03	1338.79	1329.1	1.397228571	9.69	6.935157352	610.0483029	37.2274	42
		38.77	350	490.78	1340.55	1328.36	1.402228571	12.19	8.693304536	764.7030066	46.66501	
7	k	38.77	350	493.28	1343.19	1216.5	1.409371429	126.69	89.89113688	7907.237387	482.5289	487
		38.77	350	496.07	1345.79	1215.93	1.417342857	129.86	91.6221501	8059.505262	491.8208	
8	s	38.7	350	494.01	1390.84	1323.15	1.411457143	67.69	47.95753122	4218.564778	257.4324	215
		38.7	350	492.37	1396.31	1350.96	1.406771429	45.35	32.23693564	2835.708965	173.0455	
9	k	38.77	350	500.25	1349.73	1290.17	1.429285714	59.56	41.67116442	3665.587072	223.6877	260
		38.77	350	499.38	1350.96	1272.1	1.4268	78.86	55.27053546	4861.850229	296.6881	
10	k	38.77	350	500.25	1520	1390	1.429285714	130	90.95452274	8000.777693	488.2371	540
	s	38.77	350	498.32	1438	1281	1.423771429	157	110.2705089	9699.90058	591.9238	

									per 6"x6" square	per total surface area	total	avg per shaft
Shaft #	tester	beaker tare (g)	beaker volume (mL)	full beaker (g)	Before weight (g)	After weight (g)	putty density (g/mL)	putty used (g)	void volume (cm^3)(mL)	void volume (cm^3)	void volume (in^3)	
11	k	38.77	350	496.87	1345.32	1320.96	1.419628571	24.36	17.15941796	1509.421239	92.11047	71
		38.77	350	498.32	1347.37	1333.91	1.423771429	13.46	9.453764649	831.596572	50.7471	
12	k	38.77	350	490.03	1340.92	1323.08	1.400085714	17.84	12.74207702	1120.851635	68.39851	59
		38.77	350	489.99	1339.25	1326.1	1.399971429	13.15	9.393048838	826.2557303	50.42118	
13	s	38.7	350	488.31	1388.08	1340.11	1.395171429	47.97	34.38287154	3024.475346	184.5647	169
		38.7	350	493.42	1393.91	1353.62	1.409771429	40.29	28.57910097	2513.949022	153.4105	
14	s	38.7	350	485.23	1383.62	1307.7	1.386371429	75.92	54.76165942	4817.087154	293.9565	299
		38.7	350	487.09	1386.89	1307.82	1.391685714	79.07	56.81598883	4997.795407	304.984	
15	s	38.7	350	491.2	1392.76	1324.62	1.403428571	68.14	48.55252443	4270.903114	260.6263	263
		38.7	350	489.37	1393.83	1324.61	1.3982	69.22	49.50650837	4354.819924	265.7472	
16	k	38.77	350	491.21	1340.6	1320.26	1.403457143	20.34	14.49278313	1274.851788	77.79617	73
		38.77	350	490.18	1339.9	1322.34	1.400514286	17.56	12.53825125	1102.922185	67.30439	
17	s	38.7	350	486.51	1385.83	1376.91	1.390028571	8.92	6.417134283	564.4806138	34.4467	38
		38.7	350	489.34	1388.96	1378.01	1.398114286	10.95	7.831977766	688.9367468	42.04147	
18	k	38.77	350	489.86	1339.19	1325.42	1.3996	13.77	9.838525293	865.4418859	52.81247	47
		38.77	350	490.44	1337.62	1326.64	1.401257143	10.98	7.835820896	689.2748061	42.0621	
19	s	38.7	350	487.53	1388.28	1377.1	1.392942857	11.18	8.026172748	706.0190296	43.08389	43
		38.7	350	490.84	1392.6	1381.23	1.4024	11.37	8.107529949	713.1755827	43.52061	
20	k	38.77	350	490.69	1332.3	1323.26	1.401971429	9.04	6.448062932	567.2012398	34.61272	33
		38.77	350	489.05	1338.4	1330.4	1.397285714	8	5.725385952	503.6312525	30.73344	
21	s	38.7	350	484.64	1374.17	1200.68	1.384685714	173.49	125.2919693	11021.25725	672.5579	578
		38.7	350	481.74	1379.9	1256.14	1.3764	123.76	89.91572217	7909.400022	482.6609	
22	k	38.77	350	483.61	1333.62	1324.43	1.381742857	9.19	6.65102045	585.0543156	35.70218	30
		38.77	350	495.75	1345.36	1339.17	1.416428571	6.19	4.370146243	384.4181413	23.45862	

									per 6"x6" square	per total surface area	total	avg per shaft
Shaft #	tester	beaker tare (g)	beaker volume (mL)	full beaker (g)	Before weight (g)	After weight (g)	putty density (g/mL)	putty used (g)	void volume (cm^3)(mL)	void volume (cm^3)	void volume (in^3)	
23	k	38.77	350	498.89	1348.44	1336.57	1.4254	11.87	8.327487021	732.5240174	44.70133	48
		38.77	350	498.14	1347.7	1334.07	1.423257143	13.63	9.576625045	842.4039369	51.40661	

APPENDIX C
SURFACE POTENTIAL MAPPING RAW DATA & STATISTICAL DISTRIBUTION

Table C-1: Shaft 1 Surface Potential Mapping Raw Data (mV)

	0"`	3"	6"	9"	12"	15"	18"	21"
0"	-266	-289	-333	-337	-313	-298	-296	-289
3"	-279	-292	-316	-317	-311	-301	-300	-293
6"	-290	-302	-312	-312	-308	-306	-307	-303
9"	-290	-308	-315	-312	-309	-310	-308	-307
12"	-307	-316	-315	-318	-317	-314	-311	-302
15"	-309	-317	-319	-325	-324	-322	-320	-311
18"	-314	-323	-324	-332	-330	-328	-327	-320
21"	-323	-330	-330	-338	-338	-342	-331	-322
24"	-327	-330	-338	-344	-345	-348	-337	-329
27"	-328	-333	-338	-344	-347	-349	-338	-337

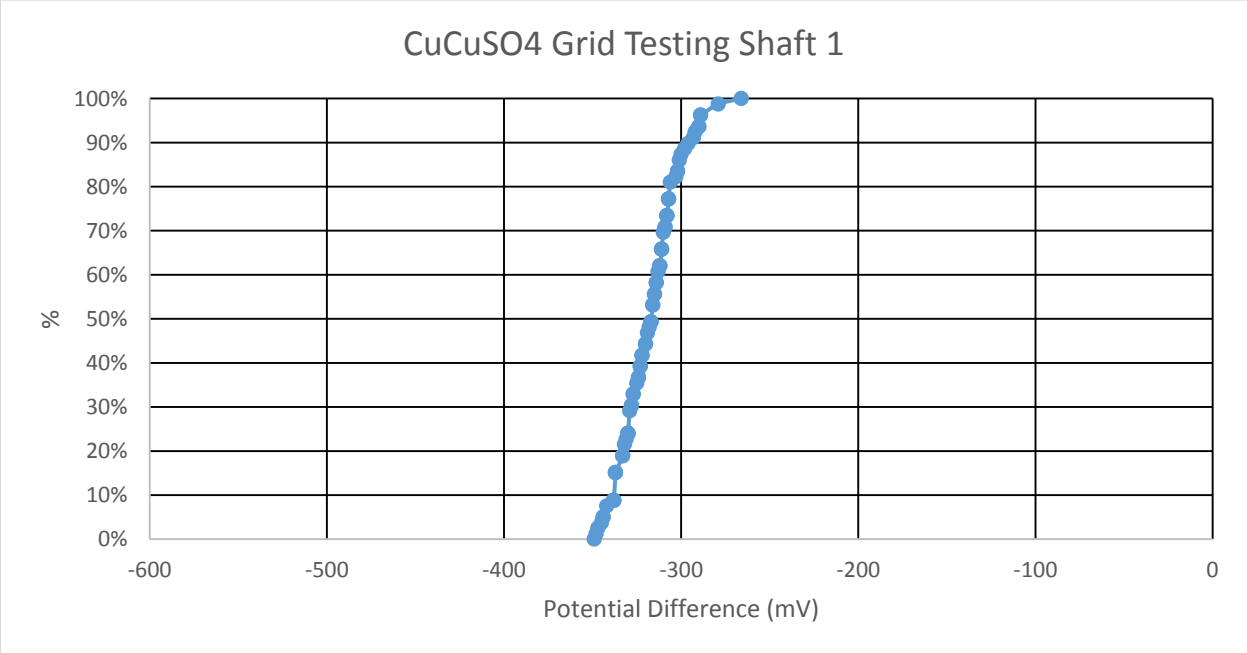

Figure C-1: Shaft 1 Surface Potential Mapping Data Distribution

Table C-2: Shaft 2 Surface Potential Mapping Raw Data (mV)

	0”	3”	6”	9”	12”	15”	18”	21”
0”	-384	-387	-406	-421	-434	-438	-431	-411
3”	-402	-398	-416	-431	-454	-456	-446	-434
6”	-400	-403	-420	-442	-460	-464	-461	-454
9”	-392	-408	-430	-452	-466	-474	-472	-465
12”	-402	-417	-447	-463	-476	-470	-462	-459
15”	-402	-416	-445	-463	-474	-478	-463	-462
18”	-395	-410	-460	-468	-482	-477	-458	-449
21”	-396	-404	-466	-483	-492	-485	-469	-449
24”	-389	-400	-444	-470	-481	-472	-461	-440
27”	-390	-398	-428	-467	-472	-472	-461	-447

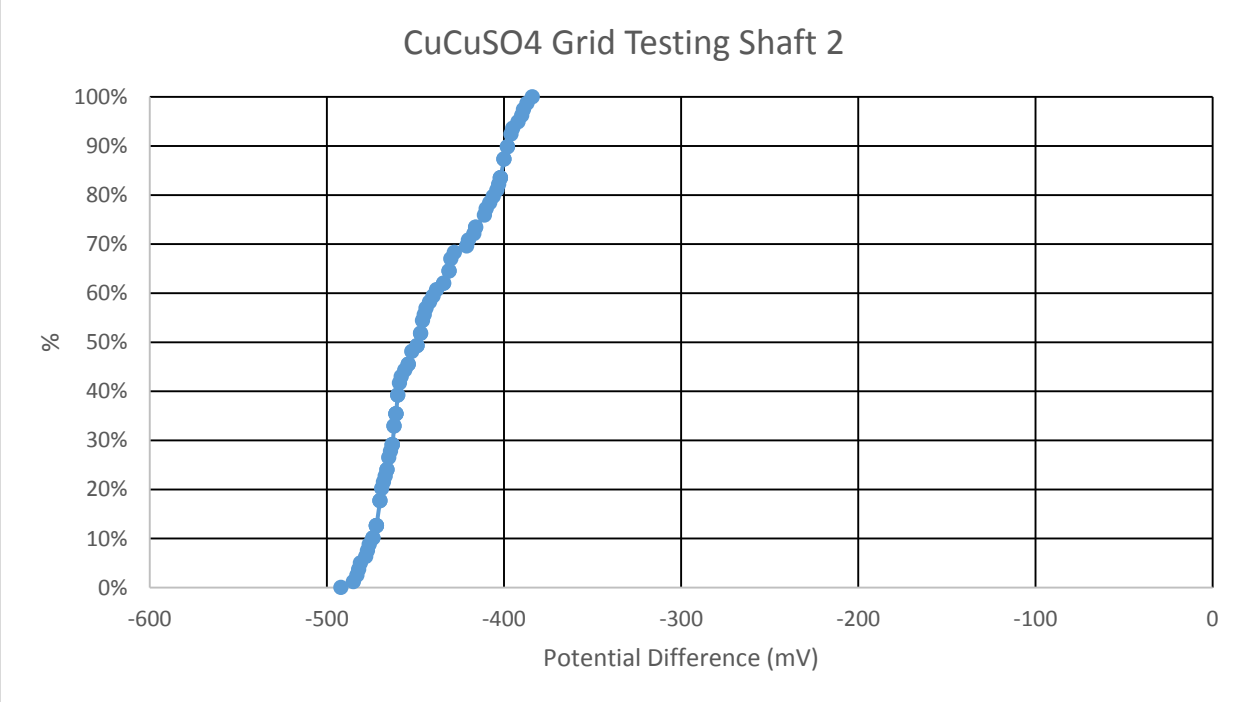

Figure C-2: Shaft 2 Surface Potential Mapping Data Distribution

Table C-3: Shaft 3 Surface Potential Mapping Raw Data (mV)

	0"	3"	6"	9"	12"	15"	18"	21"
0"	-372	-382	-389	-390	-396	-396	-384	-379
3"	-373	-378	-381	-382	-393	-386	-381	-378
6"	-374	-374	-377	-377	-379	-380	-373	-379
9"	-376	-368	-372	-359	-361	-360	-363	-379
12"	-370	-364	-369	-352	-351	-353	-351	-369
15"	-374	-366	-360	-350	-349	-353	-346	-361
18"	-377	-360	-364	-352	-356	-355	-355	-354
21"	-379	-361	-380	-359	-364	-367	-370	-378
24"	-379	-367	-378	-368	-368	-380	-382	-383
27"	-373	-367	-374	-376	-376	-378	-381	-388

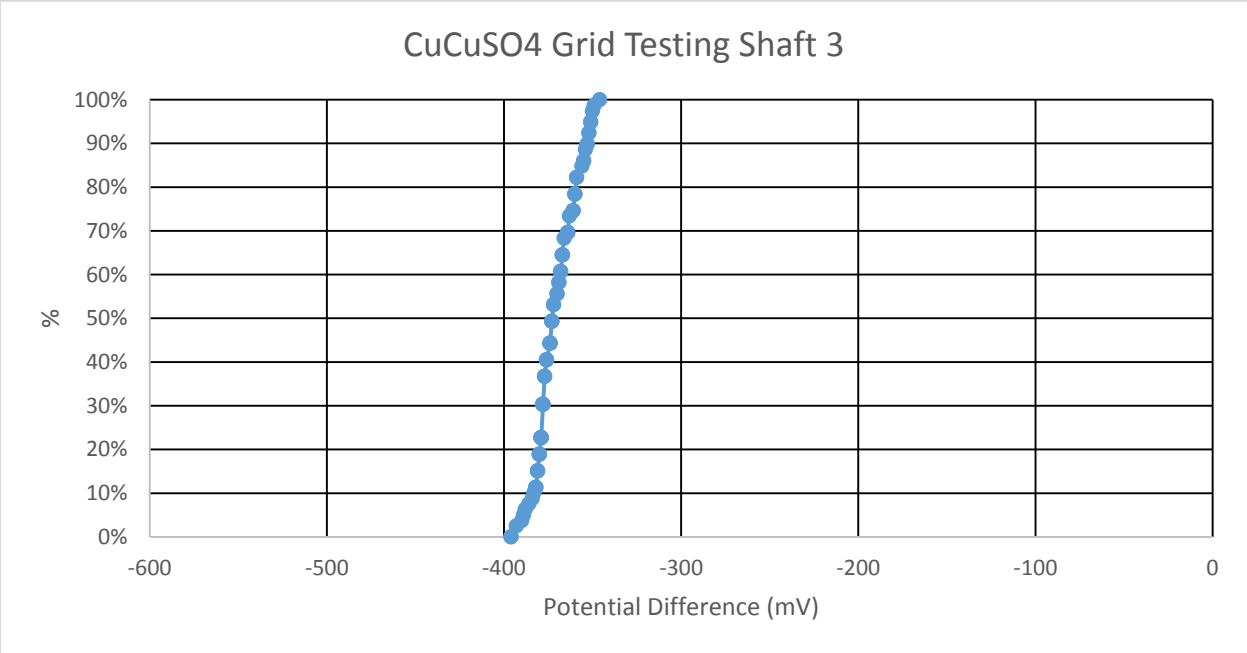

Figure C-3: Shaft 3 Surface Potential Mapping Data Distribution

Table C-4: Shaft 4 Surface Potential Mapping Raw Data (mV)

	0"	3"	6"	9"	12"	15"	18"	21"
0"	-411	-441	-447	-462	-472	-454	-437	-425
3"		-443	-453	-463	-472	-453	-433	-423
6"	-442	-444	-447	-467	-473	-459	-434	-419
9"	-429	-434	-439	-463	-474	-458	-427	-415
12"		-427	-435	-458	-470	-458	-433	-409
15"		-429	-435	-454	-461	-450	-437	-414
18"	-425	-426	-444	-458	-473	-459	-445	-433
21"	-413	-425	-437	-470	-471	-461	-451	-439
24"	-420	-422	-430	-452	-466	-458	-449	-439
27"	-418	-417	-423	-449	-459	-463	-451	-443

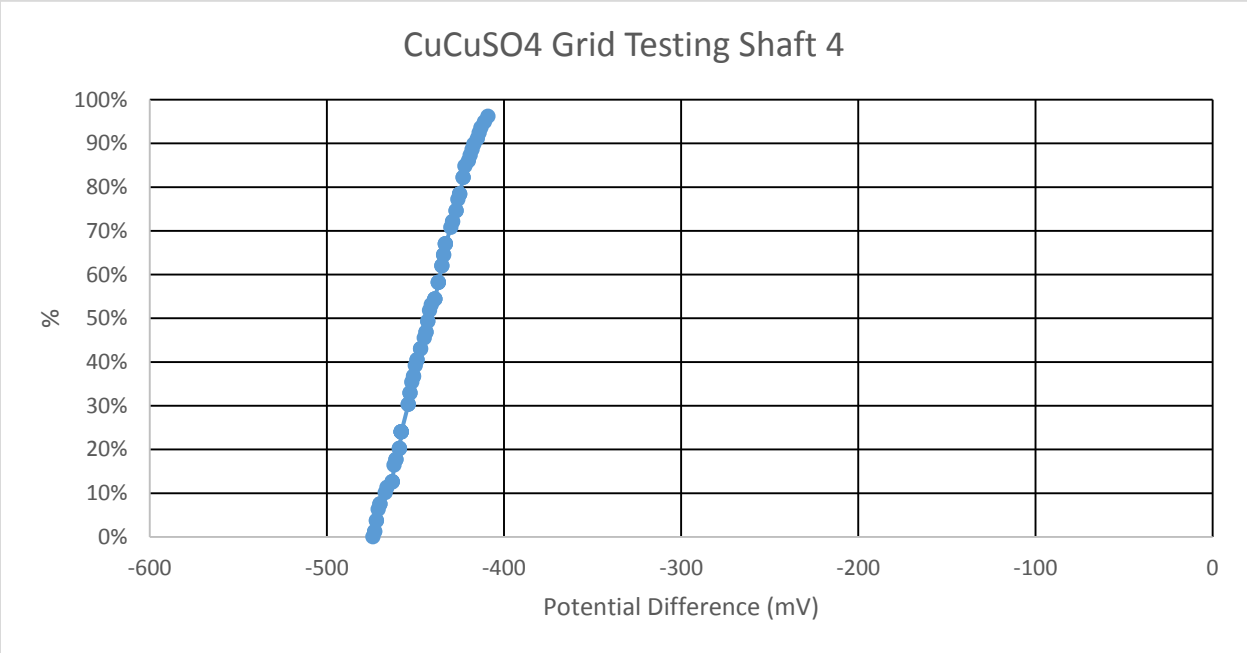

Figure C-4: Shaft 4 Surface Potential Mapping Data Distribution

Table C-5: Shaft 5 Surface Potential Mapping Raw Data (mV)

	0"	3"	6"	9"	12"	15"	18"	21"
0"	-400	-408	-425	-447	-469	-482	-484	-475
3"	-408	-413	-428	-456	-476	-489	-494	-489
6"	-413	-416	-432	-460	-473	-482	-492	-485
9"	-413	-415	-433	-457	-466	-467	-470	-464
12"	-407	-402	-422	-450	-459	-465	-463	-455
15"	-390	-402	-416	-440	-441	-445	-459	-449
18"	-394	-402	-413	-433	-433	-435	-437	-426
21"	-392	-407	-416	-441	-448	-450	-457	-450
24"	-401	-416	-435	-452	-457	-469	-469	-469
27"	-412	-420	-432	-450	-460	-465	-469	-457

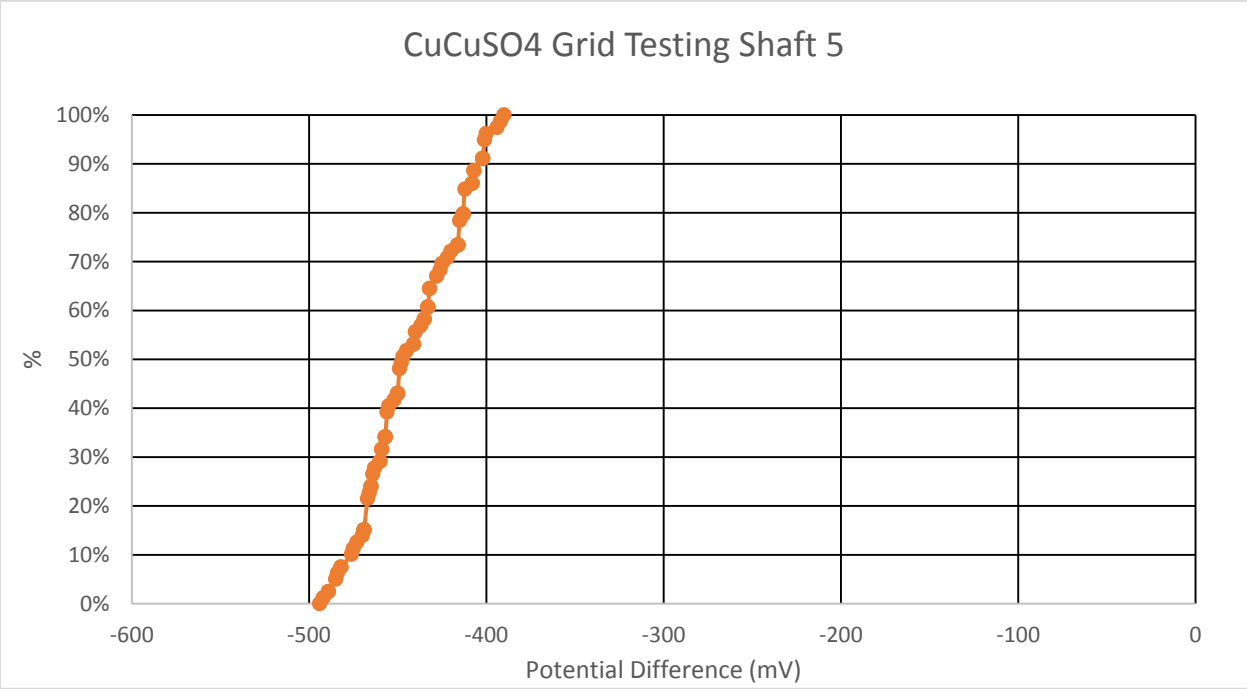

Figure C-5: Shaft 5 Surface Potential Mapping Data Distribution

Table C-6: Shaft 6 Surface Potential Mapping Raw Data (mV)

	0"	3"	6"	9"	12"	15"	18"	21"
0"	-160	-148	-144	-139	-129	-131	-141	-155
3"	-168	-157	-143	-135	-130	-131	-141	-153
6"	-170	-163	-158	-147	-136	-138	-138	-142
9"	-168	-161	-153	-140	-128	-127	-140	-144
12"	-169	-161	-155	-145	-134	-129	-141	-146
15"	-170	-164	-157	-130	-142	-139	-143	-152
18"	-172	-167	-163	-136	-148	-149	-150	-152
21"	-174	-172	-166	-159	-155	-156	-156	-153
24"	-174	-174	-167	-168	-156	-159	-159	-160
27"	-176	-174	-161	-165	-159	-161	-161	-157

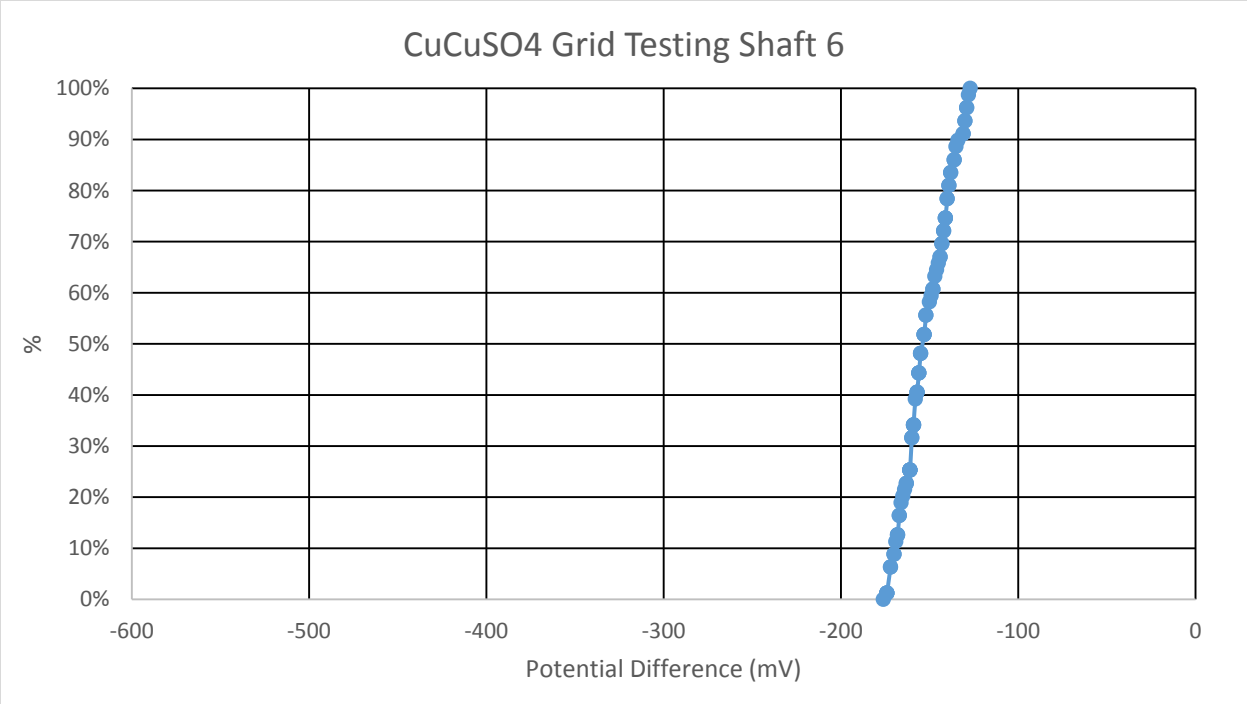

Figure C-6: Shaft 6 Surface Potential Mapping Data Distribution

Table C-7: Shaft 7 Surface Potential Mapping Raw Data (mV)

	0"	3"	6"	9"	12"	15"	18"	21"
0"	-331	-331	-329	-338	-344	-350	-361	-361
3"	-339	-340	-339	-343	-345	-354	-372	-382
6"	-340	-346	-345	-348	-351	-366	-386	-402
9"	-352	-352	-354	-356	-361	-375	-398	-409
12"	-357	-358	-362	-364	-380	-398	-419	-422
15"	-354	-363	-373	-376	-398	-421	-444	-437
18"	-365	-364	-374	-383	-399	-430	-468	-454
21"	-364	-368	-377	-393	-400	-436	-462	-475
24"	-366	-369	-378	-395	-416	-436	-459	-466
27"	-364	-363	-378	-393	-415	-442	-458	-480

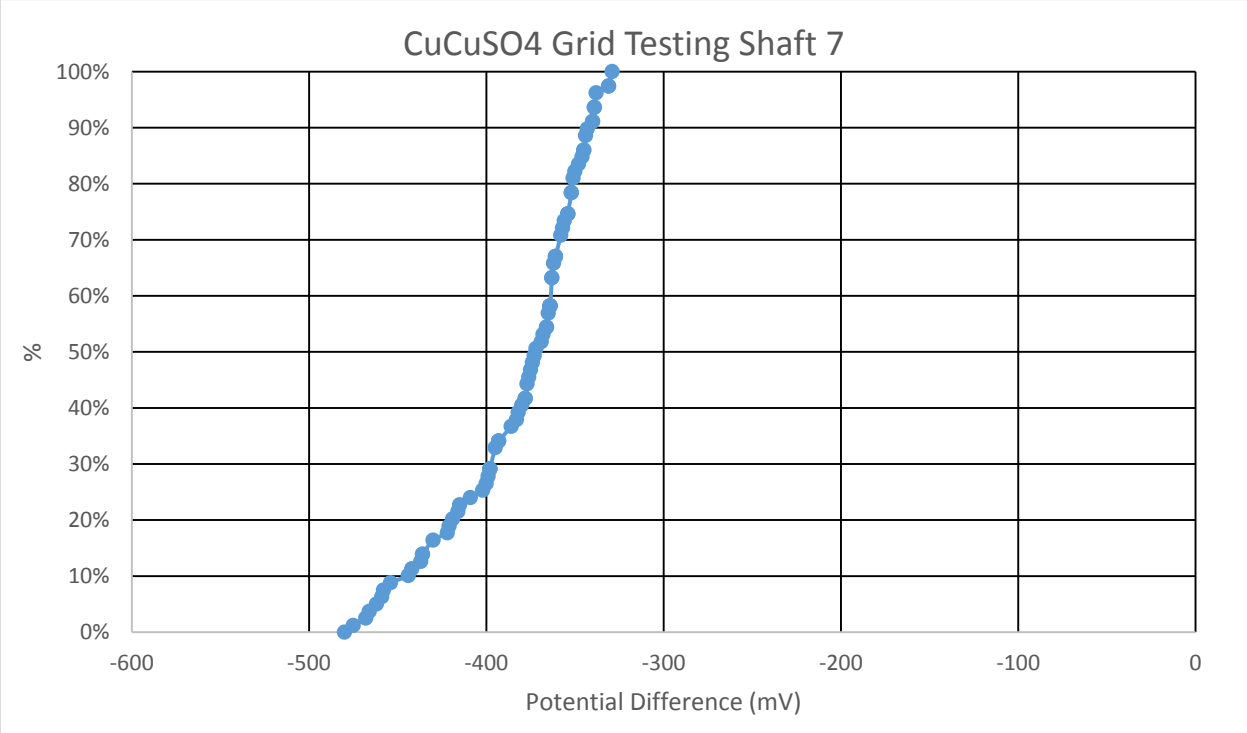

Figure C-7: Shaft 7 Surface Potential Mapping Data Distribution

Table C-8: Shaft 8 Surface Potential Mapping Raw Data (mV)

	0"	3"	6"	9"	12"	15"	18"	21"
0"	-239	-243	-234	-233	-215	-211	-210	-215
3"	-233	-241	-237	-236	-218	-213	-220	-216
6"	-223	-221	-237	-235	-222	-213	-216	-209
9"	-226	-232	-235	-225	-213	-209	-208	-209
12"	-234	-235	-231	-227	-218	-217	-214	-212
15"	-255	-247	-239	-234	-226	-227	-229	-225
18"	-251	-238	-232	-227	-223	-212	-227	-219
21"	-245	-242	-236	-233	-223	-216	-215	-216
24"	-243	-238	-234	-230	-215	-214	-218	-223
27"	-240	-239	-233	-224	-219	-211	-209	-216

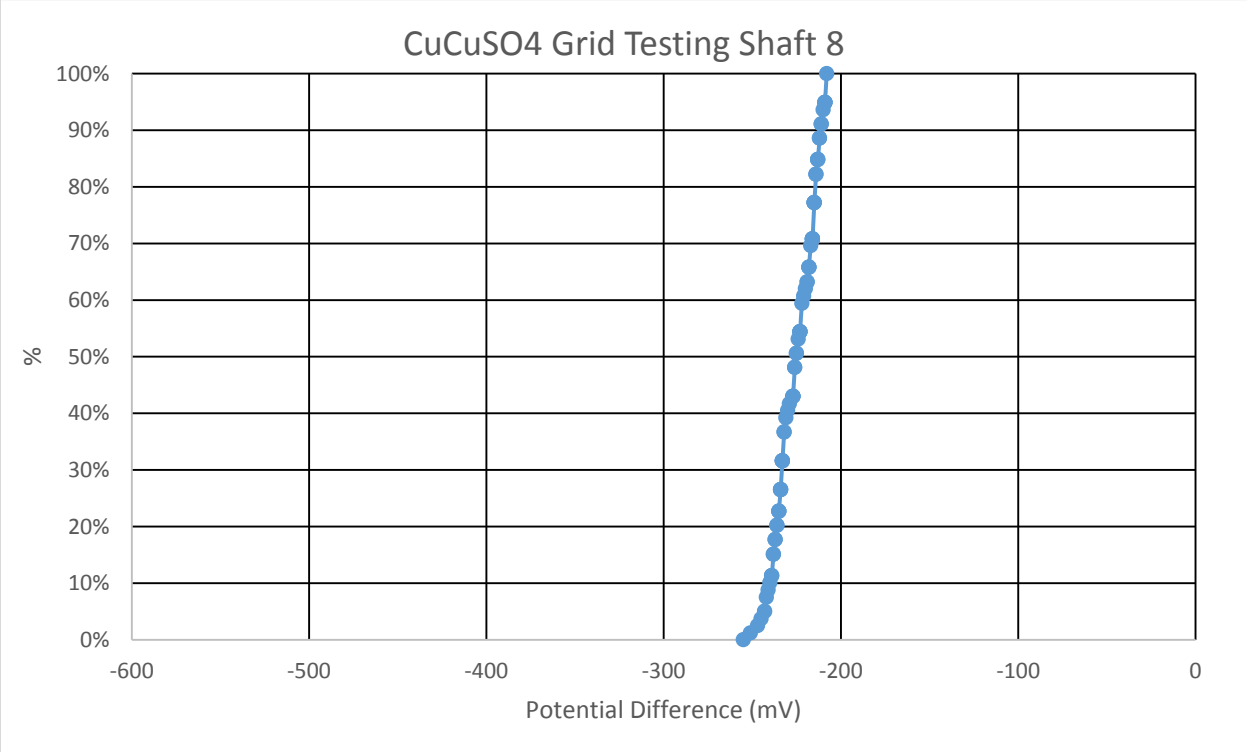

Figure C-8: Shaft 8 Surface Potential Mapping Data Distribution

Table C-9: Shaft 9 Surface Potential Mapping Raw Data (mV)

	0"	3"	6"	9"	12"	15"	18"	21"
0"	-362	-364	-372	-381	-391	-410	-423	-424
3"	-356	-364	-368	-373	-385	-402	-420	-418
6"	-359	-359	-367	-383	-393	-413	-427	-430
9"	-362	-367	-370	-384	-397	-416	-427	-423
12"	-363	-366	-373	-382	-400	-415	-425	-419
15"	-372	-371	-375	-385	-399	-416	-421	-417
18"	-371	-372	-375	-379	-392	-403	-409	-410
21"	-365	-366	-367	-373	-392	-392	-396	-404
24"	-363	-365	-368	-375	-387	-387	-390	-396
27"	-357	-356	-366	-369	-383	-383	-387	-389

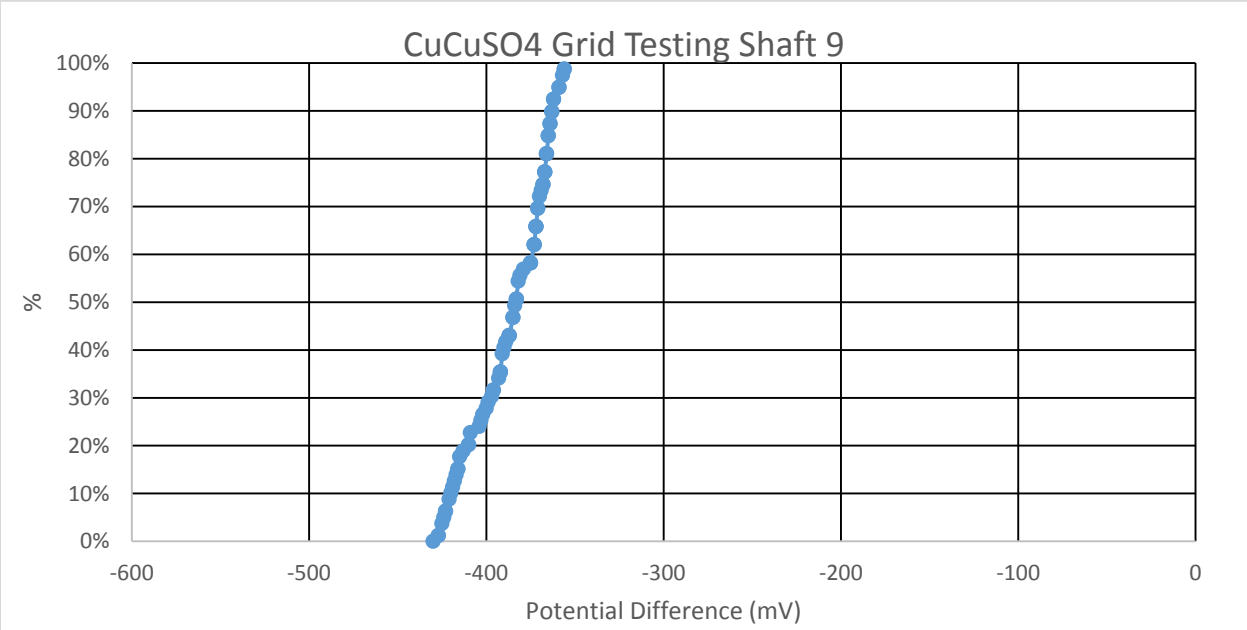

Figure C-9: Shaft 9 Surface Potential Mapping Data Distribution

Table C-10: Shaft 11 Surface Potential Mapping Raw Data (mV)

	0"	3"	6"	9"	12"	15"	18"	21"
0"	-263	-271	-268	-267	-266	-265	-266	-258
3"	-264	-273	-272	-274	-272	-274	-271	-260
6"	-269	-278	-280	-281	-280	-287	-283	-266
9"	-272	-282	-283	-287	-287	-291	-282	-269
12"	-273	-283	-287	-288	-287	-285	-280	-273
15"	-285	-295	-292	-295	-290	-290	-293	-274
18"	-289	-299	-298	-298	-293	-3030	-293	-271
21"	-297	-299	-296	-290	-287	-286	-287	-268
24"	-299	-312	-310	-308	-296	-297	-285	-278
27"	-305	-318	-322	-326	-291	-297	-289	-278

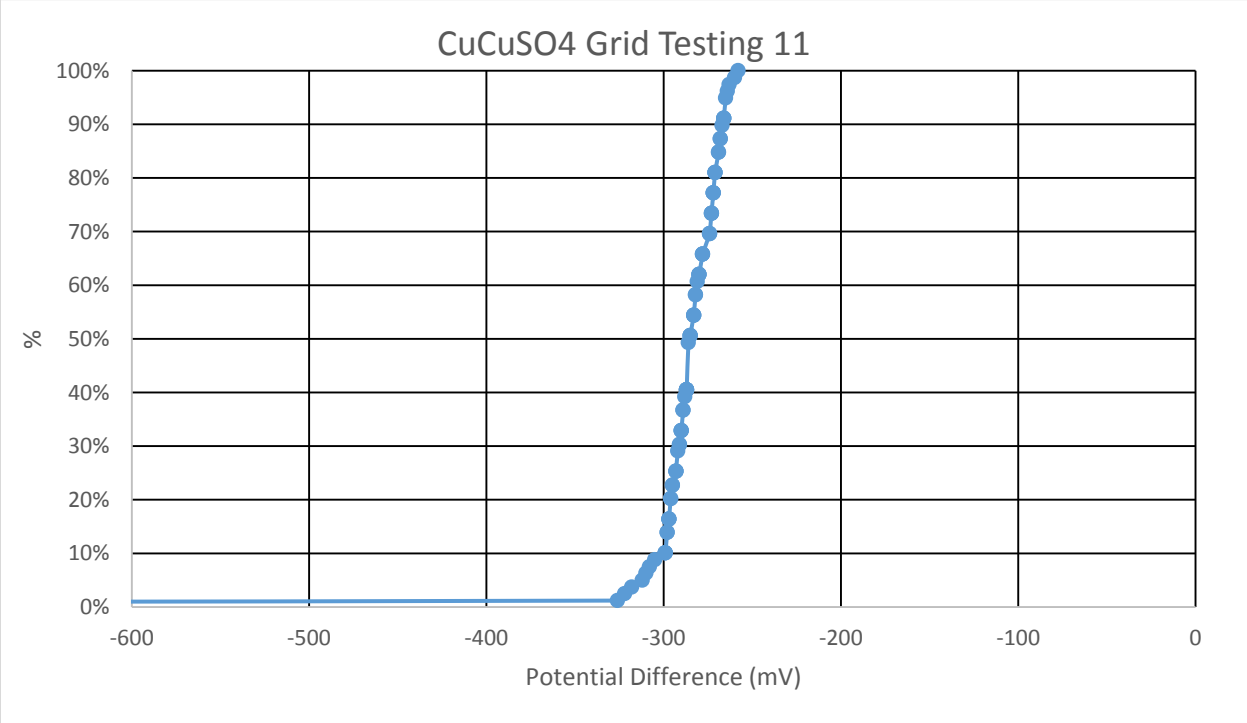

Figure C-10: Shaft 11 Surface Potential Mapping Data Distribution

Table C-11: Shaft 12 Surface Potential Mapping Raw Data (mV)

	0"	3"	6"	9"	12"	15"	18"	21"
0"	-184	-188	-181	-176	-173	-174	-175	-170
3"	-195	-201	-189	-186	-181	-176	-175	-173
6"	-196	-201	-197	-191	-179	-172	-171	-168
9"	-204	-210	-200	-190	-179	-174	-170	-170
12"	-225	-217	-201	-193	-185	-179	-171	-170
15"	-220	-220	-206	-193	-191	-178	-176	-172
18"	-226	-222	-210	-206	-199	-187	-183	-187
21"	-220	-220	-213	-205	-195	-189	-185	-185
24"	-219	-221	-212	-204	-206	-186	-188	-181
27"	-218	-221	-212	-206	-199	-192	-186	-187

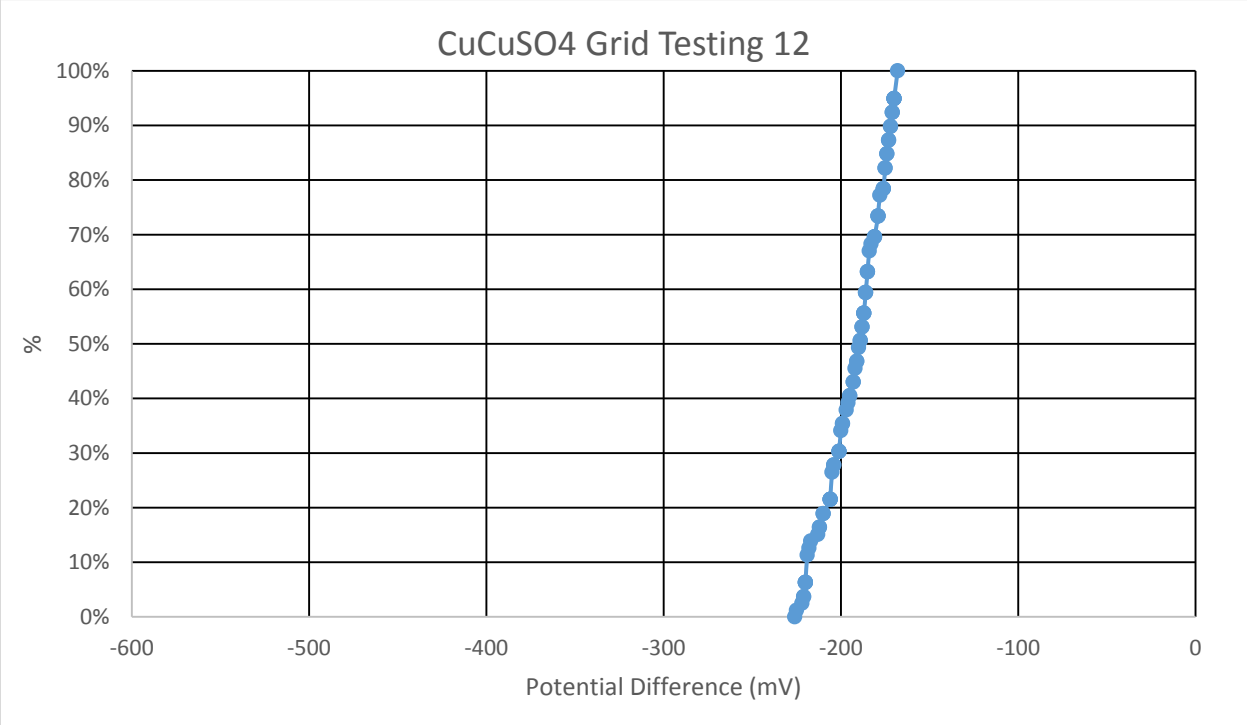

Figure C-11: Shaft 12 Surface Potential Mapping Data Distribution

Table C-12: Shaft 13 Surface Potential Mapping Raw Data (mV)

	0"	3"	6"	9"	12"	15"	18"	21"
0"	-306	-300	-291	-288	-286	-285	-285	-289
3"	-305	-298	-291	-291	-290	-285	-286	-286
6"	-305	-299	-294	-289	-286	-284	-287	-285
9"	-303	-297	-293	-290	-285	-286	-285	-284
12"	-304	-299	-294	-291	-286	-285	-282	-282
15"	-307	-300	-296	-291	-285	-281	-280	-278
18"	-303	-302	-294	-290	-286	-283	-278	-278
21"	-297	-300	-300	-293	-288	-286	-283	-277
24"	-309	-302	-302	-293	-290	-288	-284	-280
27"	-310	-306	-301	-293	-289	-285	-283	-278

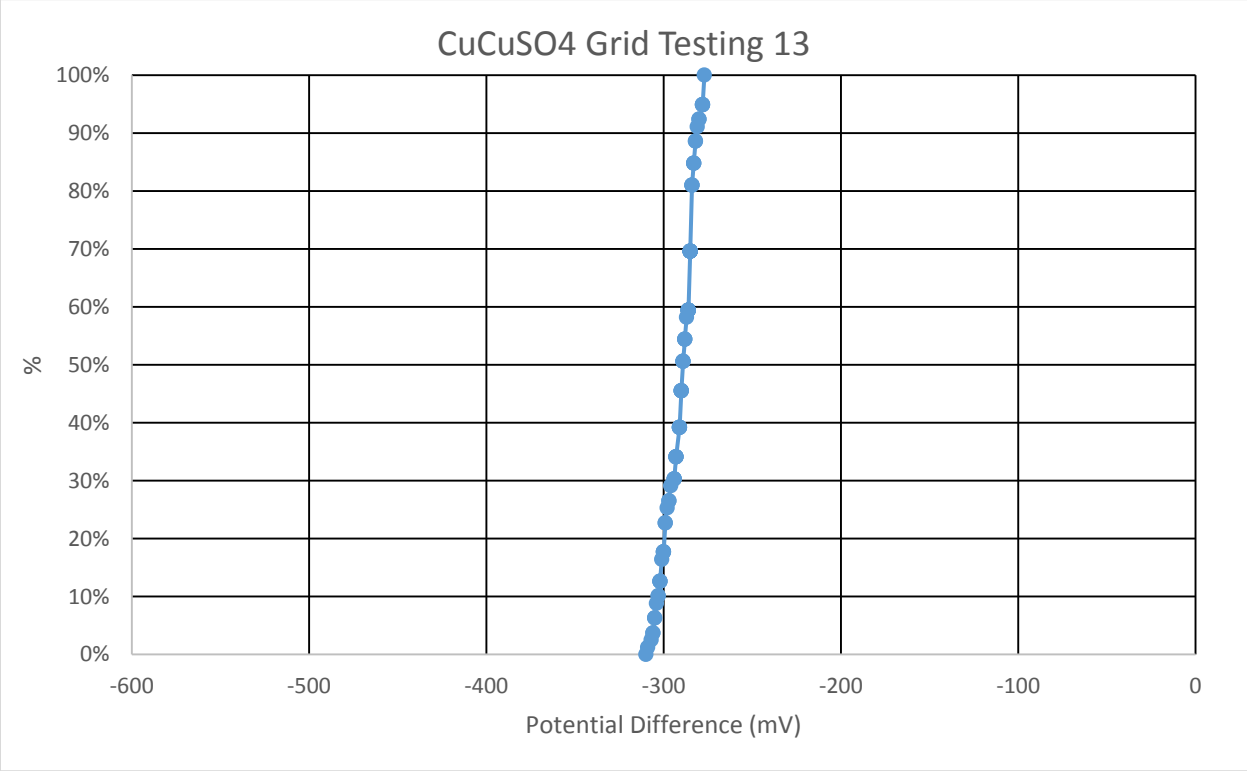

Figure C-12: Shaft 13 Surface Potential Mapping Data Distribution

Table C-13: Shaft 14 Surface Potential Mapping Raw Data (mV)

	0"	3"	6"	9"	12"	15"	18"	21"
0"	-315	-300	-291	-282	-273	-248	-255	-263
3"	-307	-296	-292	-284	-235	-214	-230	-251
6"	-298	-299	-294	-289	-280	-243	-245	-268
9"	-300	-294	-291	-285	-280	-276	-253	-281
12"	-298	-293	-288	-285	-285	-280	-270	-268
15"	-302	-295	-288	-284	-281	-281	-275	-279
18"	-297	-293	-289	-284	-279	-277	-276	-278
21"	-300	-296	-291	-284	-278	-276	-276	-277
24"	-301	-297	-291	-283	-274	-262	-262	-270
27"	-304	-298	-294	-286	-277	-270	-267	-273

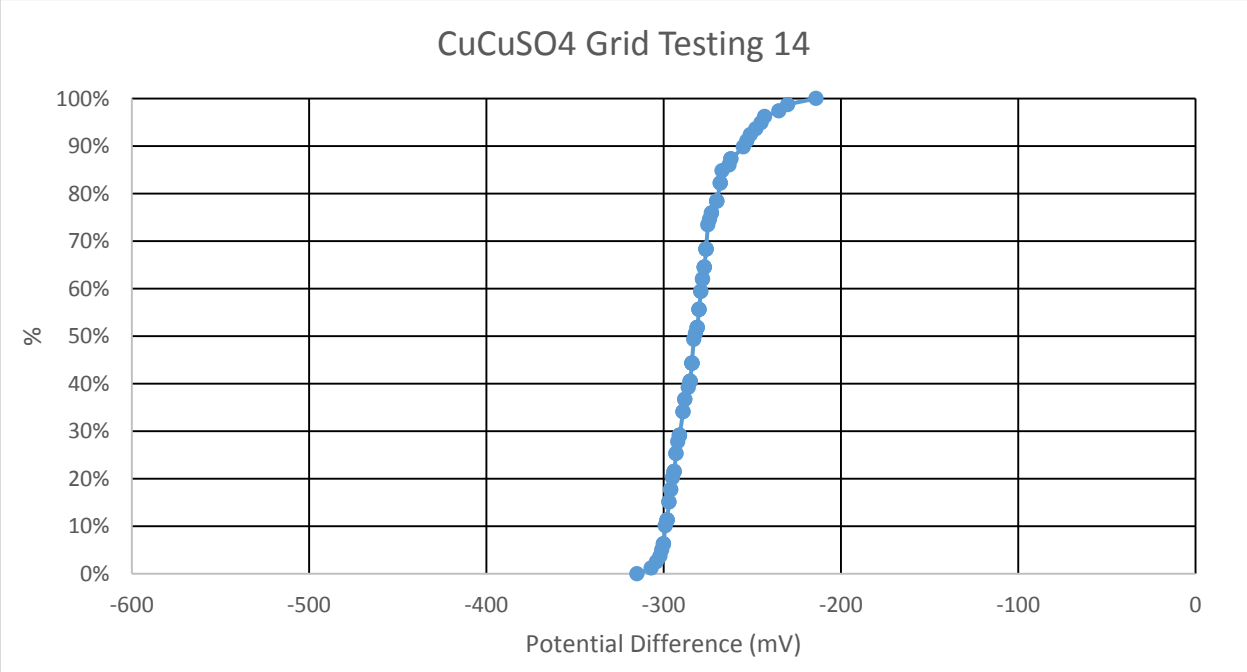

Figure C-13: Shaft 14 Surface Potential Mapping Data Distribution

Table C-14: Shaft 15 Surface Potential Mapping Raw Data (mV)

	0"	3"	6"	9"	12"	15"	18"	21"
0"			-349	-350	-351	-340	-339	-347
3"			-339	-345	-340	-338	-338	-341
6"		-337	-336	-338	-340	-330	-335	-336
9"		-335	-334	-333	-327	-328	-331	-334
12"			-330	-330	-327	-327	-329	-334
15"		-332	-337	-331	-328	-330	-332	-336
18"		-337	-336	-335	-332	-331	-334	-337
21"		-344	-336	-335	-328	-327	-333	-339
24"		-349	-348	-341	-338	-332	-337	-341
27"	-362	-357	-344	-341	-337	-333	-336	-337

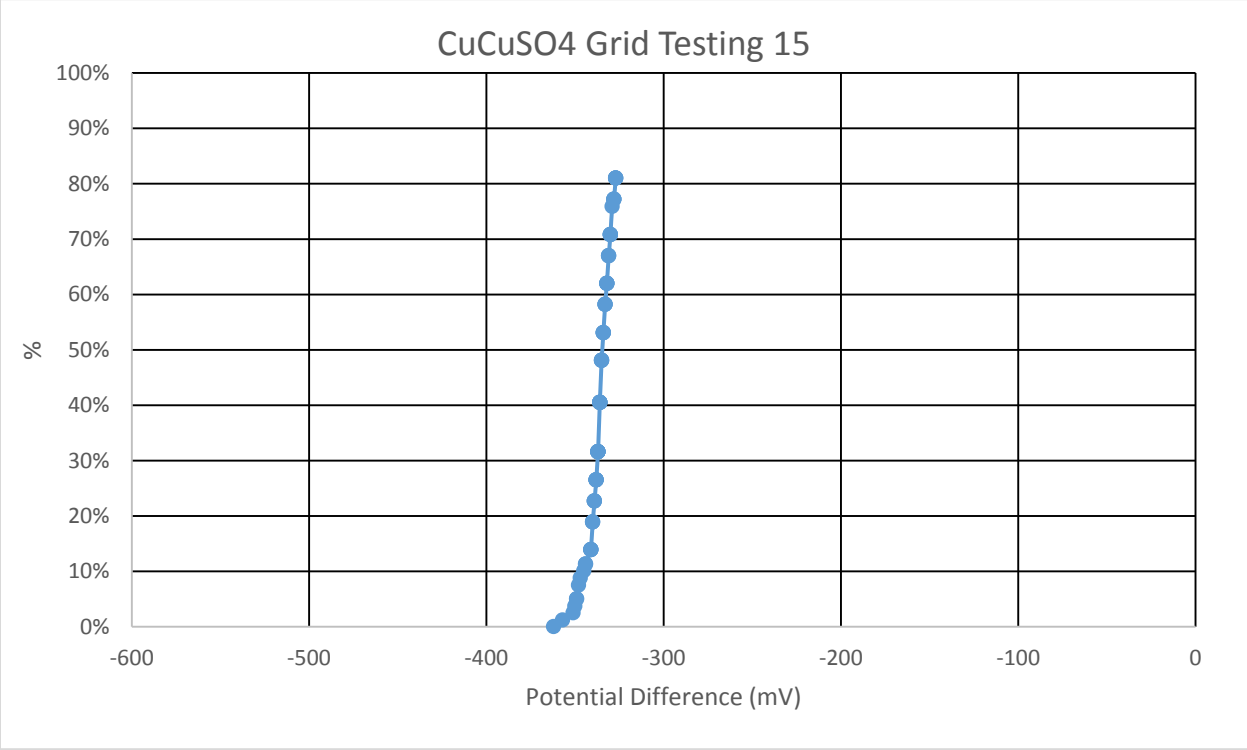

Figure C-14: Shaft 15 Surface Potential Mapping Data Distribution

Table C-15: Shaft 16 Surface Potential Mapping Raw Data (mV)

	0"	3"	6"	9"	12"	15"	18"	21"
0"	-291	-278	-271	-266	-259	-256	-261	-251
3"	-298	-287	-279	-275	-269	-266	-271	-262
6"	-298	-294	-286	-278	-272	-271	-270	-264
9"	-292	-290	-283	-276	-277	-275	-271	-265
12"	-293	-290	-284	-274	-270	-273	-275	-269
15"	-292	-291	-289	-279	-278	-280	-278	-271
18"	-293	-288	-284	-278	-275	-278	-282	-275
21"	-292	-290	-285	-283	-279	-279	-284	-279
24"	-293	-290	-289	-283	-280	-283	-284	-283
27"	-289	-288	-286	-282	-280	-281	-286	-286

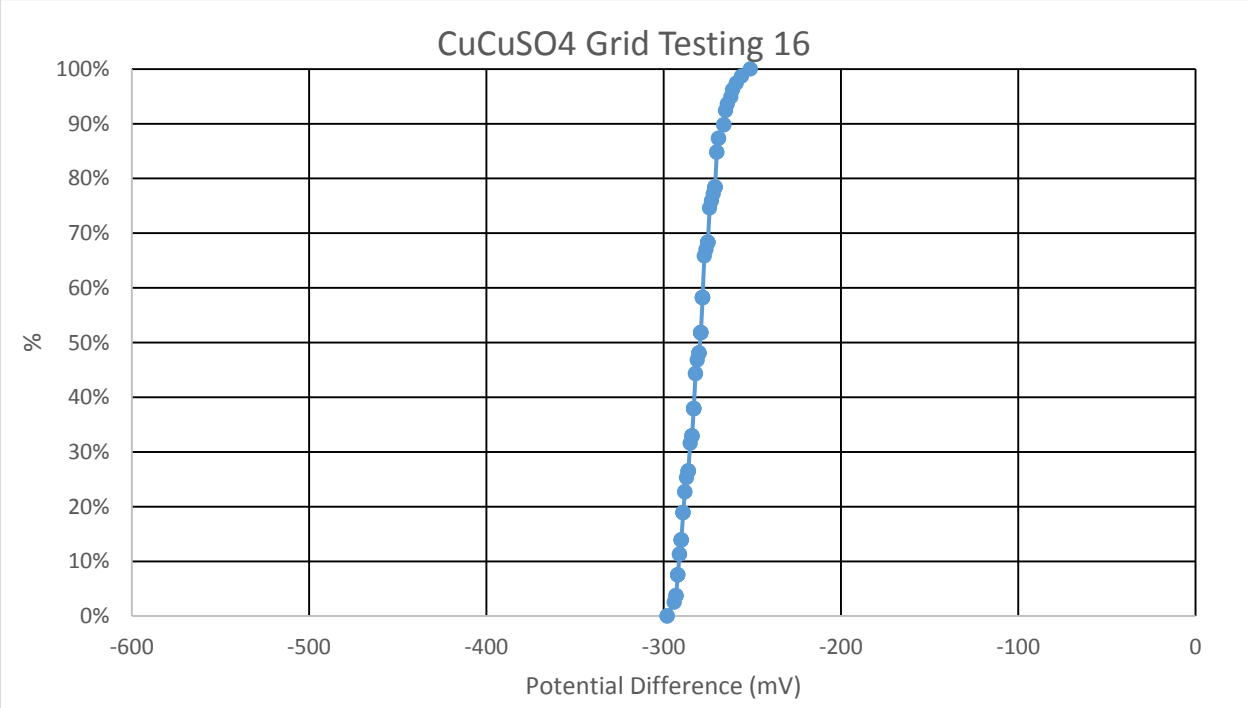

Figure C-15: Shaft 16 Surface Potential Mapping Data Distribution

Table C-16: Shaft 17 Surface Potential Mapping Raw Data (mV)

	0"	3"	6"	9"	12"	15"	18"	21"
0"	-309	-303	-301	-301	-299	-305	-304	-304
3"	-306	-306	-303	-303	-302	-299	-303	-301
6"	-309	-307	-303	-308	-304	-299	-298	-300
9"	-306	-305	-302	-299	-293	-291	-294	-293
12"	-312	-310	-304	-298	-298	-292	-296	-290
15"	-319	-312	-304	-303	-298	-295	-295	-288
18"	-322	-311	-302	-296	-293	-290	-291	-288
21"	-319	-310	-301	-300	-292	-288	-287	-285
24"	-311	-310	-302	-297	-291	-287	-285	-286
27"	-305	-306	-297	-295	-290	-286	-285	-280

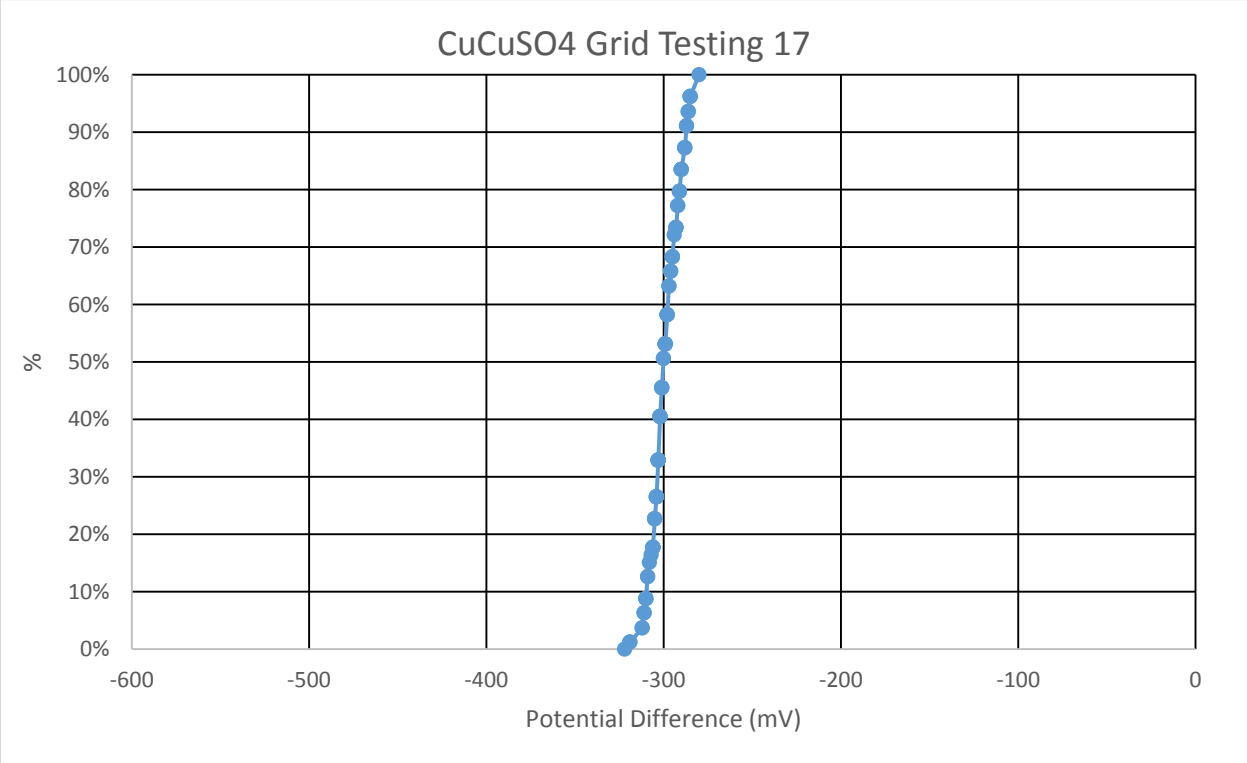

Figure C-16: Shaft 17 Surface Potential Mapping Data Distribution

Table C-17: Shaft 18 Surface Potential Mapping Raw Data (mV)

	0"	3"	6"	9"	12"	15"	18"	21"
0"	-301	-304	-291	-291	-284	-295	-300	-302
3"	-300	-302	-290	-285	-282	-290	-299	-307
6"	-299	-303	-291	-284	-282	-292	-299	-306
9"	-294	-297	-290	-286	-284	-293	-299	-304
12"	-295	-293	-285	-281	-283	-290	-293	-300
15"	-296	-298	-285	-282	-285	-291	-291	-298
18"	-296	-296	-288	-283	-292	-293	-295	-292
21"	-301	-297	-291	-288	-294	-293	-297	-303
24"	-302	-298	-291	-290	-293	-287	-294	-297
27"	-299	-297	-291	-297	-302	-295	-297	-301

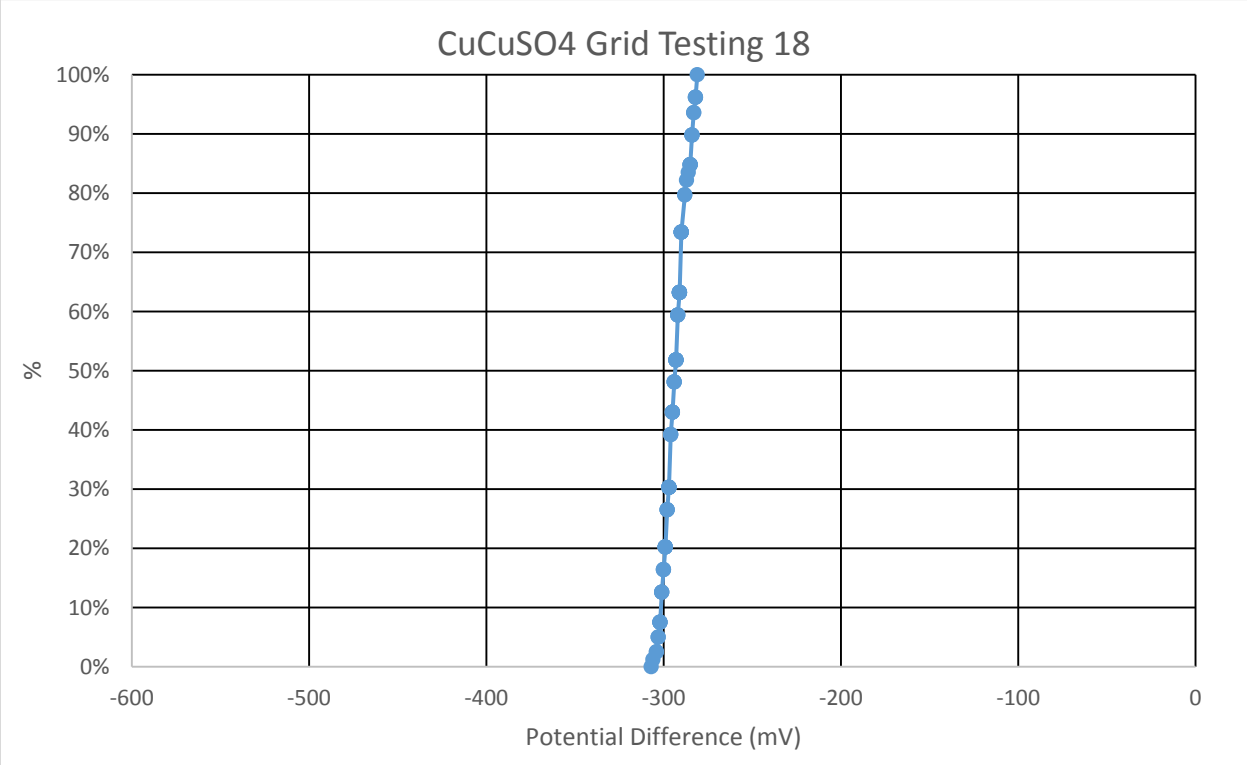

Figure C-17: Shaft 18 Surface Potential Mapping Data Distribution

Table C-18: Shaft 19 Surface Potential Mapping Raw Data (mV)

	0"	3"	6"	9"	12"	15"	18"	21"
0"	-243	-238	-234	-231	-230	-225	-229	-234
3"	-242	-242	-238	-234	-235	-230	-234	-240
6"	-246	-246	-238	-235	-231	-235	-241	-247
9"	-256	-250	-242	-234	-235	-238	-243	-255
12"	-258	-251	-241	-232	-230	-235	-248	-265
15"	-265	-259	-249	-243	-238	-240	-248	-259
18"	-263	-258	-247	-243	-240	-241	-245	-249
21"	-260	-258	-250	-243	-244	-243	-246	-245
24"	-268	-263	-255	-247	-244	-245	-248	-249
27"	-275	-263	-250	-242	-240	-239	-246	-252

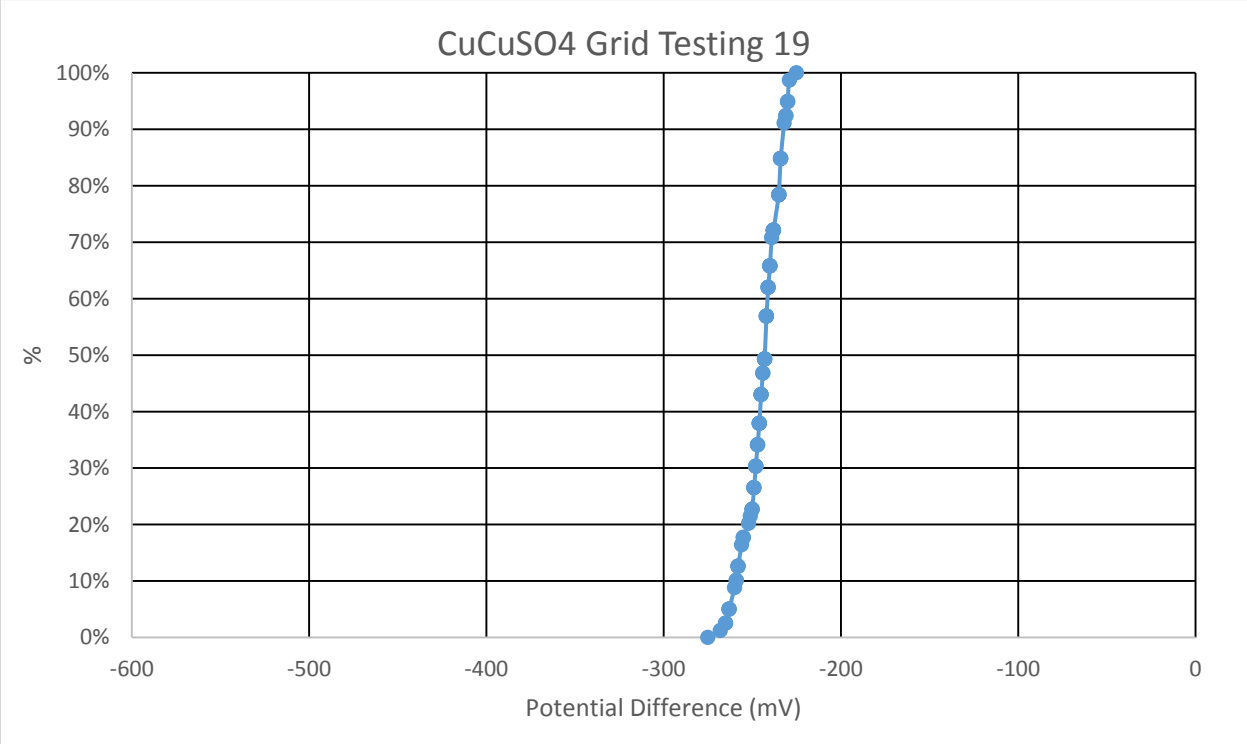

Figure C-18: Shaft 19 Surface Potential Mapping Data Distribution

Table C-19: Shaft 20 Surface Potential Mapping Raw Data (mV)

	0"	3"	6"	9"	12"	15"	18"	21"
0"	-239	-234	-225	-231	-235	-238	-243	-235
3"	-222	-231	-231	-231	-236	-236	-244	-247
6"	-239	-236	-235	-238	-239	-239	-241	-237
9"	-233	-233	-240	-241	-242	-242	-238	-242
12"	-241	-242	-241	-241	-242	-242	-242	-245
15"	-248	-244	-248	-245	-239	-239	-242	-243
18"	-253	-250	-251	-245	-245	-245	-242	-241
21"	-253	-252	-251	-246	-246	-246	-254	-245
24"	-251	-253	-250	-247	-247	-247	-250	-250
27"	-259	-259	-254	-253	-255	-255	-251	-249

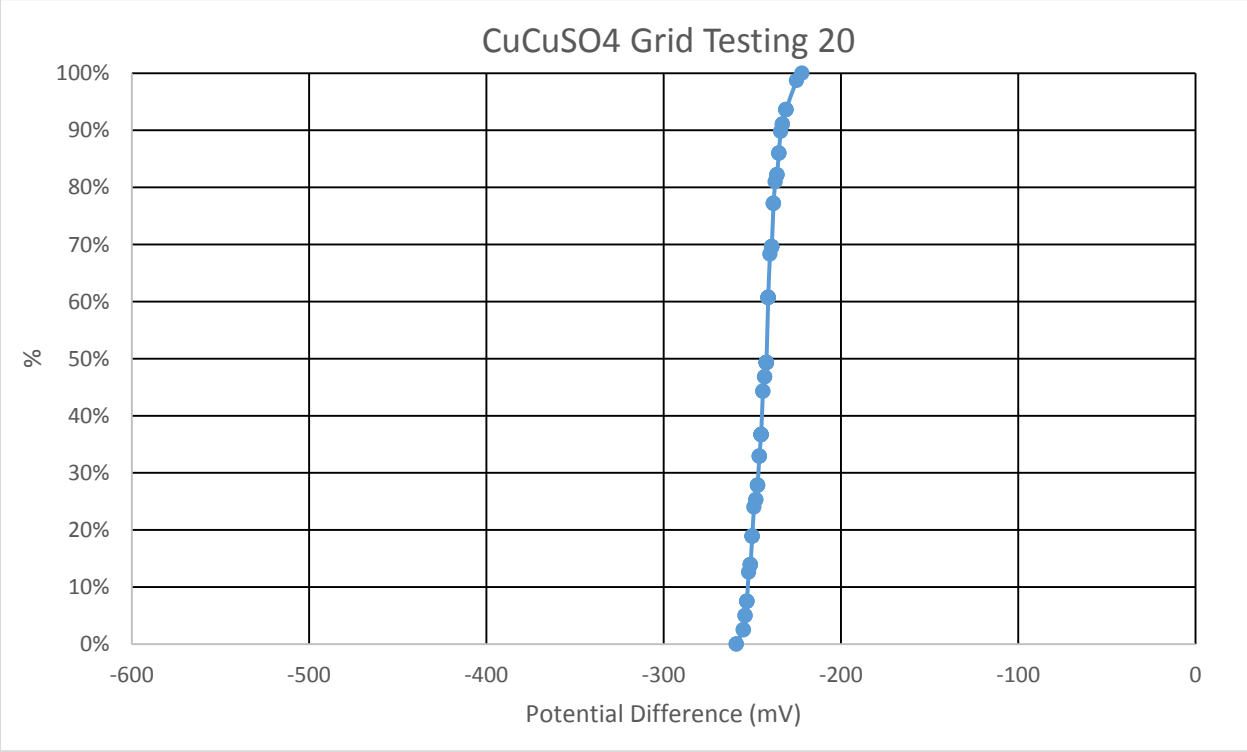

Figure C-19: Shaft 20 Surface Potential Mapping Data Distribution

Table C-20: Shaft 21 Surface Potential Mapping Raw Data (mV)

	0"	3"	6"	9"	12"	15"	18"	21"
0"	-491	-492	-495	-518	-552	-534	-548	-596
3"	-482	-489	-489	-493	-533	-524	-527	-500
6"	-480	-481	-489	-484	-508	-493	-509	-495
9"	-491	-489	-488	-497	-522	-493	-516	-502
12"	-485	-464	-488	-486	-511	-501	-522	-506
15"	-495	-494	-488	-492	-496	-494	-502	-511
18"	-500	-497	-508	-513	-536	-524	-529	-524
21"	-504	-505	-516	-528	-560	-538	-539	-516
24"	-508	-503	-508	-522	-540	-547	-556	-520
27"	-510	-510	-536	-538	-573	-558	-564	-542

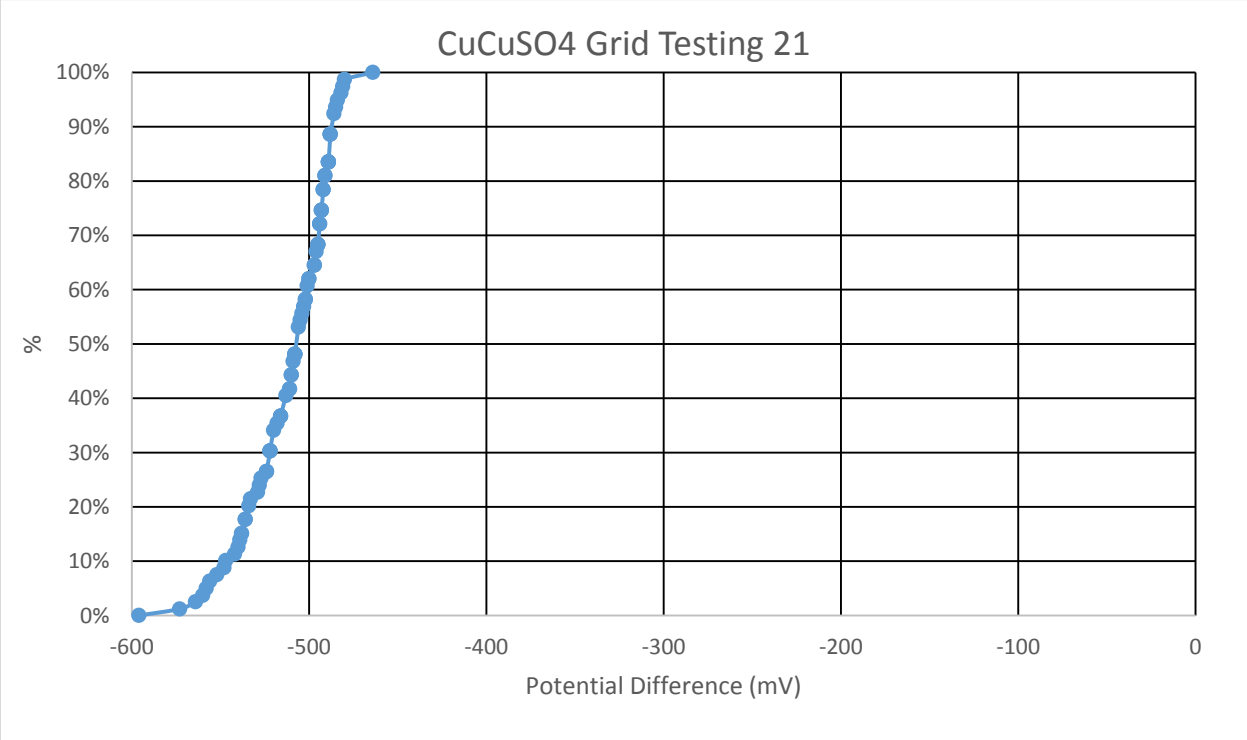

Figure C-20: Shaft 21 Surface Potential Mapping Data Distribution

Table C-21: Shaft 22 Surface Potential Mapping Raw Data (mV)

	0"	3"	6"	9"	12"	15"	18"	21"
0"	-268	-264	-248	-244	-243	-236	-230	-243
3"	-265	-273	-255	-247	-237	-237	-241	-248
6"	-281	-277	-268	-254	-244	-240	-248	-251
9"	-272	-281	-276	-261	-255	-252	-248	-250
12"	-263	-272	-261	-246	-238	-238	-237	-239
15"	-257	-259	-248	-240	-236	-234	-241	-246
18"	-261	-260	-247	-237	-237	-239	-244	-252
21"	-277	-278	-262	-249	-245	-247	-256	-269
24"	-279	-279	-266	-249	-245	-251	-259	-277
27"	-280	-279	-265	-250	246	-249	-256	-268

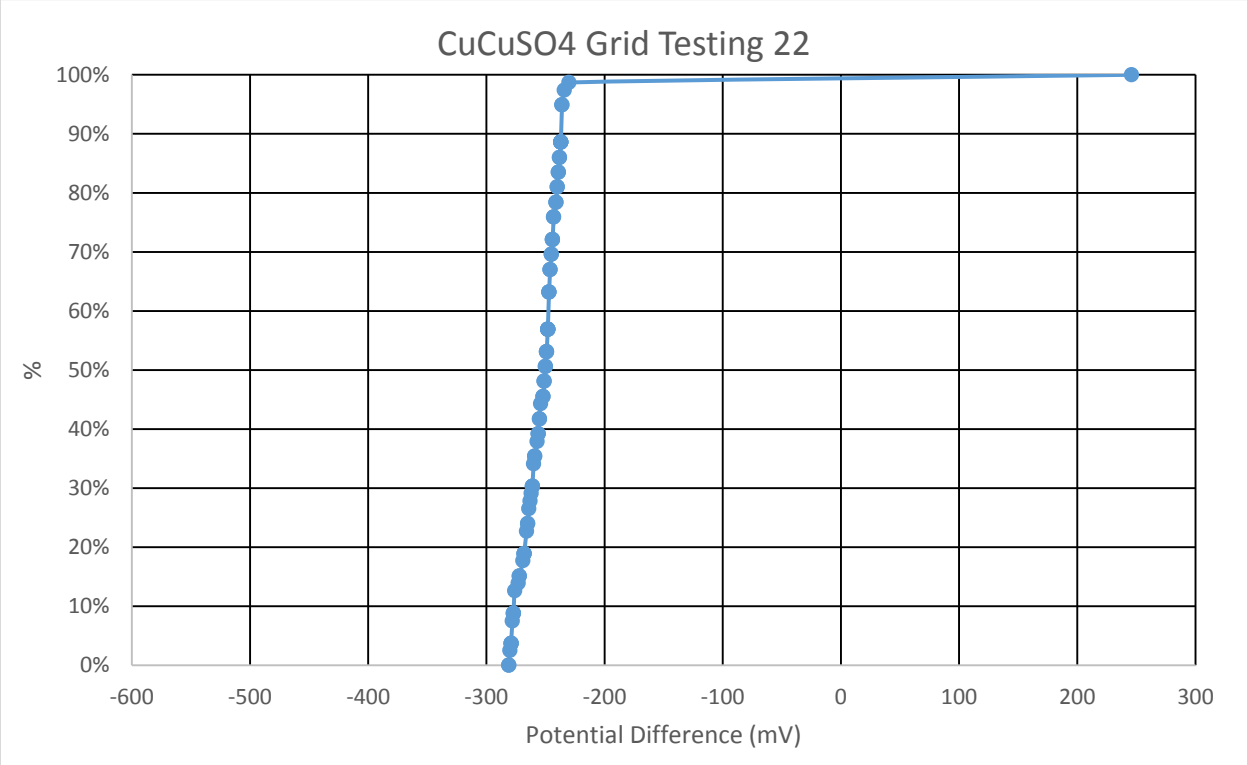

Figure C-21: Shaft 22 Surface Potential Mapping Data Distribution

Table C-22: Shaft 23 Surface Potential Mapping Raw Data (mV)

	0"	3"	6"	9"	12"	15"	18"	21"
0"	-273	-265	-264	-260	-258	-262	-263	-269
3"	-276	-263	-263	-260	-258	-262	-268	-273
6"	-272	-262	-263	-257	-258	-263	-270	-260
9"	-271	-260	-261	-255	-255	-282	-269	-261
12"	-271	-259	-258	-254	-253	-283	-271	-260
15"	-266	-256	-251	-248	-252	-255	-264	-277
18"	-265	-255	-253	-247	-249	-250	-258	-269
21"	-261	-254	-246	-243	-242	-246	-250	-257
24"	-261	-252	-246	-241	-236	-241	-245	-254
27"	-261	-254	-246	-237	-233	-238	-243	-250

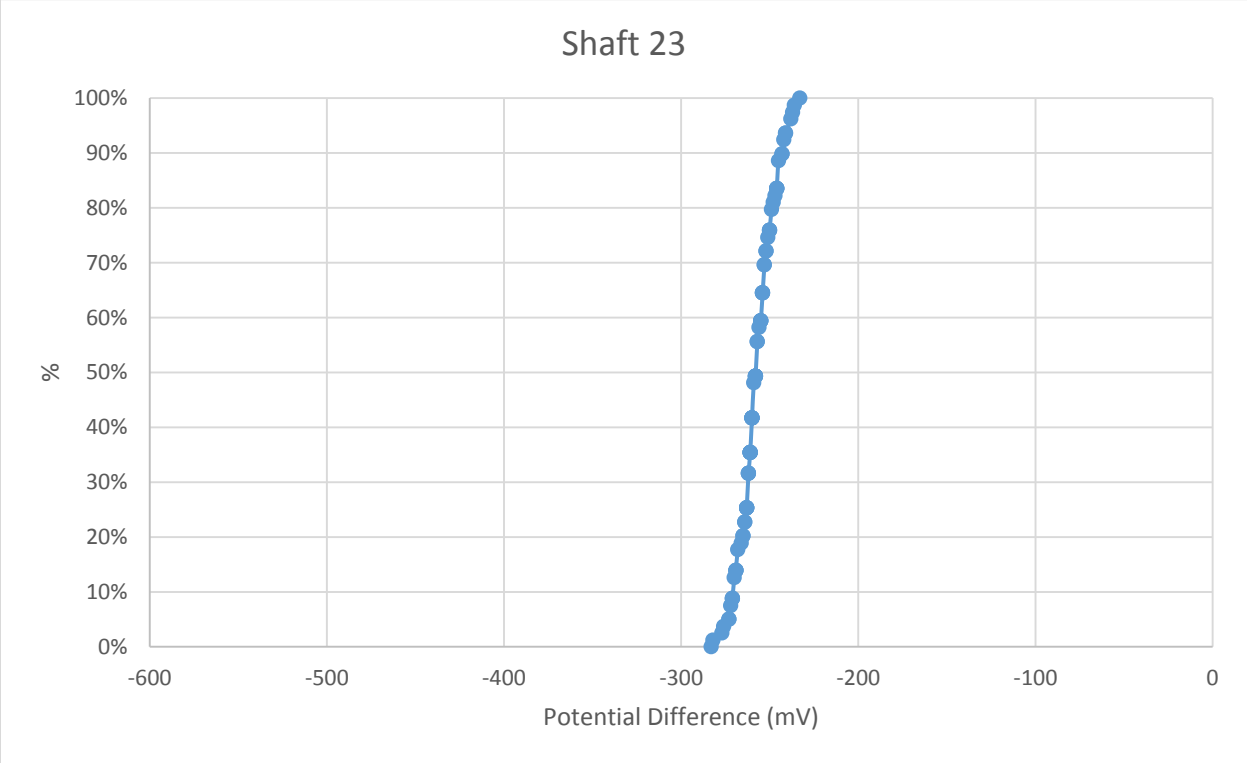

Figure C-22: Shaft 23 Surface Potential Mapping Data Distribution

Table C-23: Shaft 24 Surface Potential Mapping Raw Data (mV)

	0"	3"	6"	9"	12"	15"	18"	21"
0"	-450	-453	-449	-452	-464	-446	-413	-393
3"	-439	-447	-443	-445	-456	-441	-410	-394
6"	-436	-443	-441	-430	-464	-443	-416	-400
9"	-433	-441	-442	-442	-469	-455	-425	-404
12"	-429	-436	-438	-444	-464	-454	-423	-404
15"	-423	-429	-437	-444	-465	-456	-424	-407
18"	-414	-421	-425	-434	-454	-433	-414	-403
21"	-411	-412	-421	-425	-437	-422	-398	-394
24"	-410	-408	-408	-408	-412	-401	-390	-389
27"	-404	-399	-395	-405	-403	-395	-389	-384

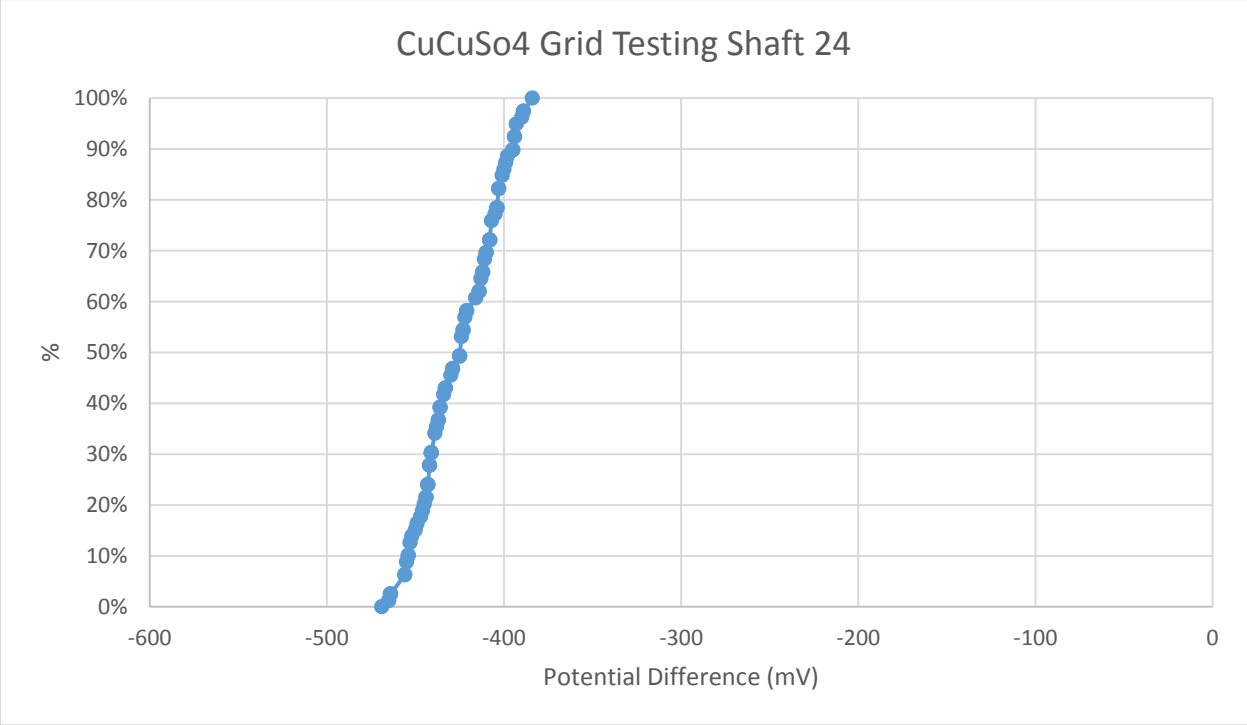

Figure C-23: Shaft 24 Surface Potential Mapping Data Distribution

APPENDIX D
CORING SPECIMEN LOGS

Shaft 6	
Slurry	water
Viscosity	26 sec
Concrete Mix	Type IV
Concrete Compressive Strength	4530 psi

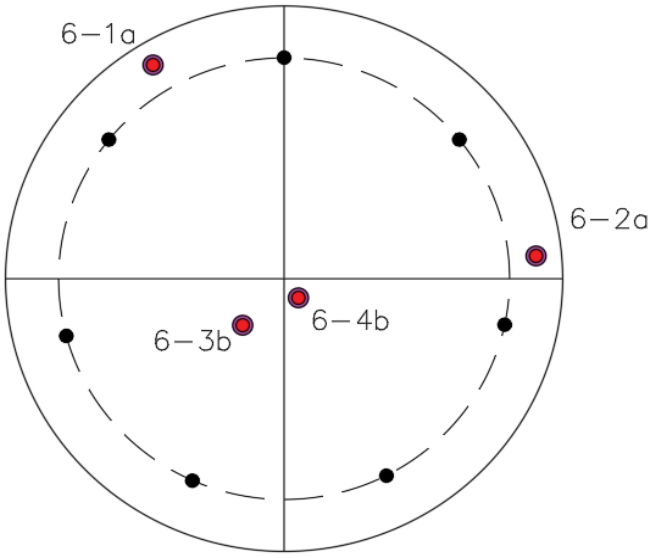

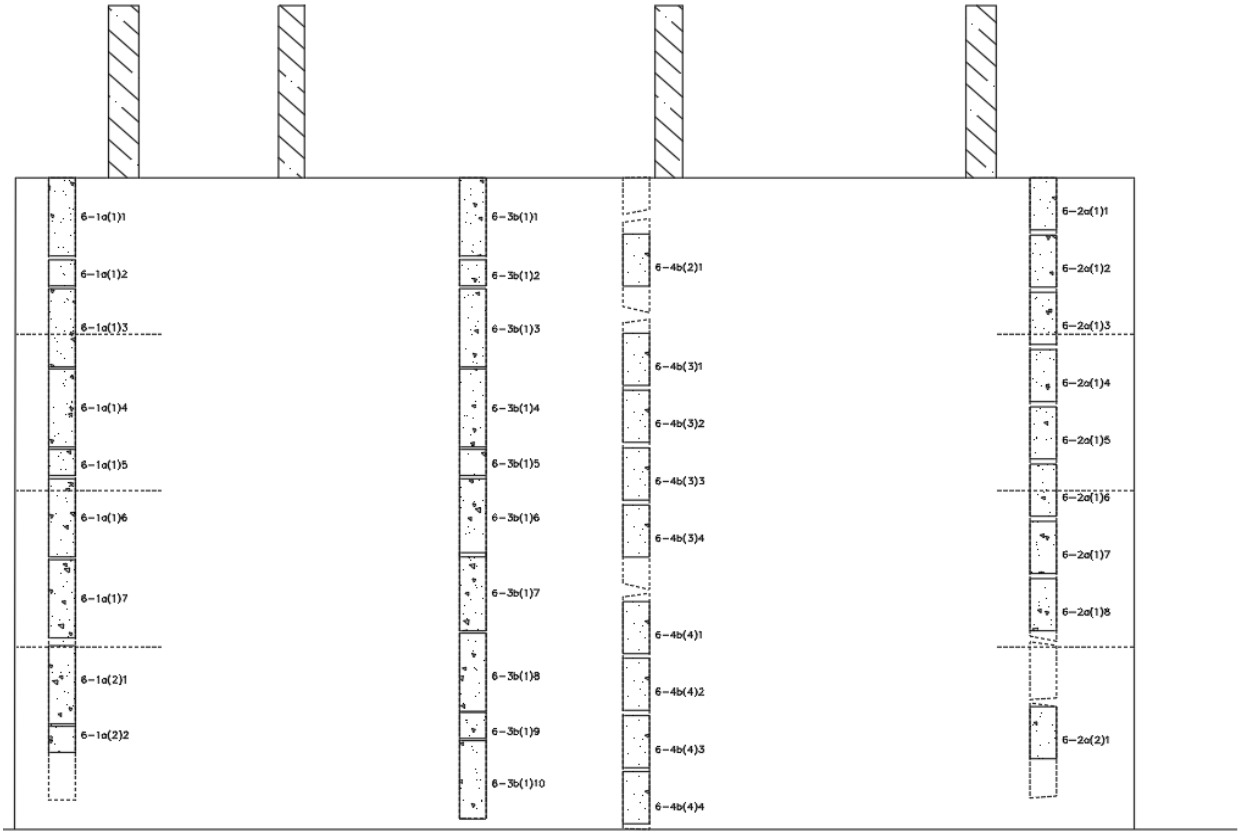

Figure D-1: Shaft 6 coring overview

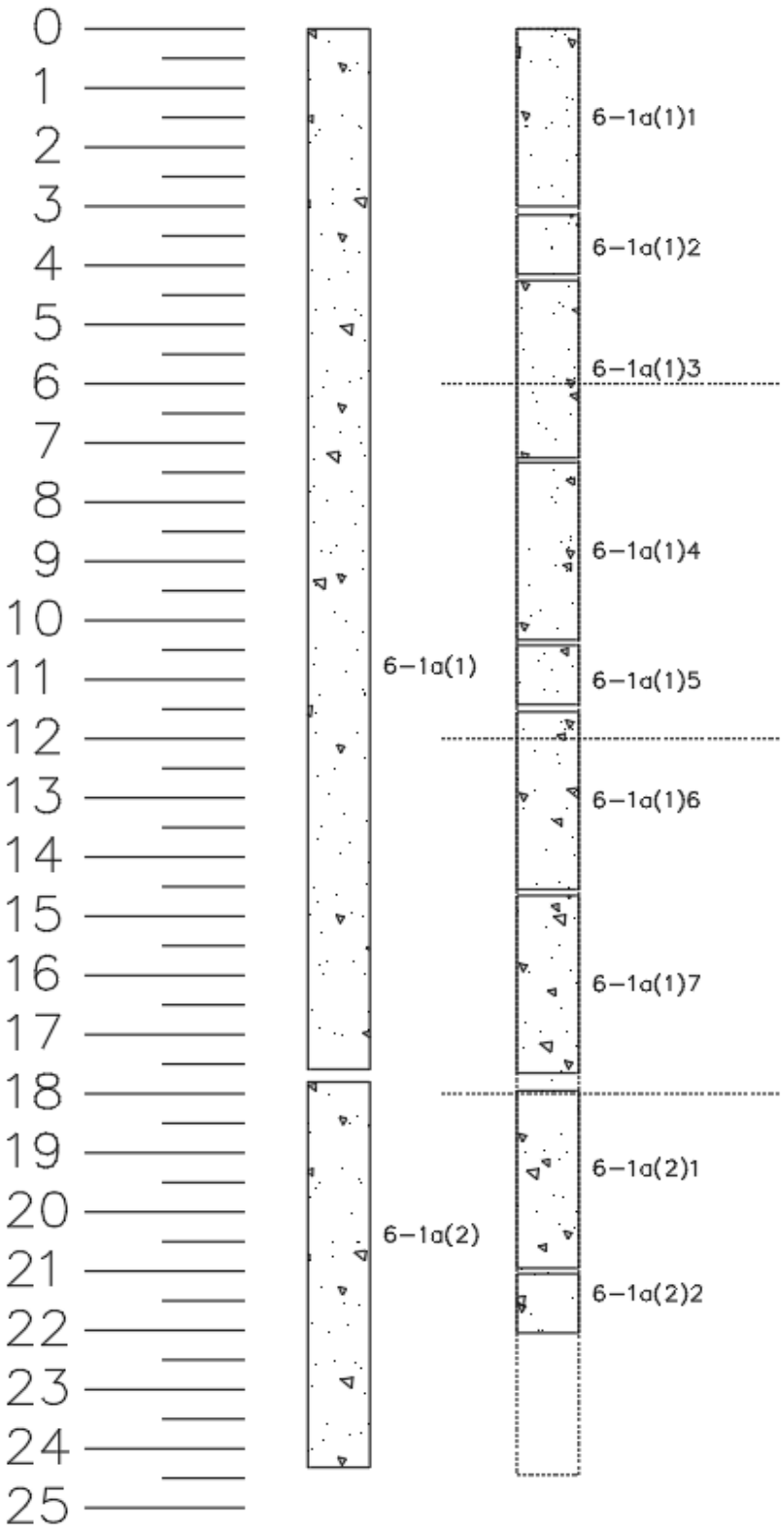

Figure D-2: 6-1a core log

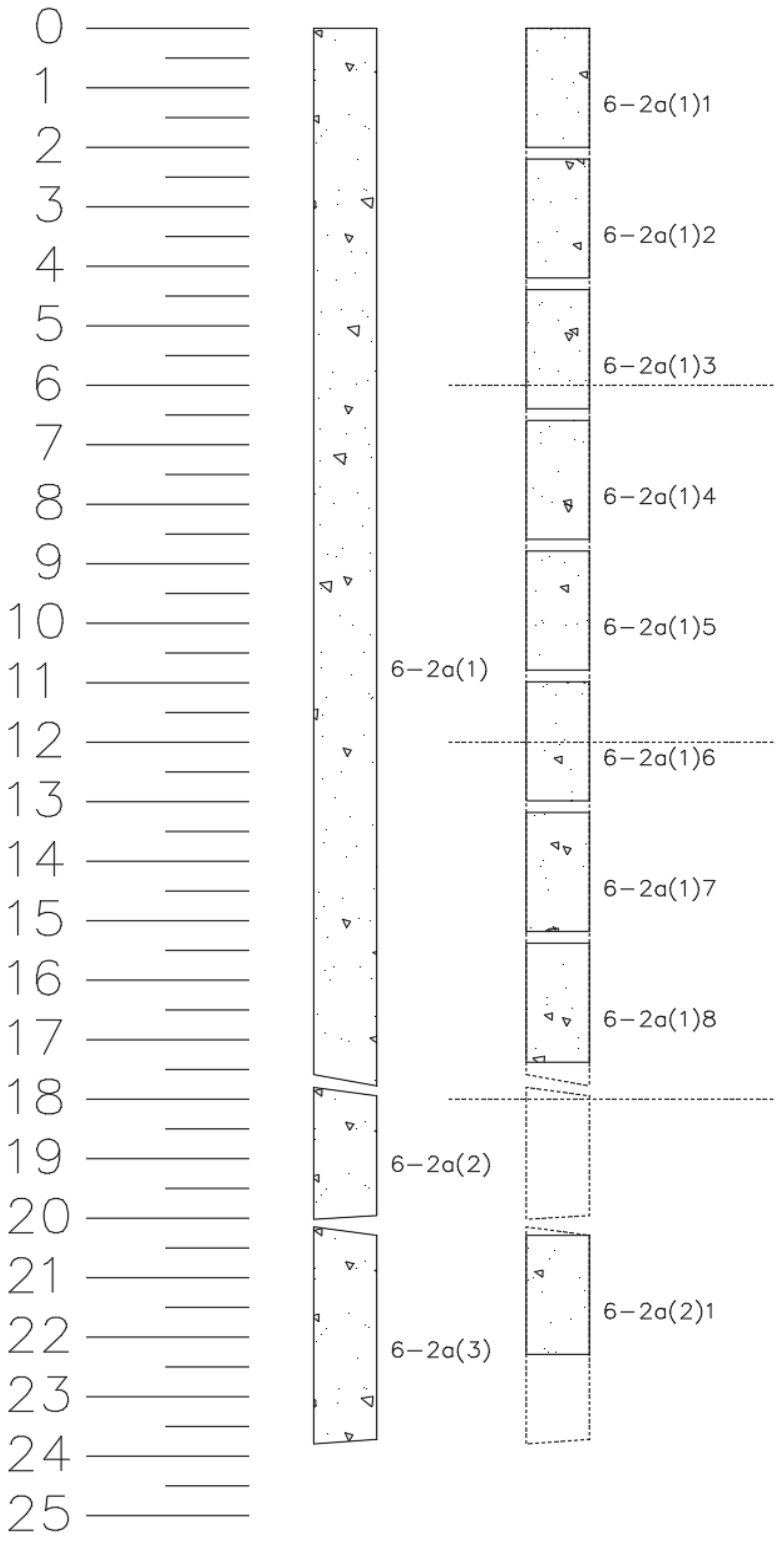

Figure D-3: 6-2a core log

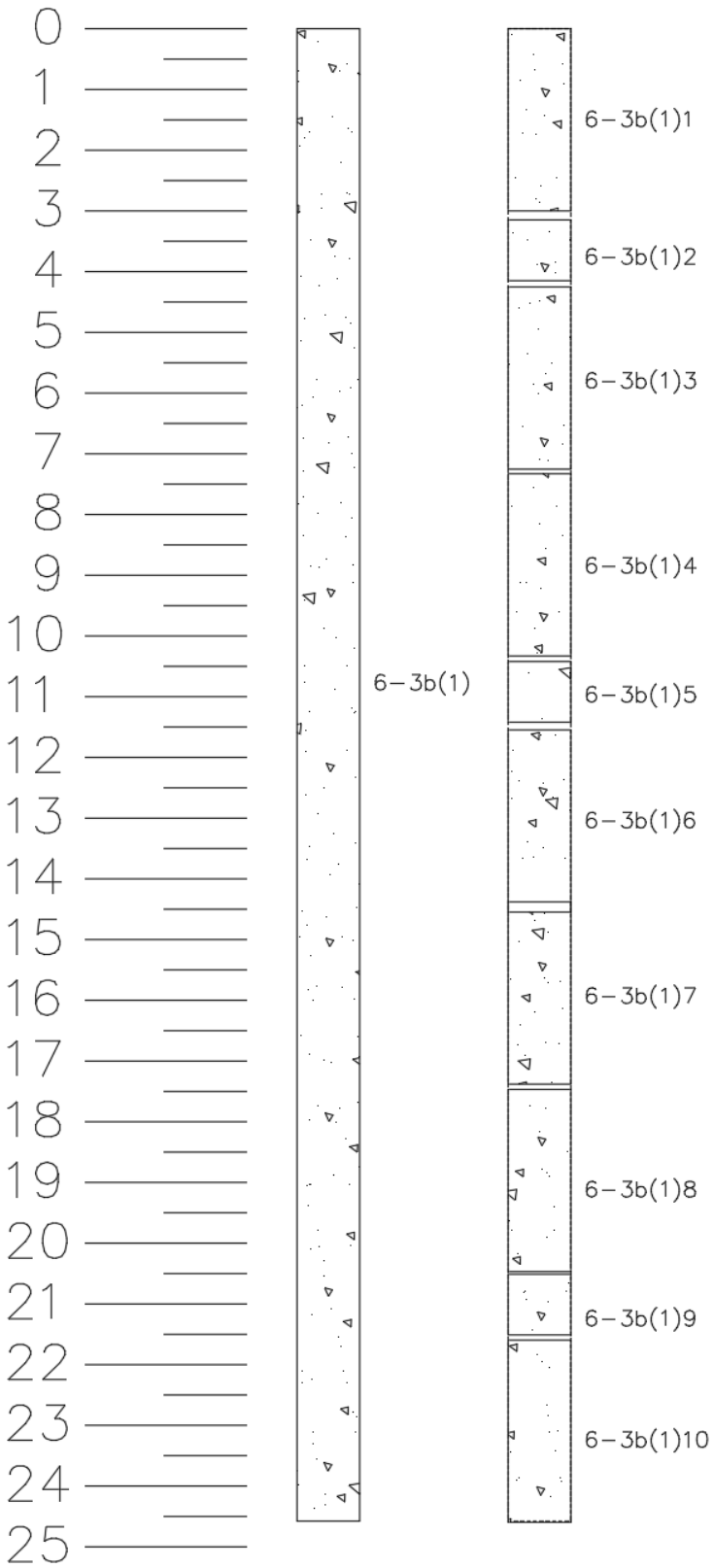

Figure D-4: 6-3b core log

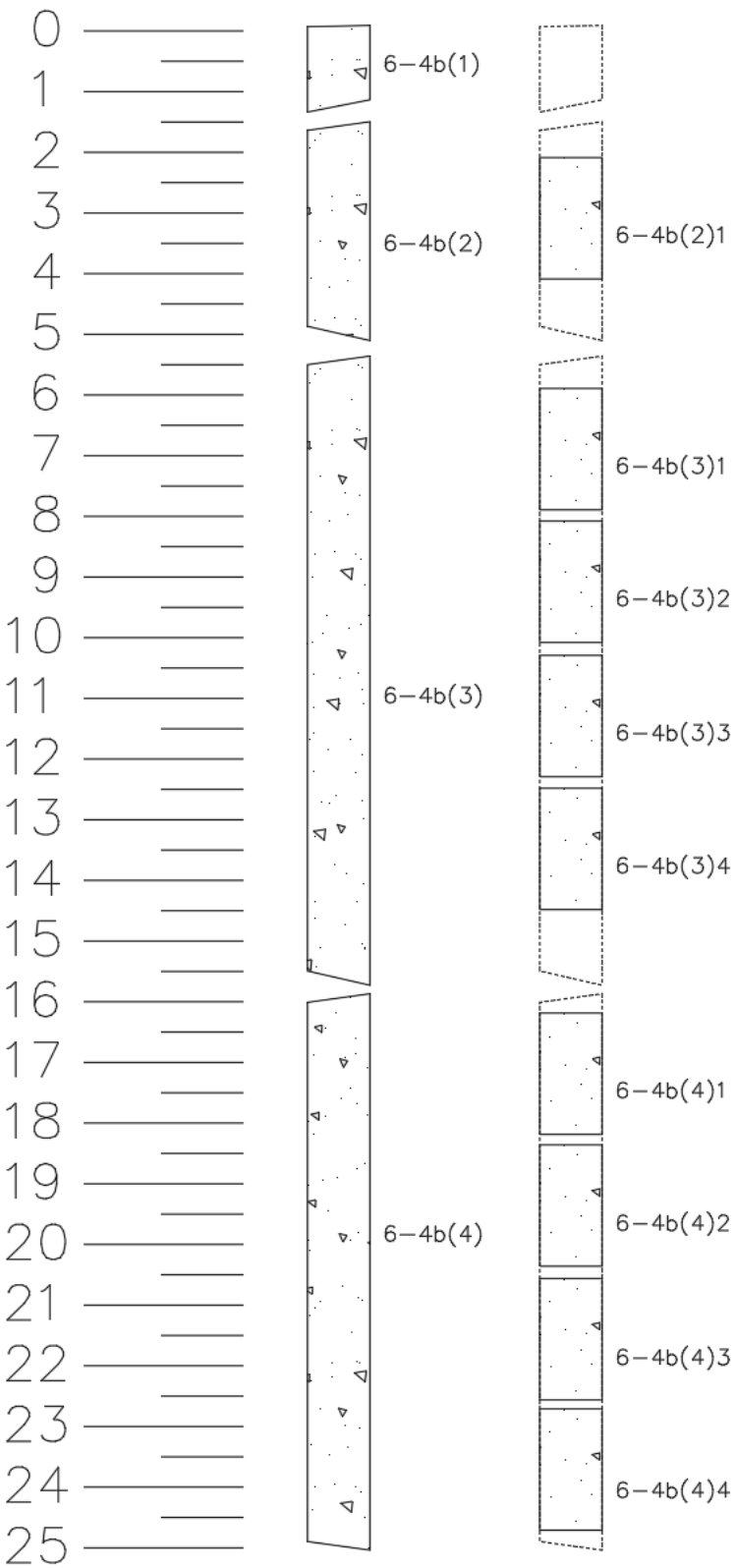

Figure D-5: 6-4b core log

Shaft 9	
Slurry	Bentonite
Viscosity	50 sec
Concrete Mix	Type IV
Concrete Compressive Strength	4530 psi

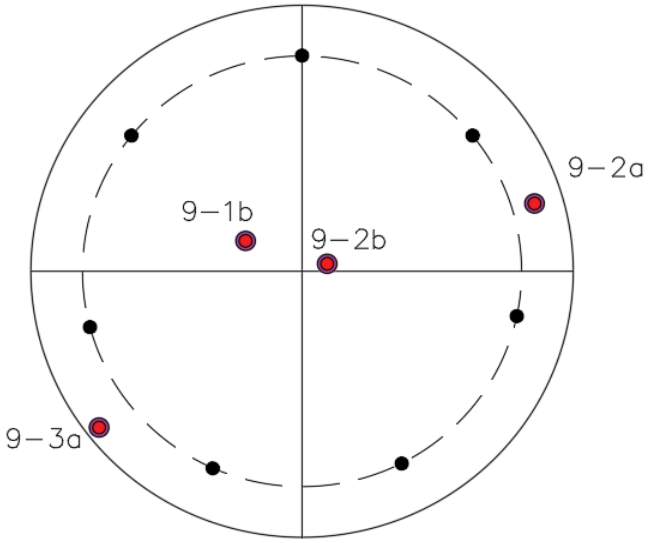

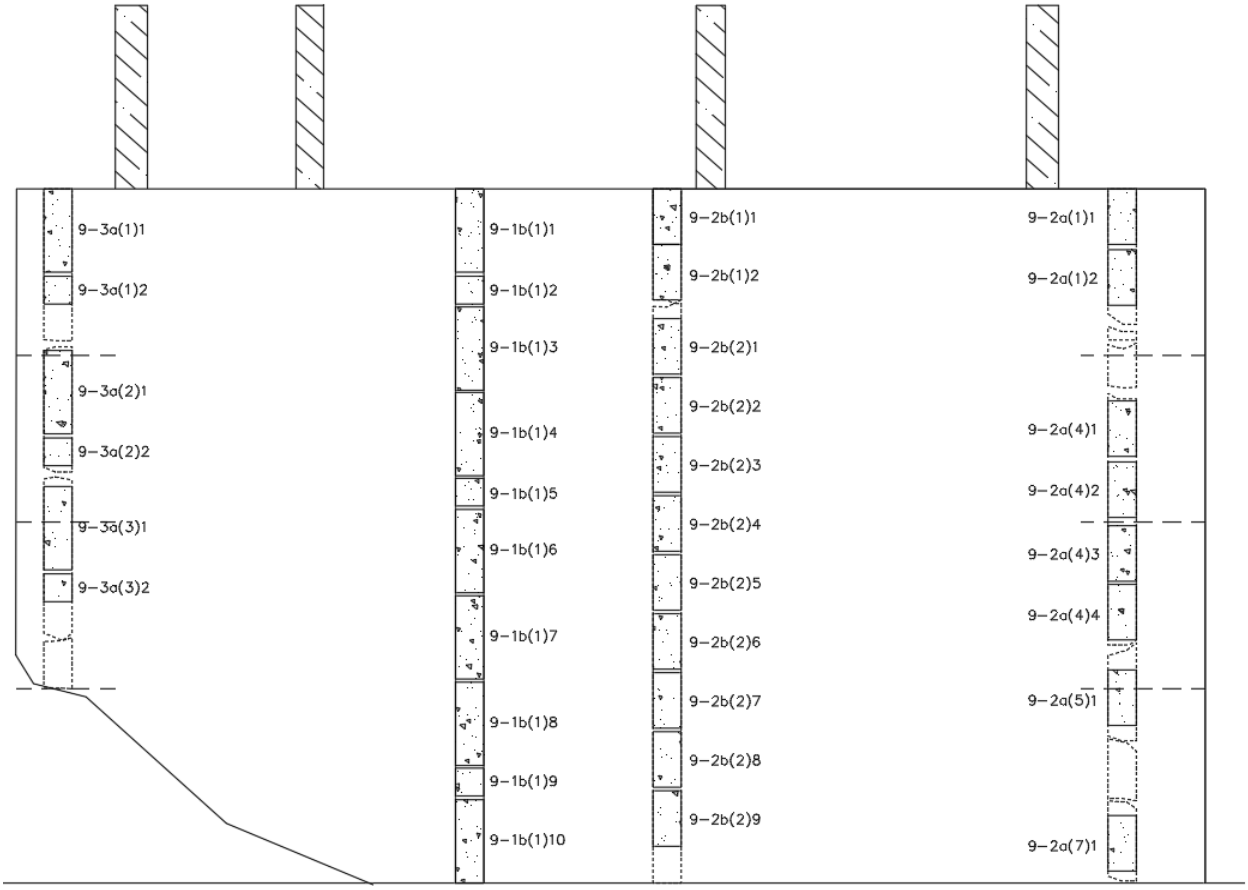

Figure D-6: Shaft 9 coring overview

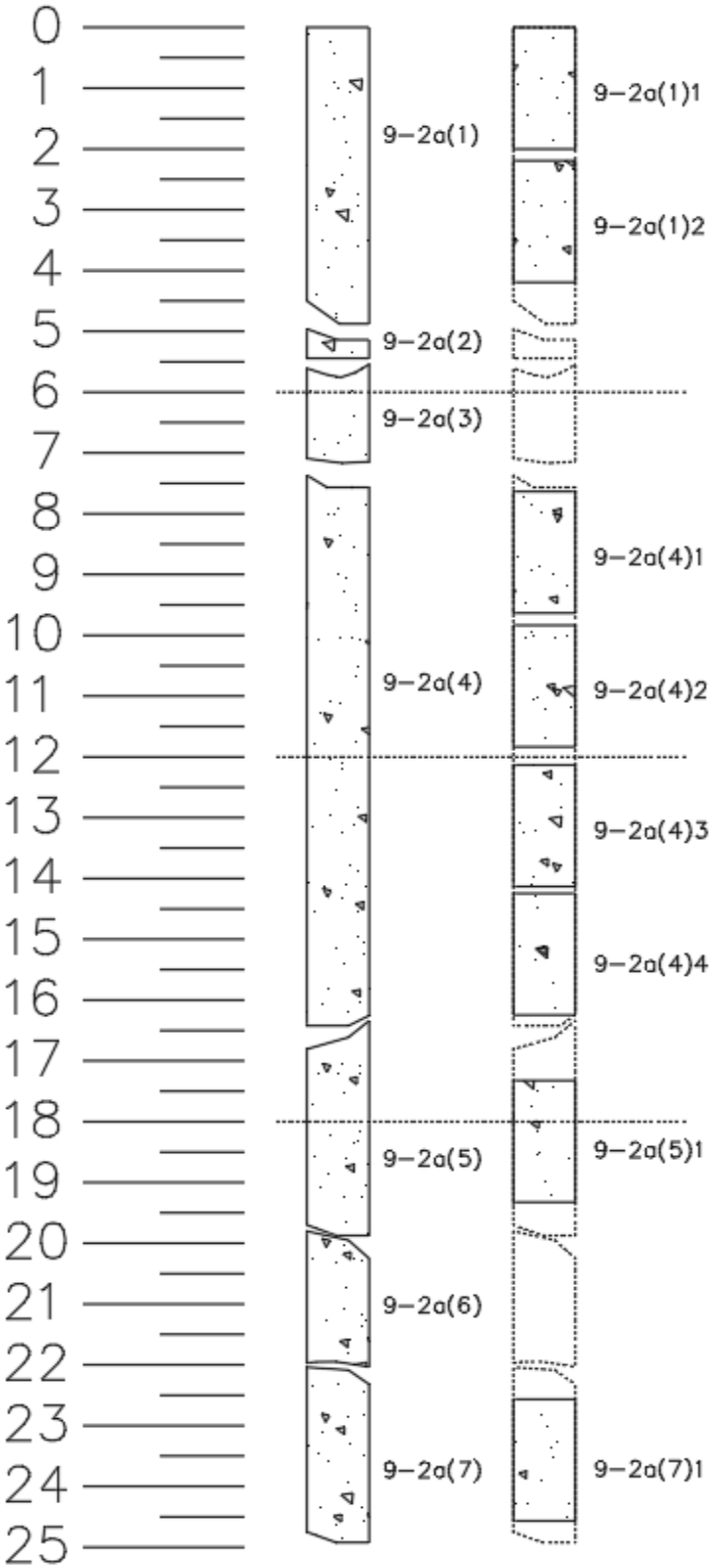

Figure D-7: 9-2a core log

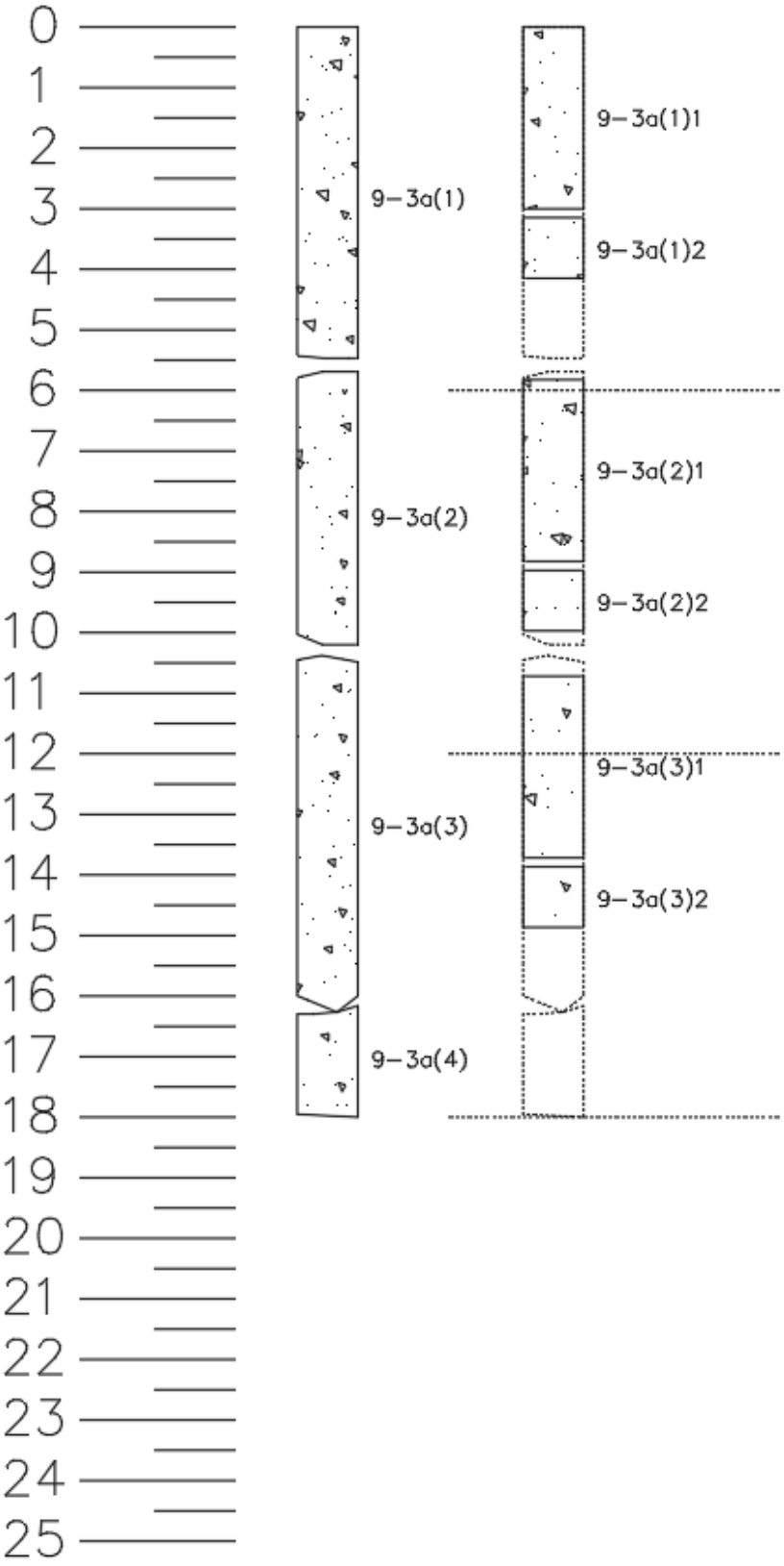

Figure D-8: 9-3a core log

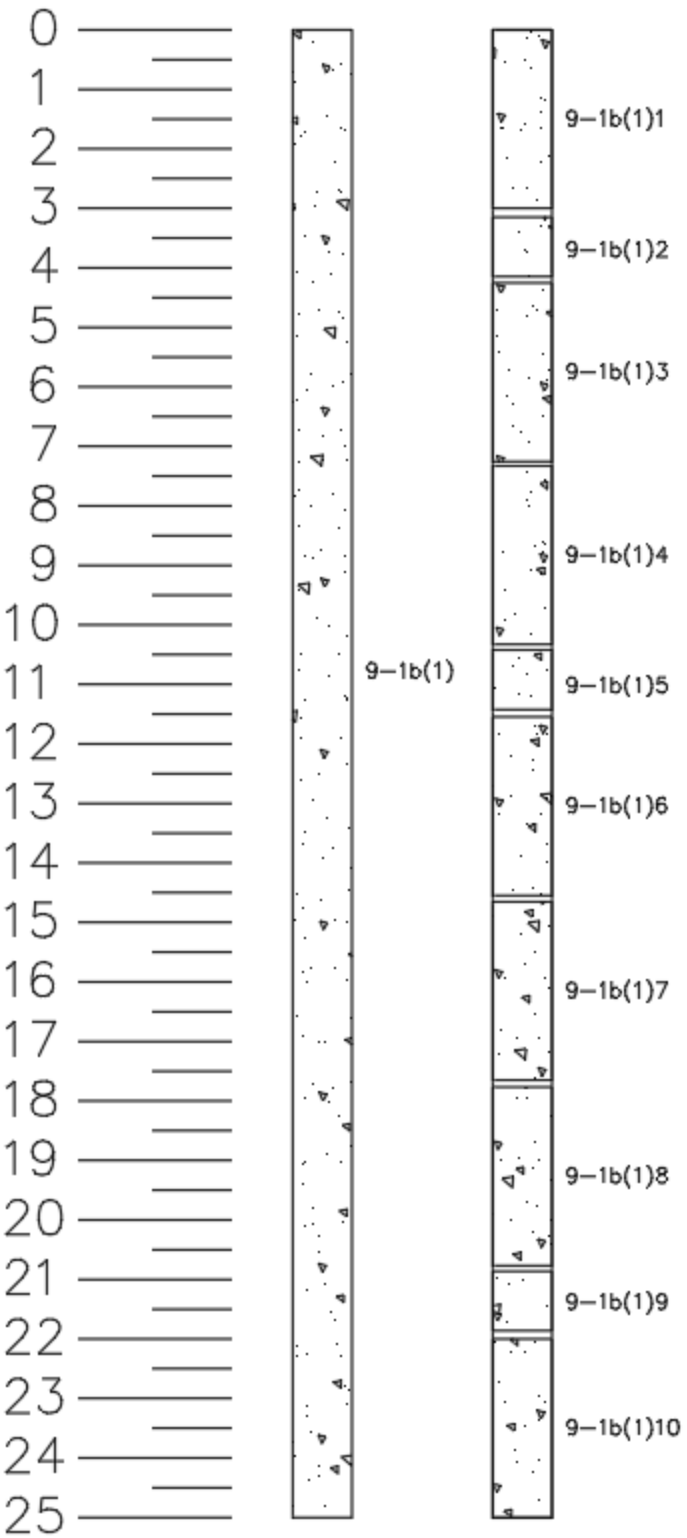

Figure D-9: 9-1b core log

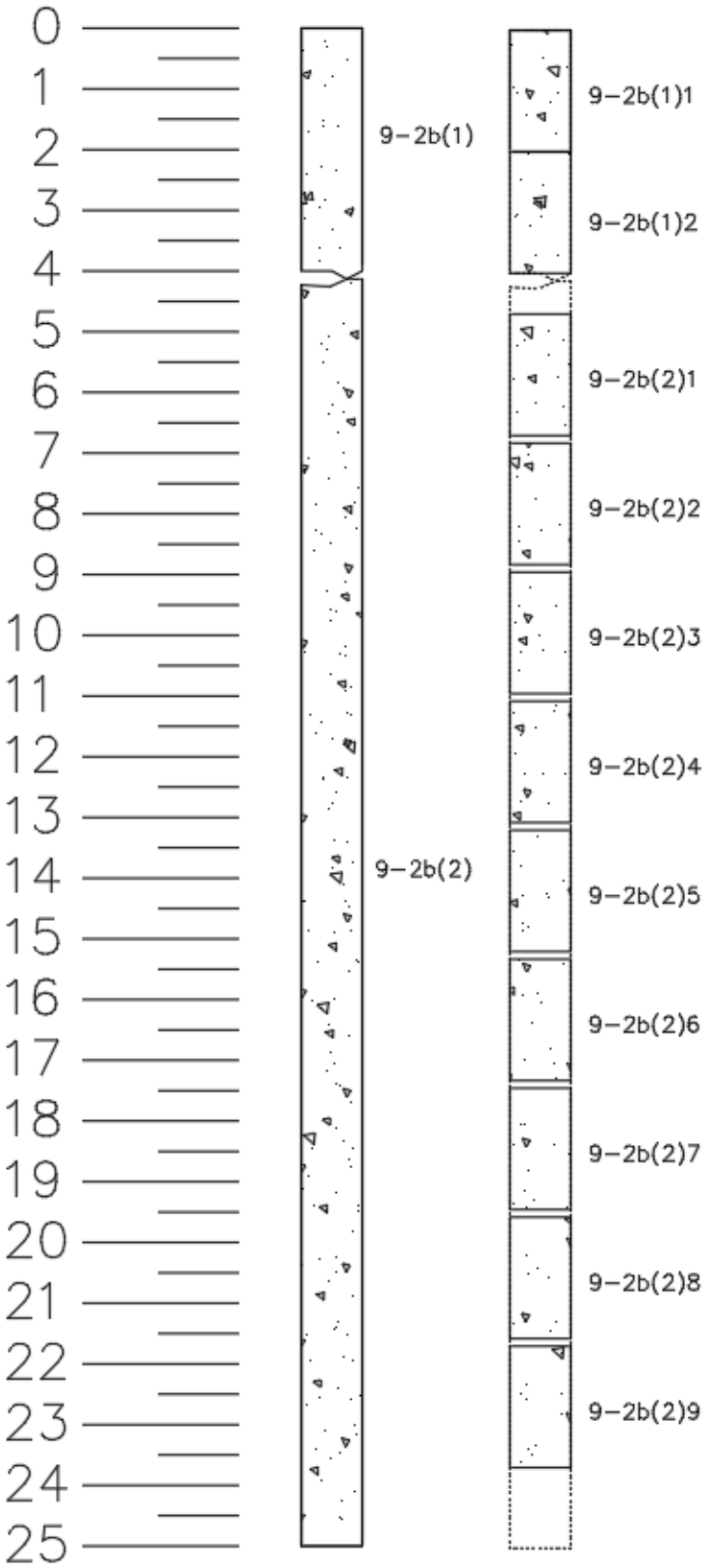

Figure D-10: 9-2b core log

Shaft 11	
Slurry	Polymer
Viscosity	65 sec
Concrete Mix	Type IV
Concrete Compressive Strength	4530 psi

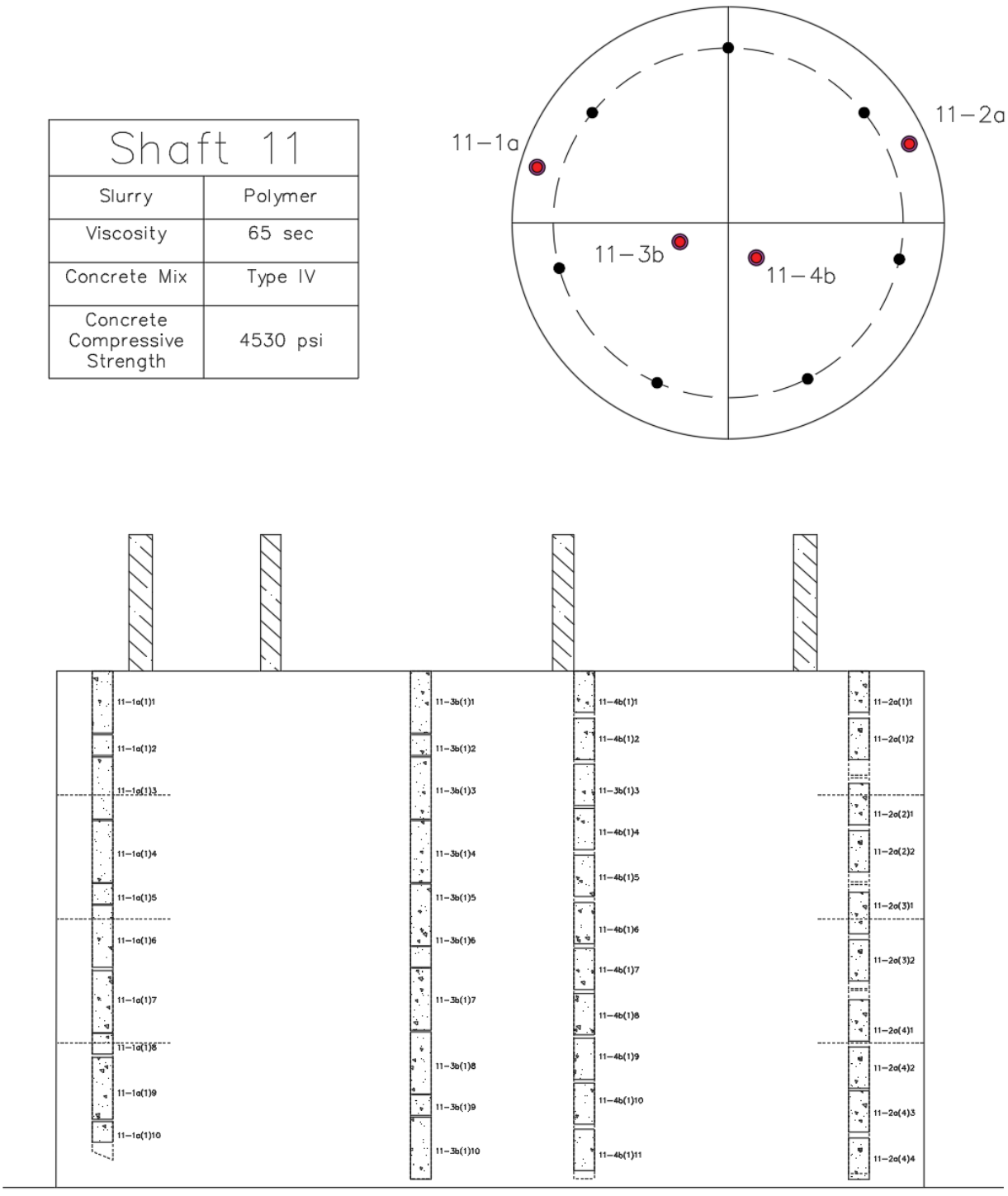

Figure D-11: Shaft 11 coring overview

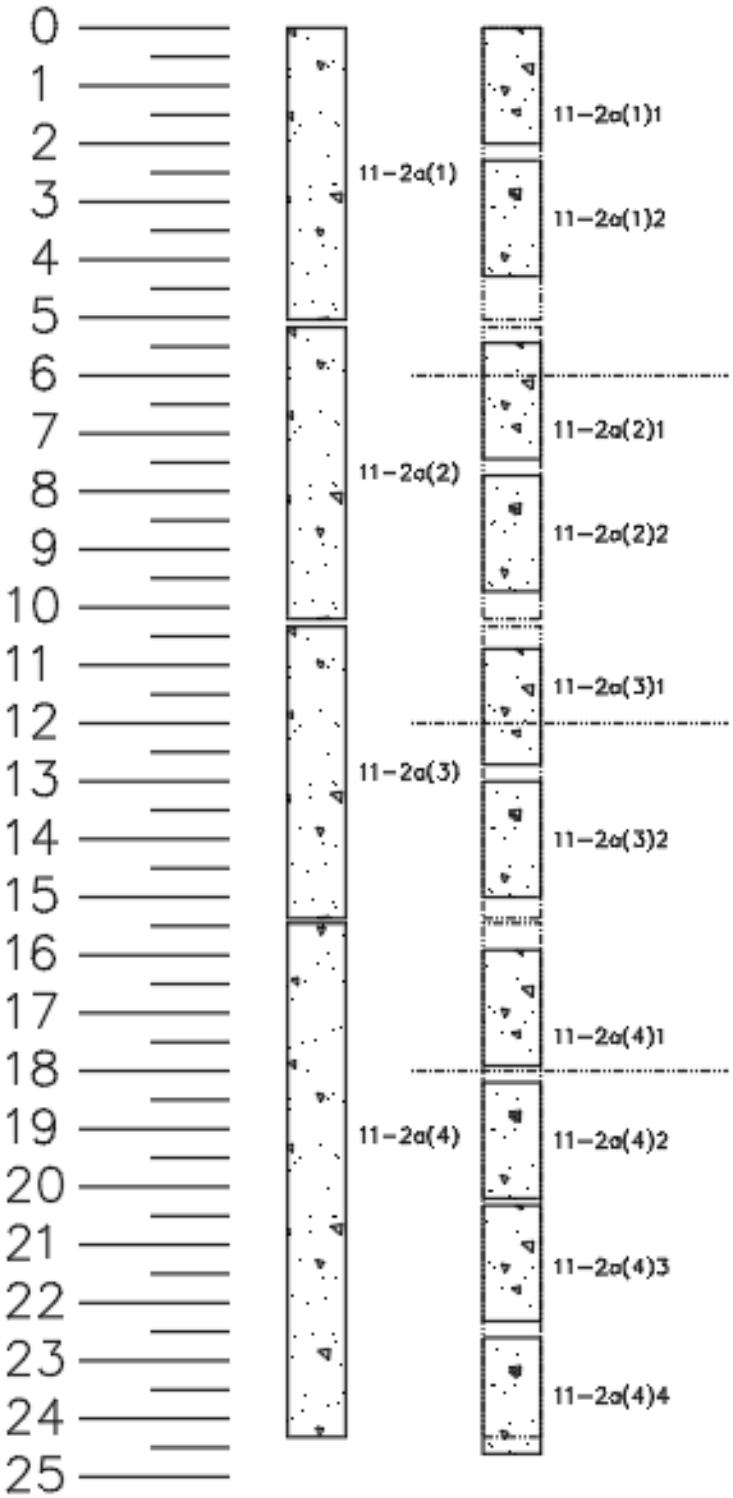

Figure D-12: 11-2a core log

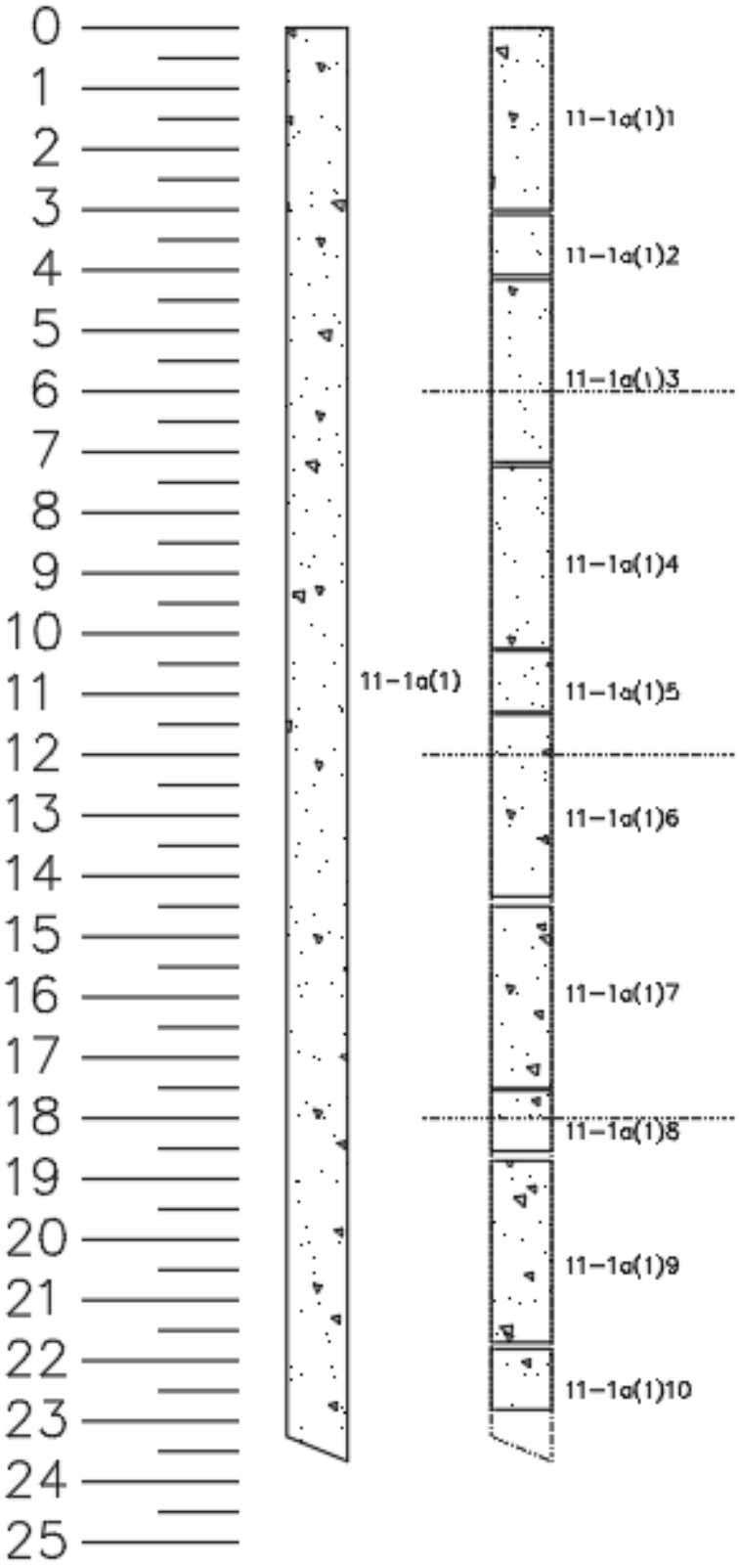

Figure D-13: 11-1a core log

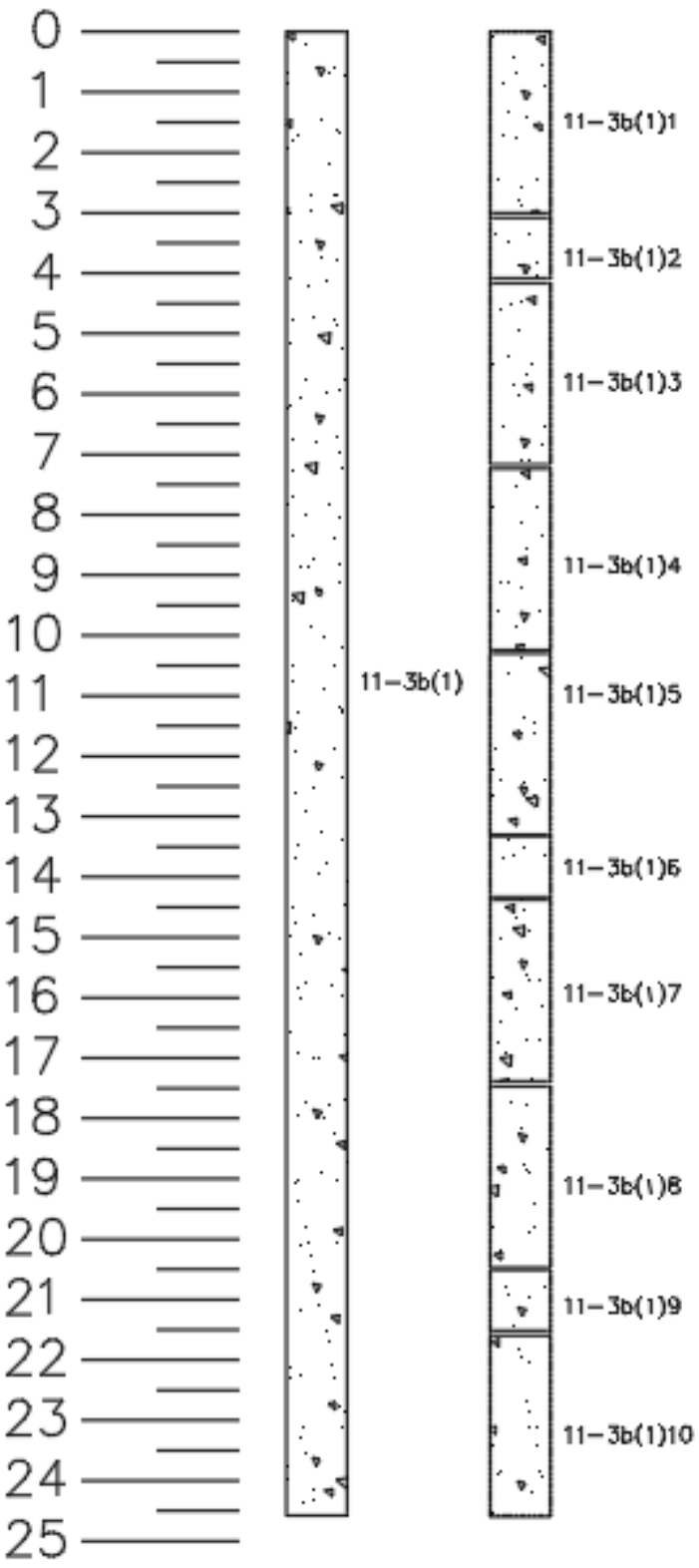

Figure D-14: 11-3b core log

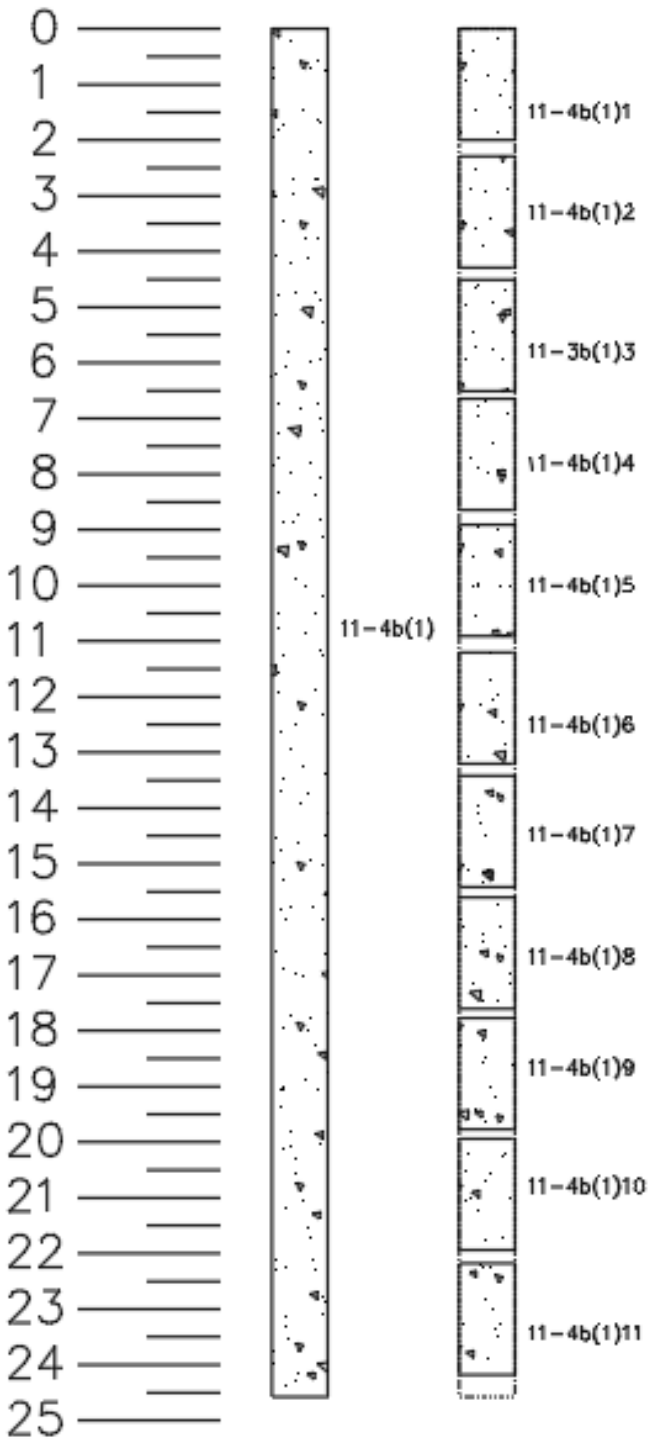

Figure D-15: 11-4b core log

APPENDIX E
CORING DATA PLOTS-

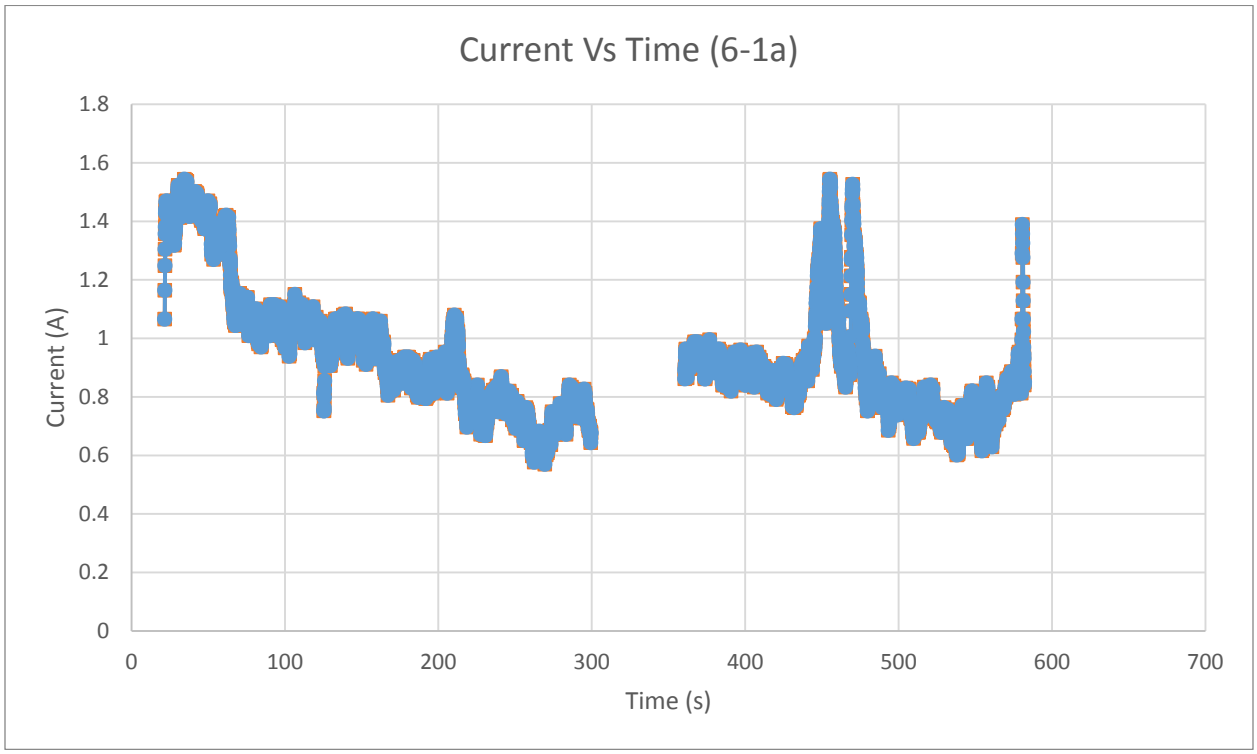

Figure E-1: Core 6-1a current vs time plot

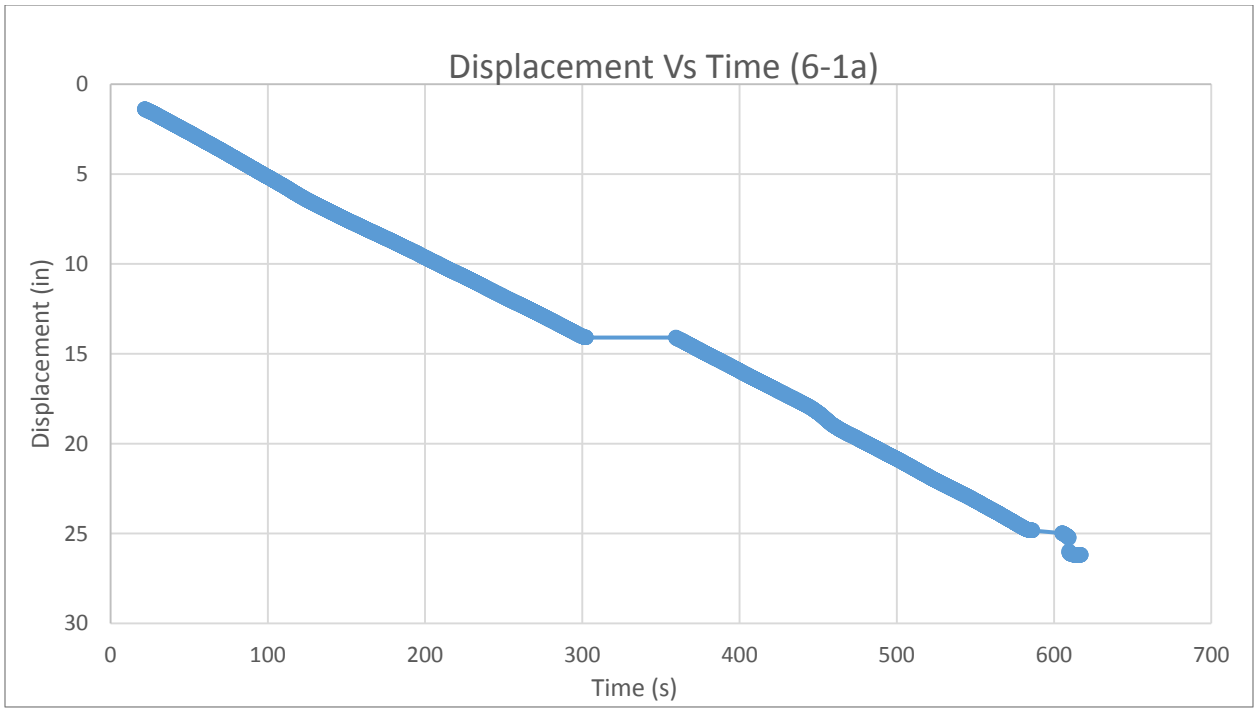

Figure E-2: Core 6-1a displacement vs time plot

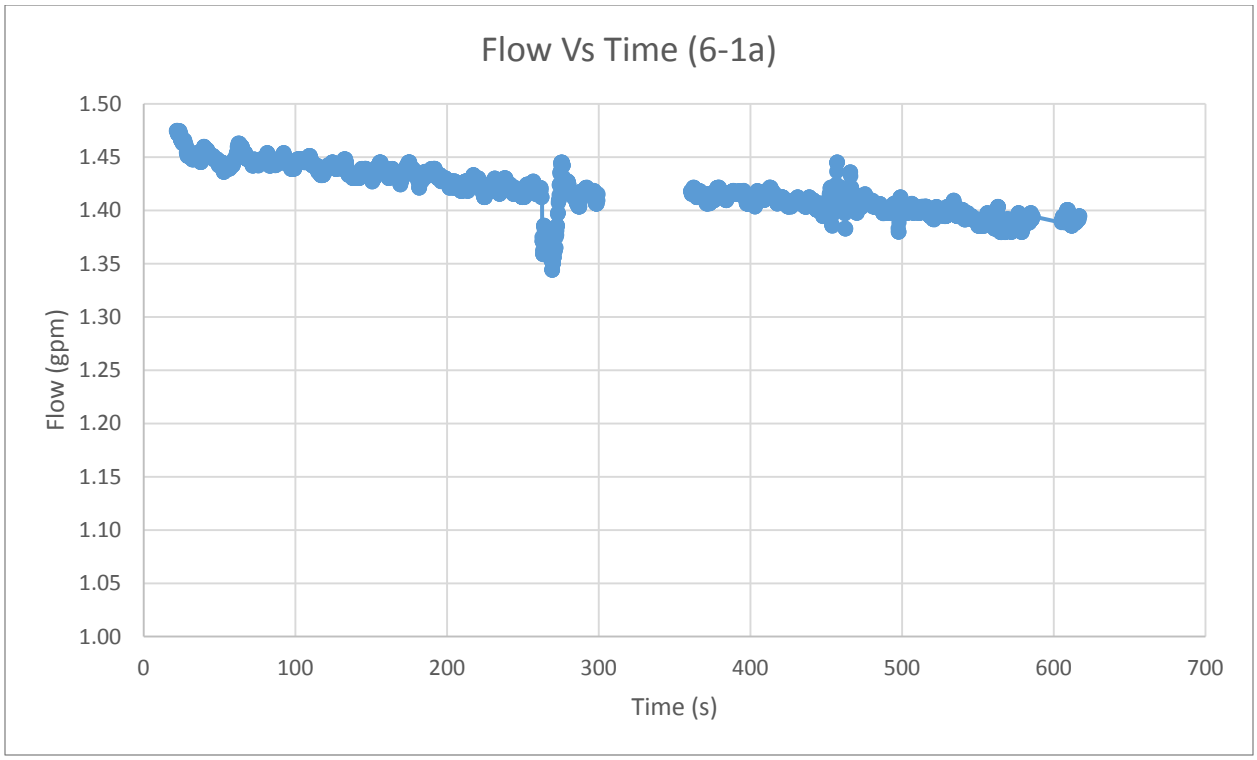

Figure E-3: Core 6-1a flow vs time plot

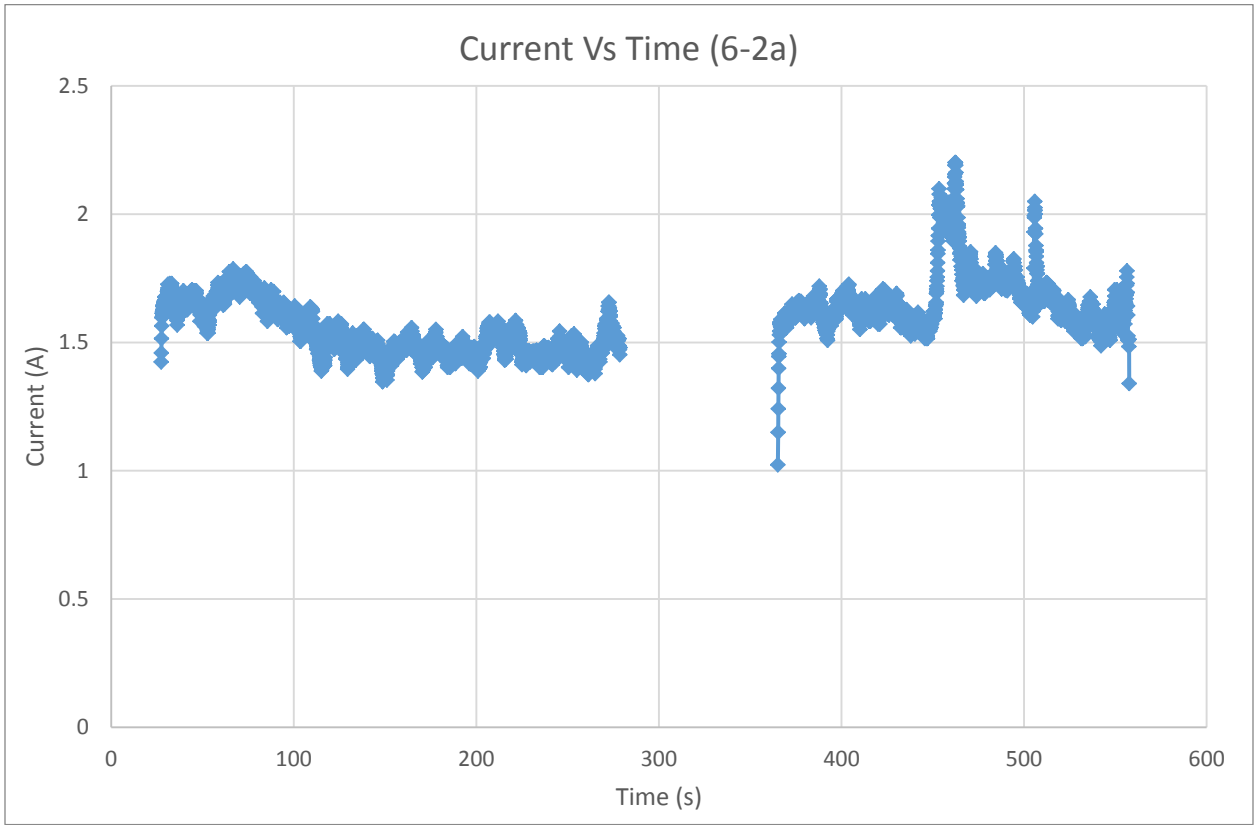

Figure E-4: Core 6-2a current vs time plot

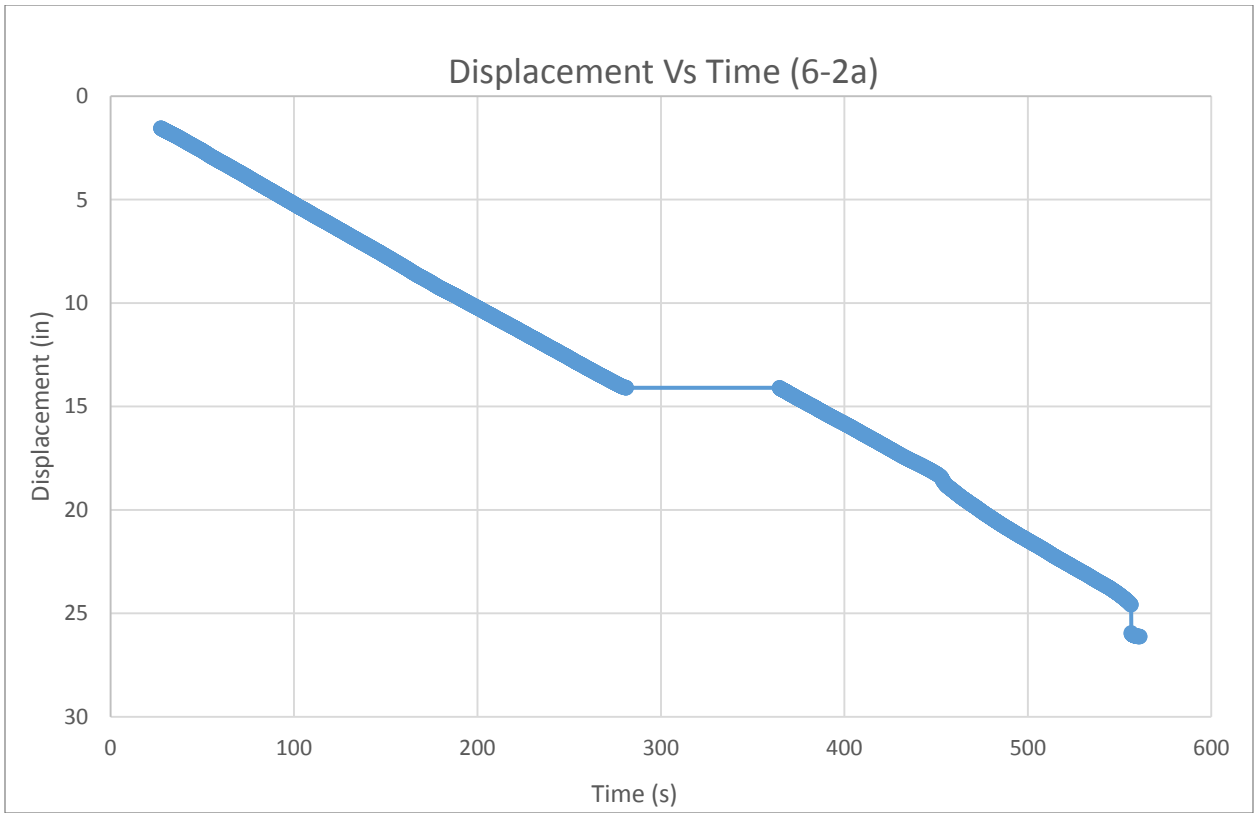

Figure E-5: Core 6-2a displacement vs time plot

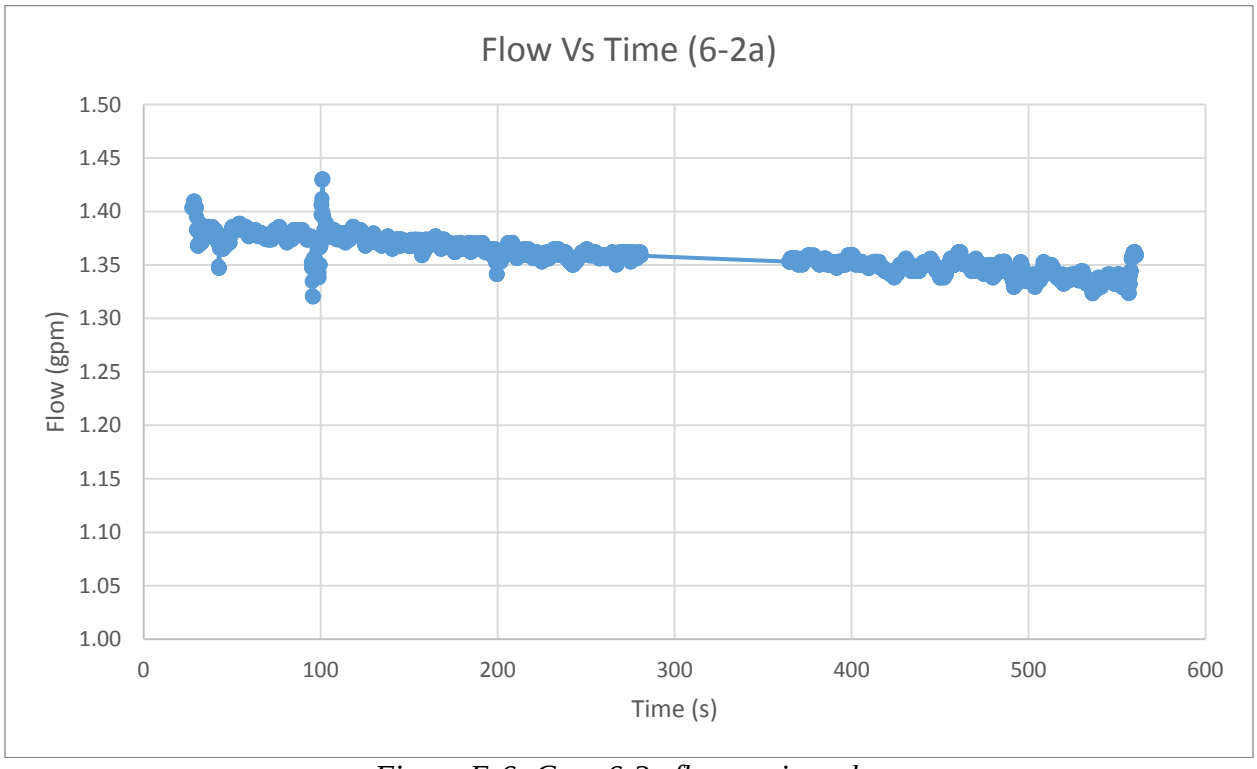

Figure E-6: Core 6-2a flow vs time plot

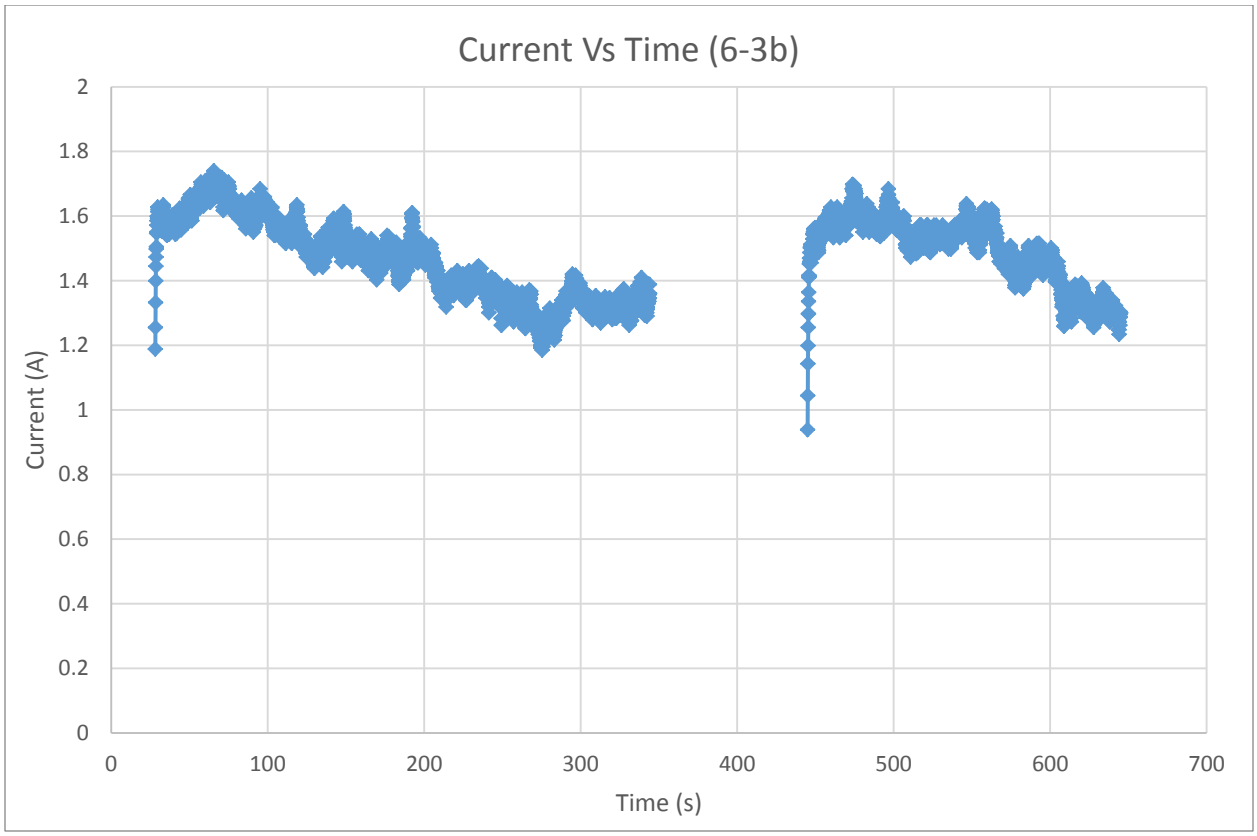

Figure E-7: Core 6-3b current vs time plot

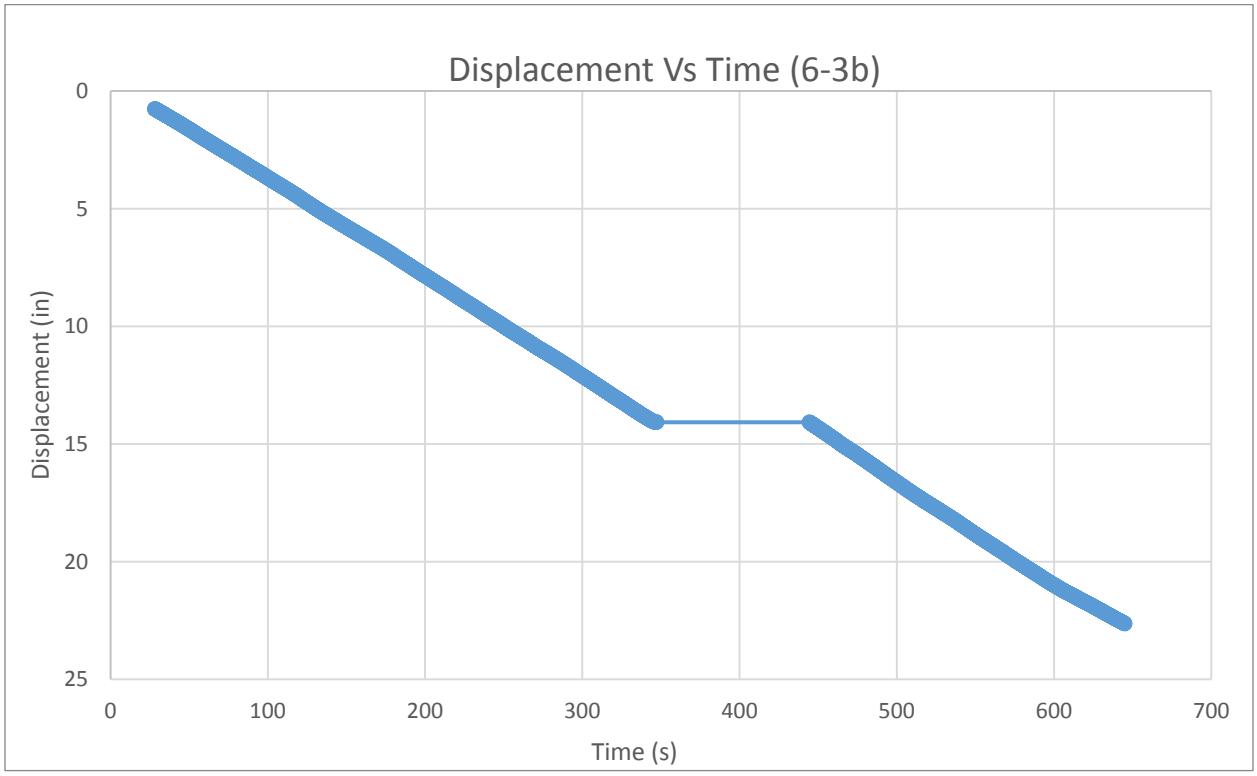

Figure E-8: Core 6-3b displacement vs time plot

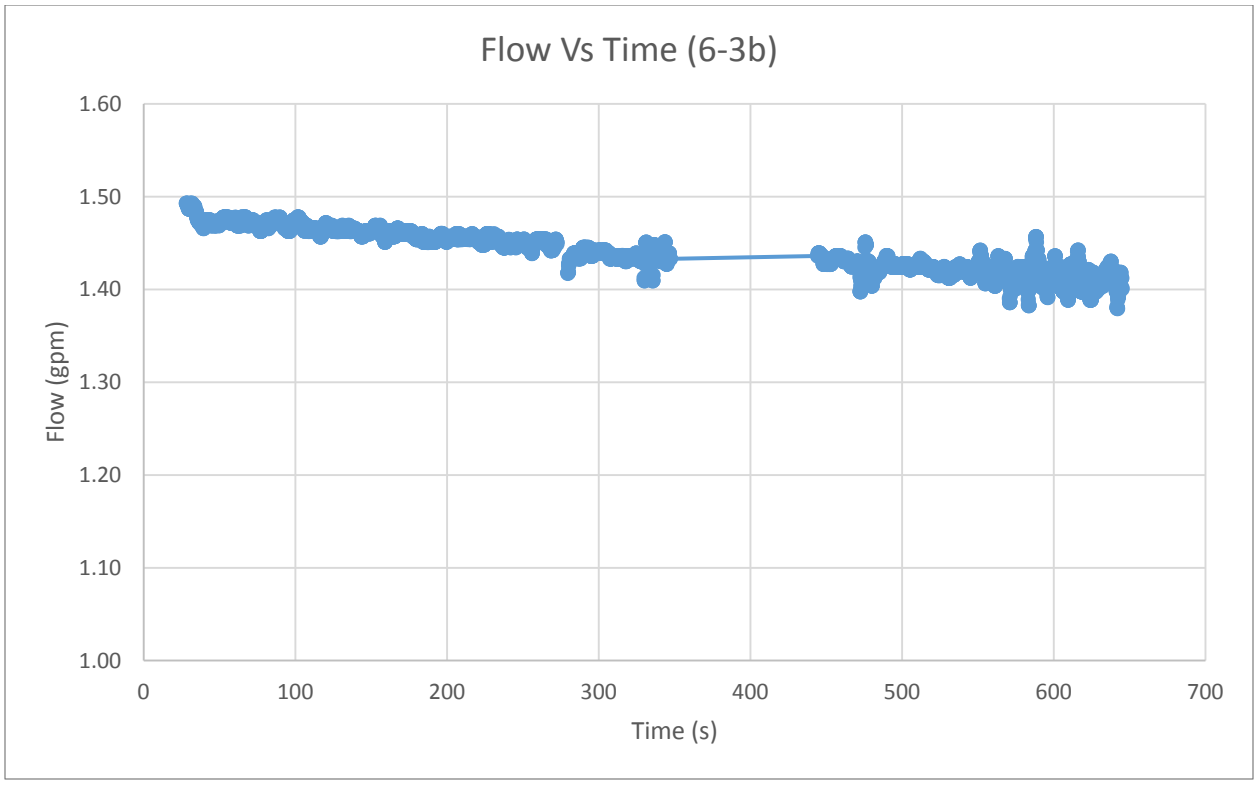

Figure E-9: Core 6-3b flow vs time plot

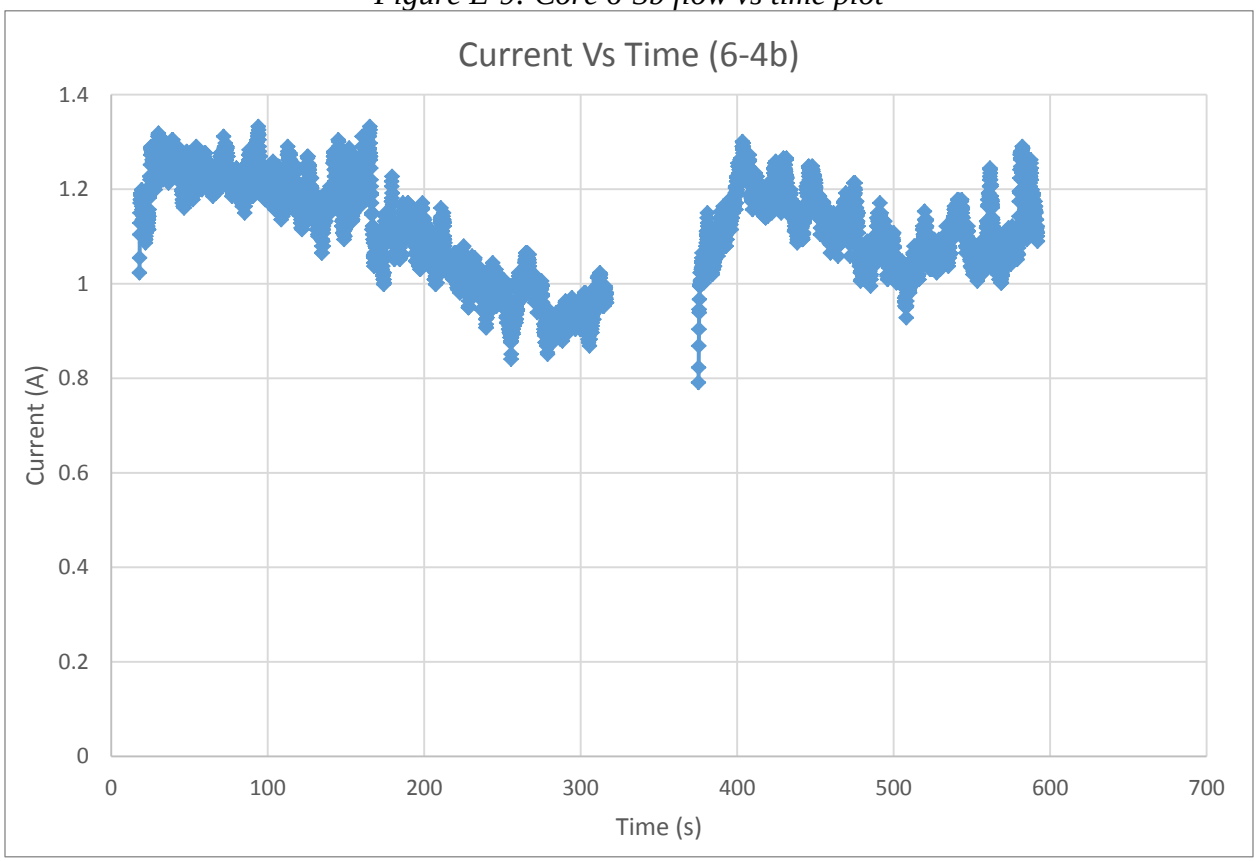

Figure E-10: Core 6-4b current vs time plot

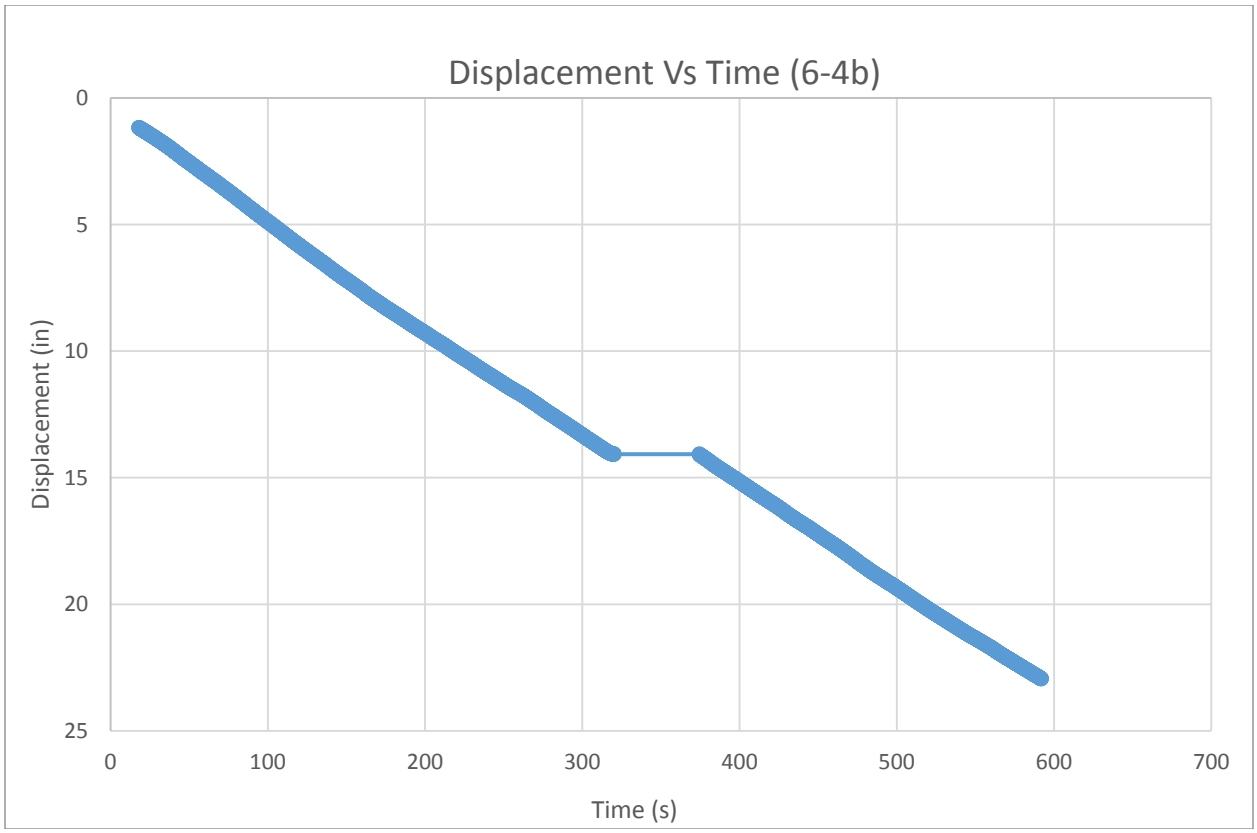

Figure E-11: Core 6-4b displacement vs time plot

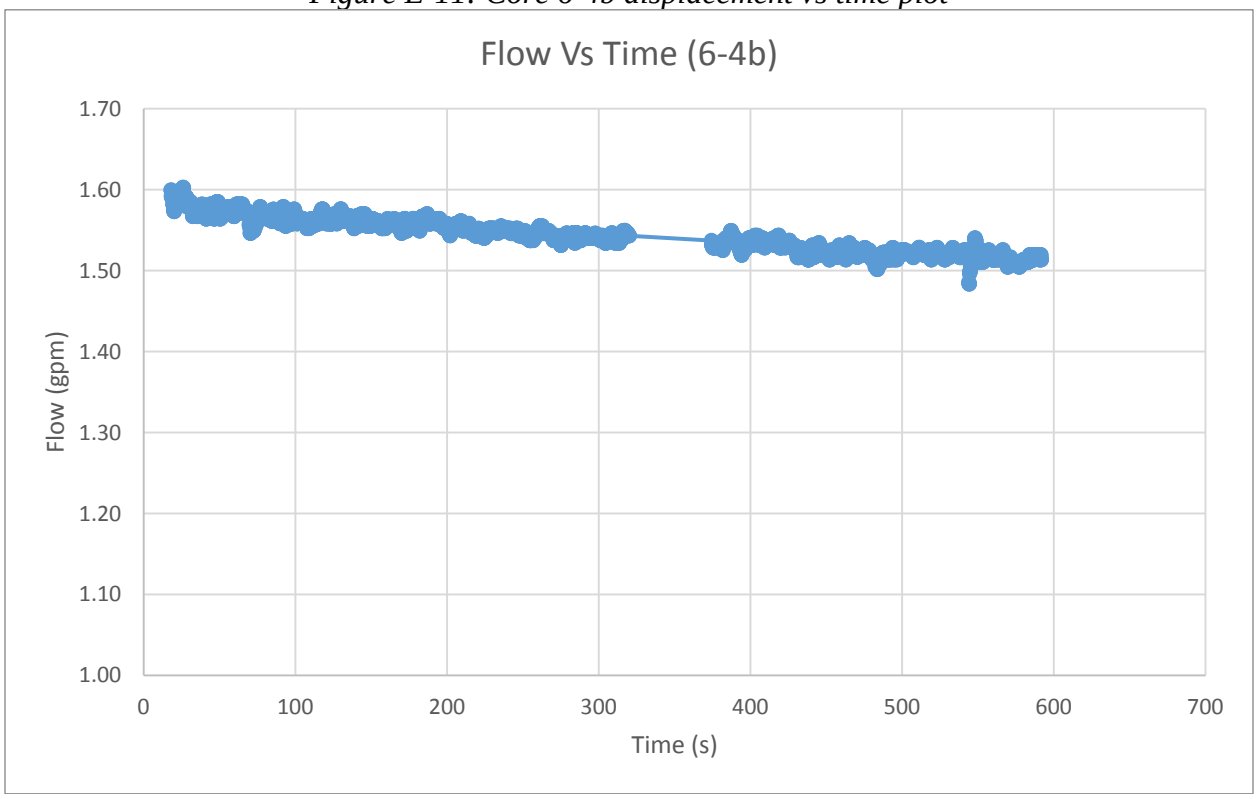

Figure E-12: Core 6-4b flow vs time plot

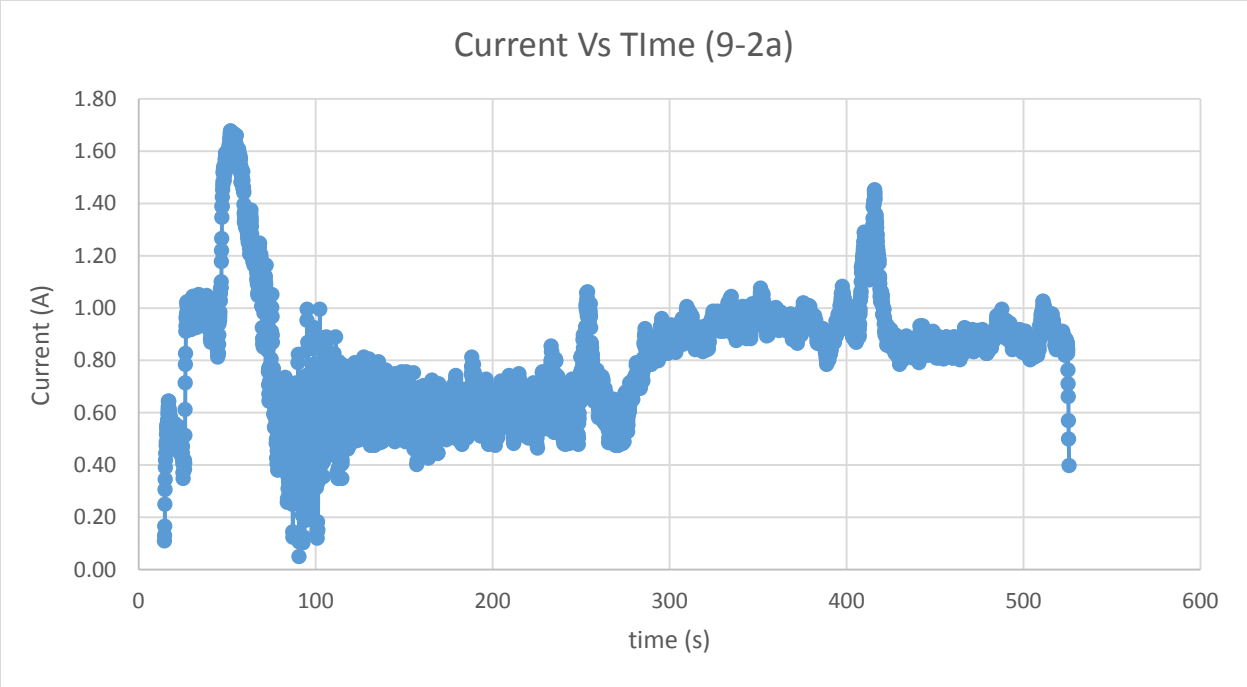

Figure E-13: Core 9-2a current vs time plot

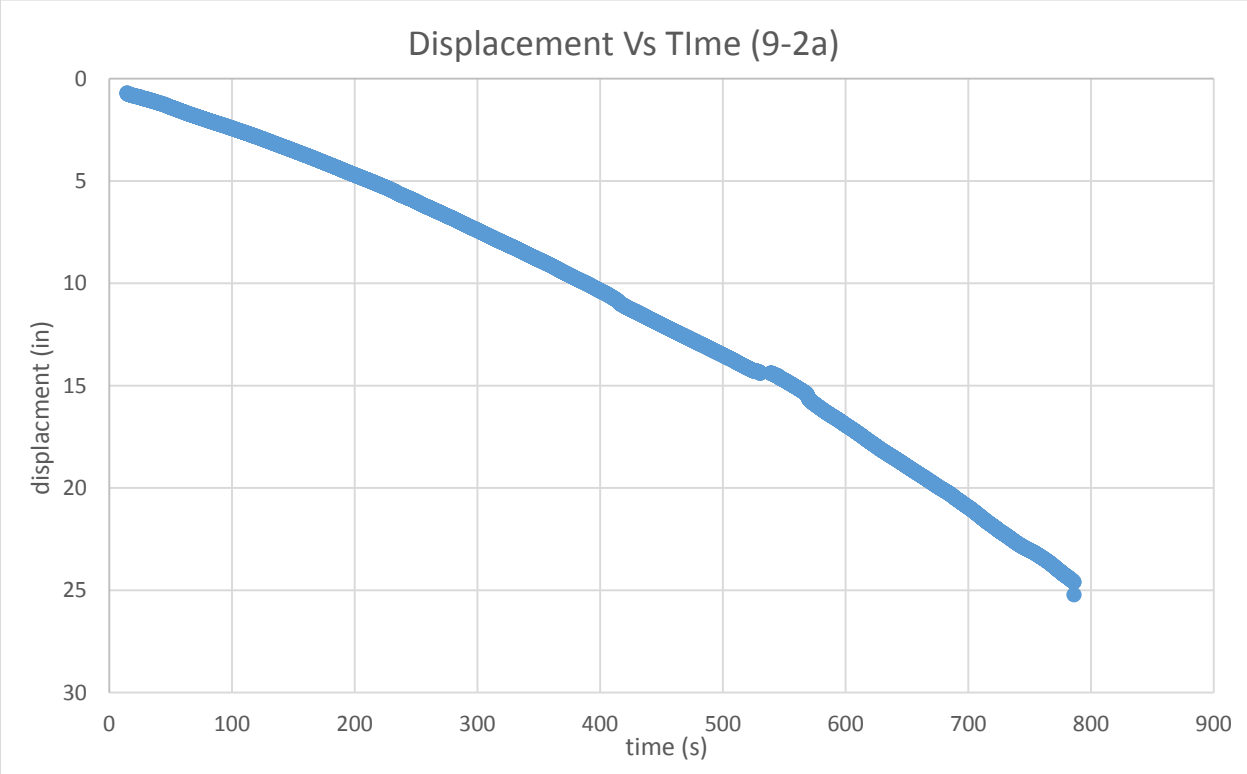

Figure E-14: Core 9-2a displacement vs time plot

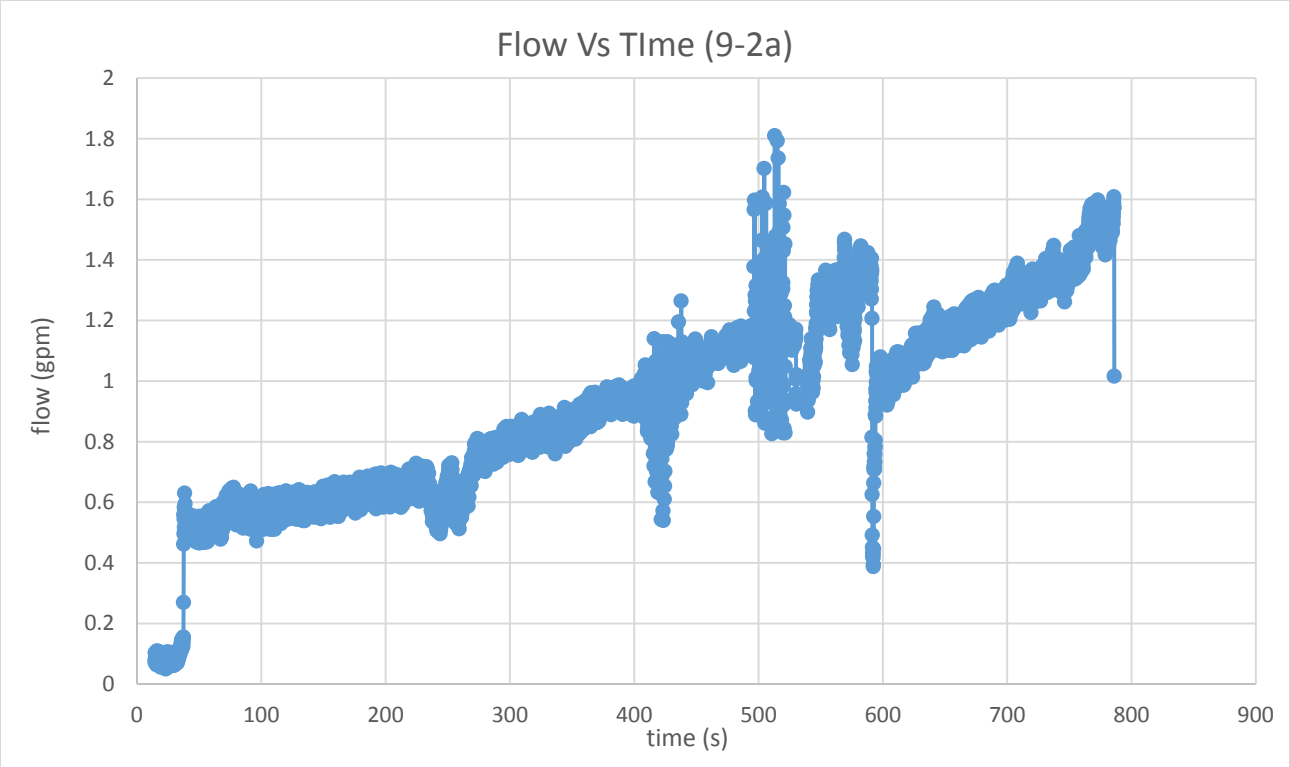

Figure E-15: Core 9-2a flow vs time plot

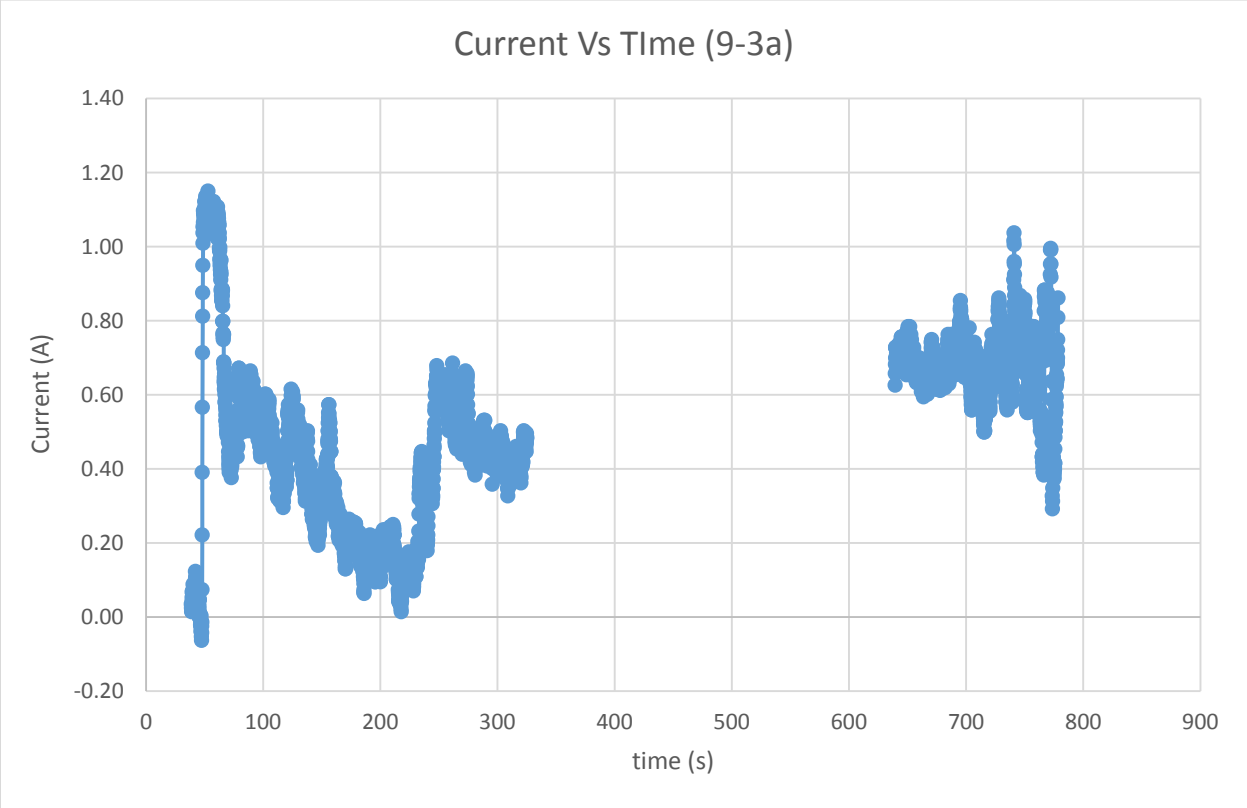

Figure E-16: Core 9-3a current vs time plot

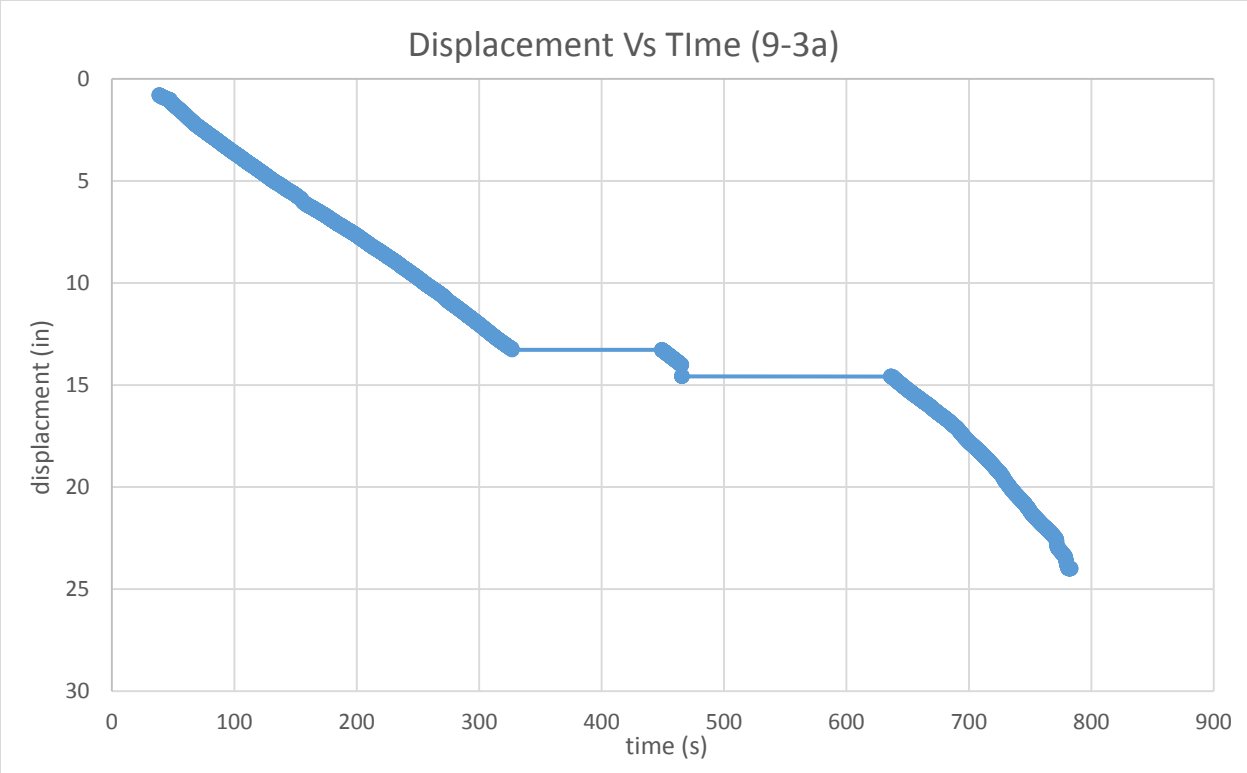

Figure E-17: Core 9-3a displacement vs time plot

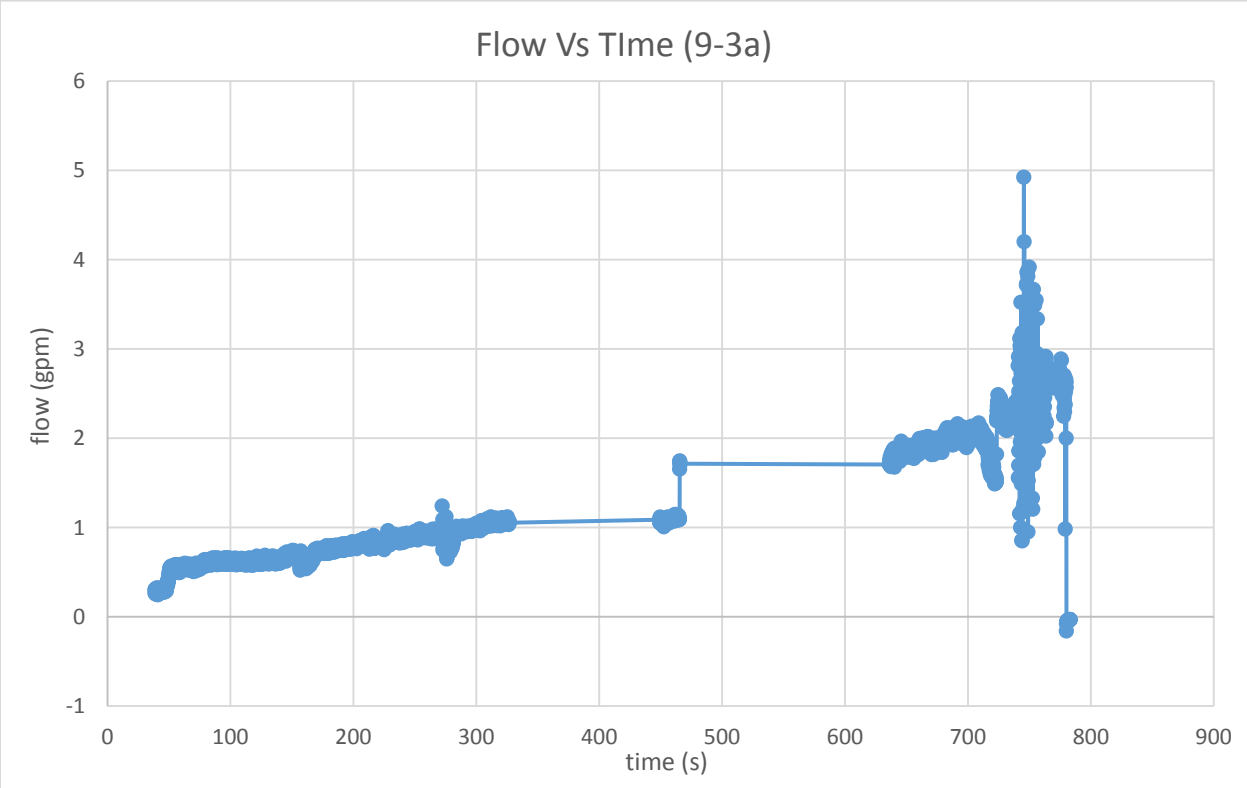

Figure E-18: Core 9-3a flow vs time plot

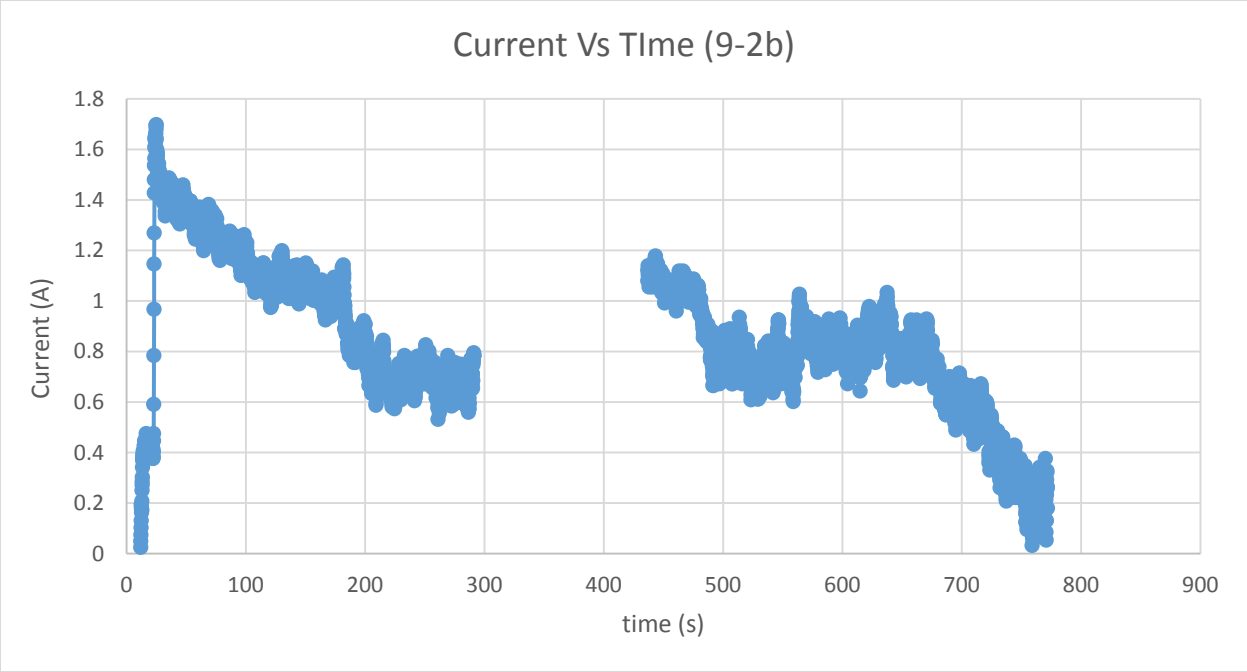

Figure E-19: Core 9-2b current vs time plot

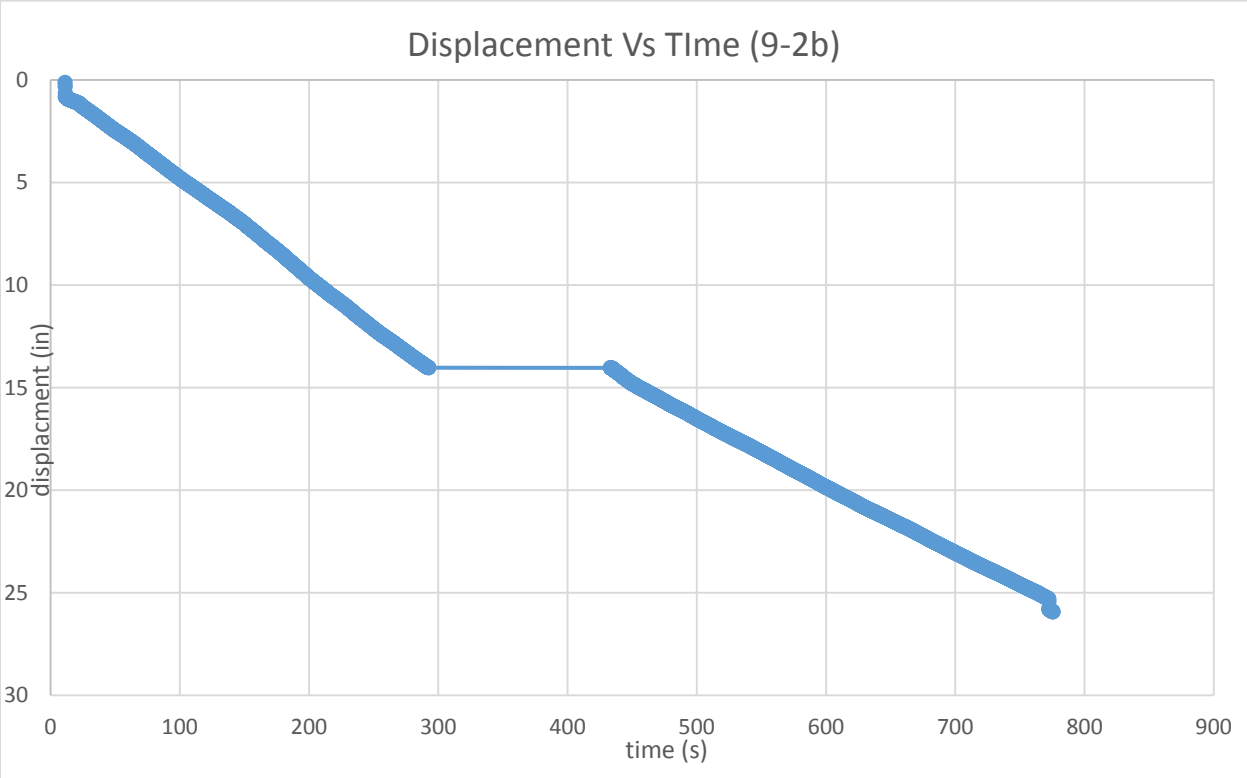

Figure E-20: Core 9-2b displacement vs time plot

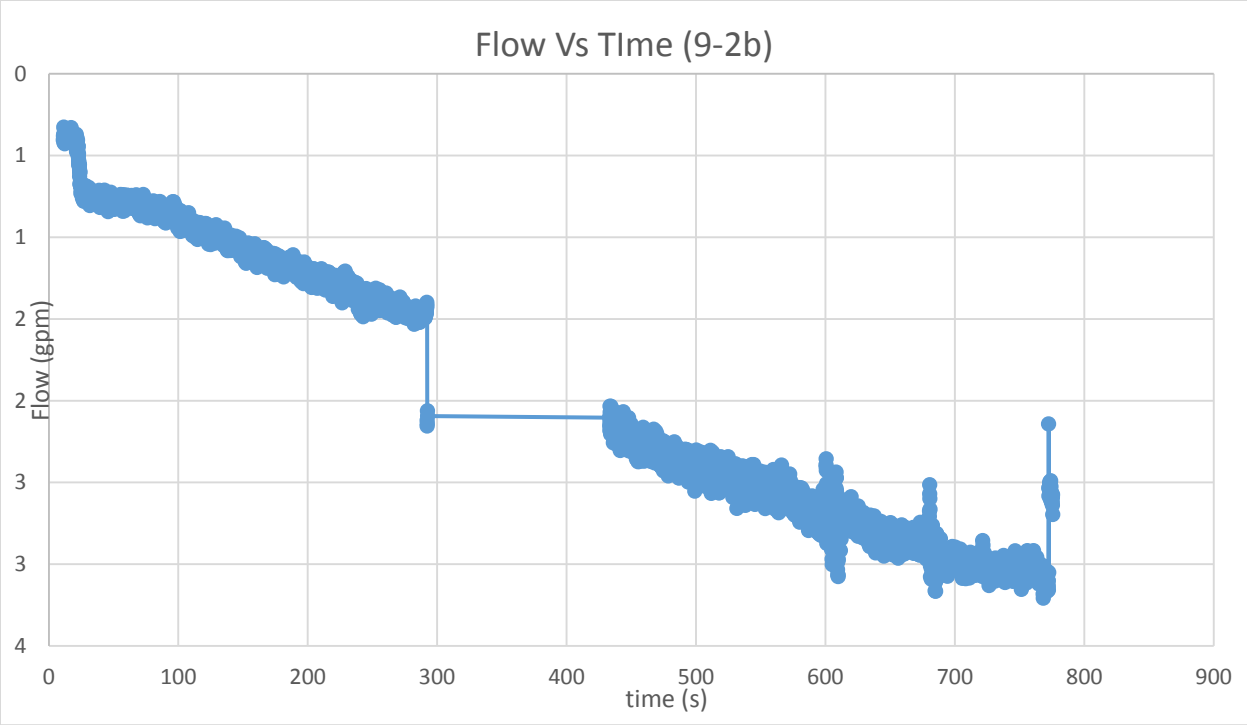

Figure E-21: Core 9-2b flow vs time plot

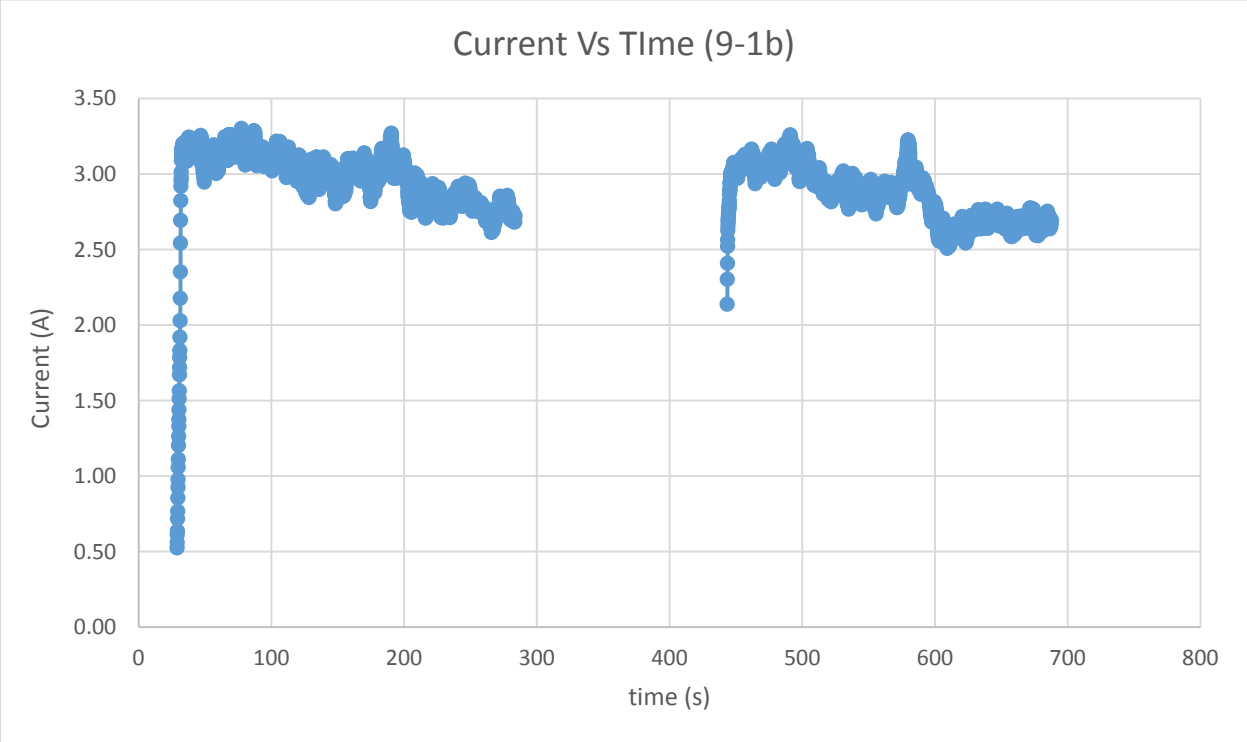

Figure E-22: Core 9-1b current vs time plot

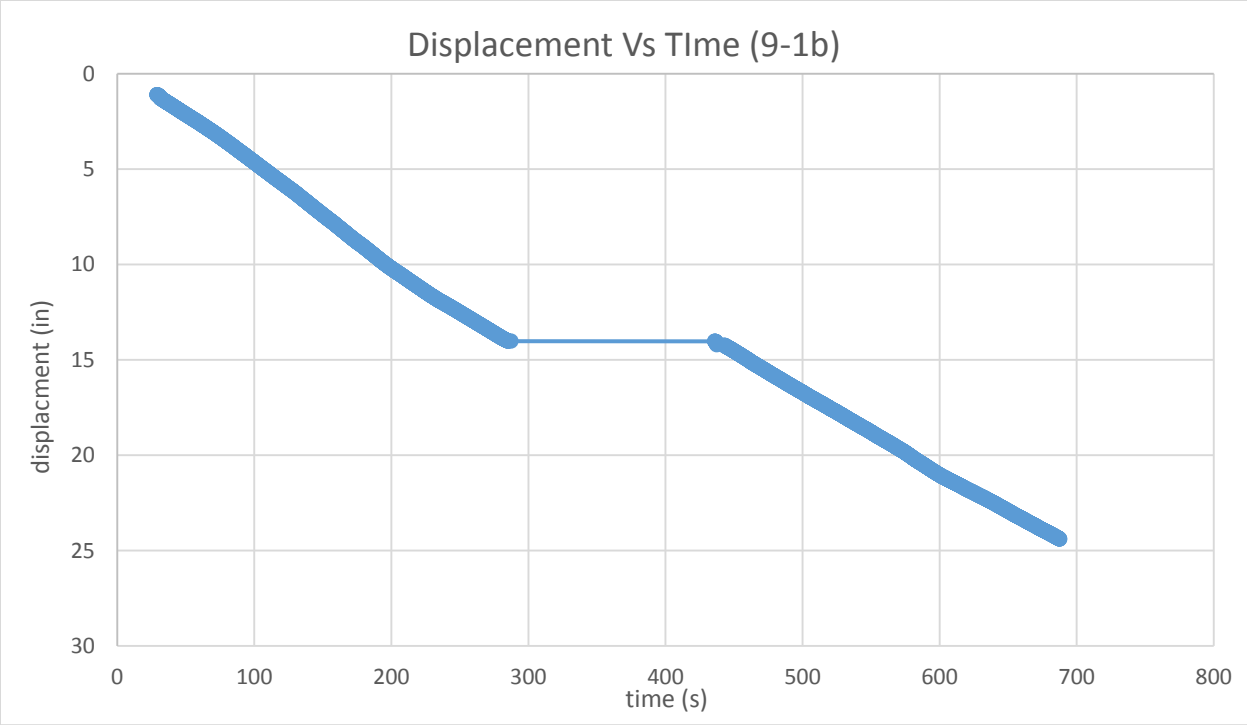

Figure E-23: Core 9-1b displacement vs time plot

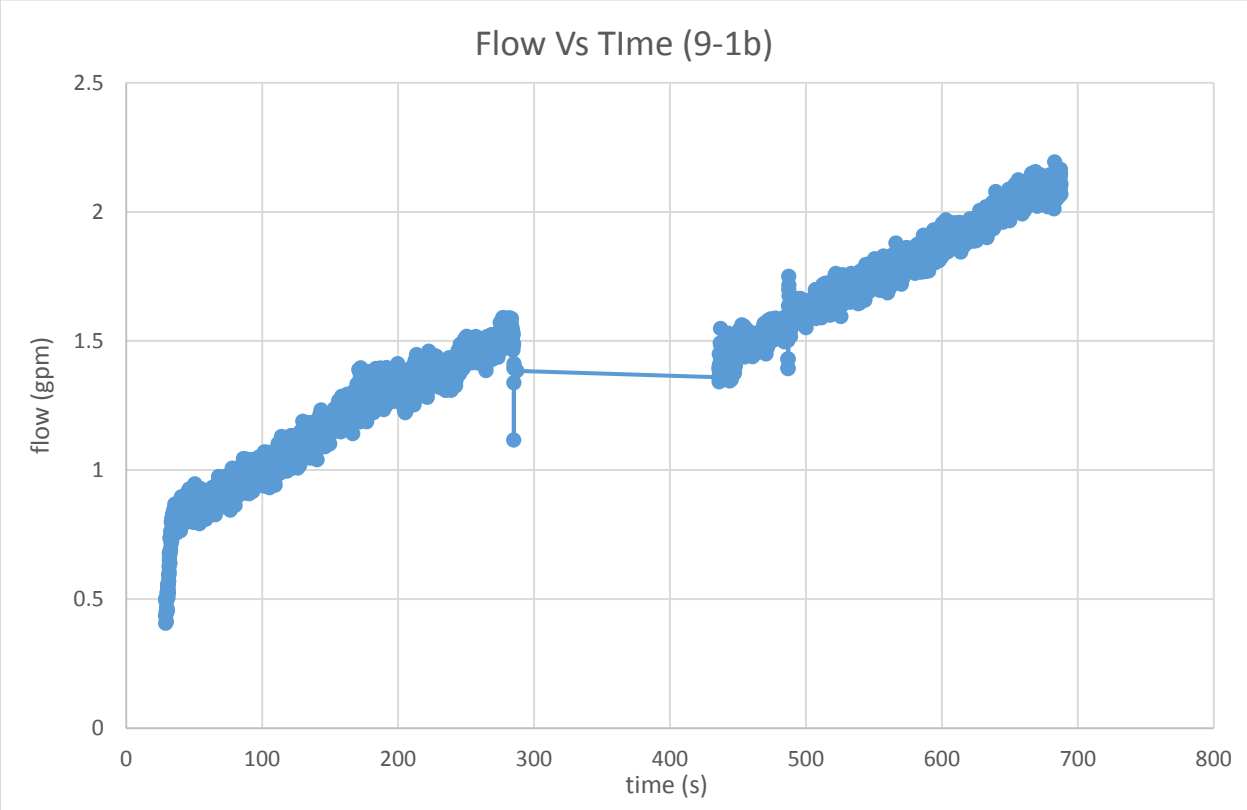

Figure E-24: Core 9-1b flow vs time plot

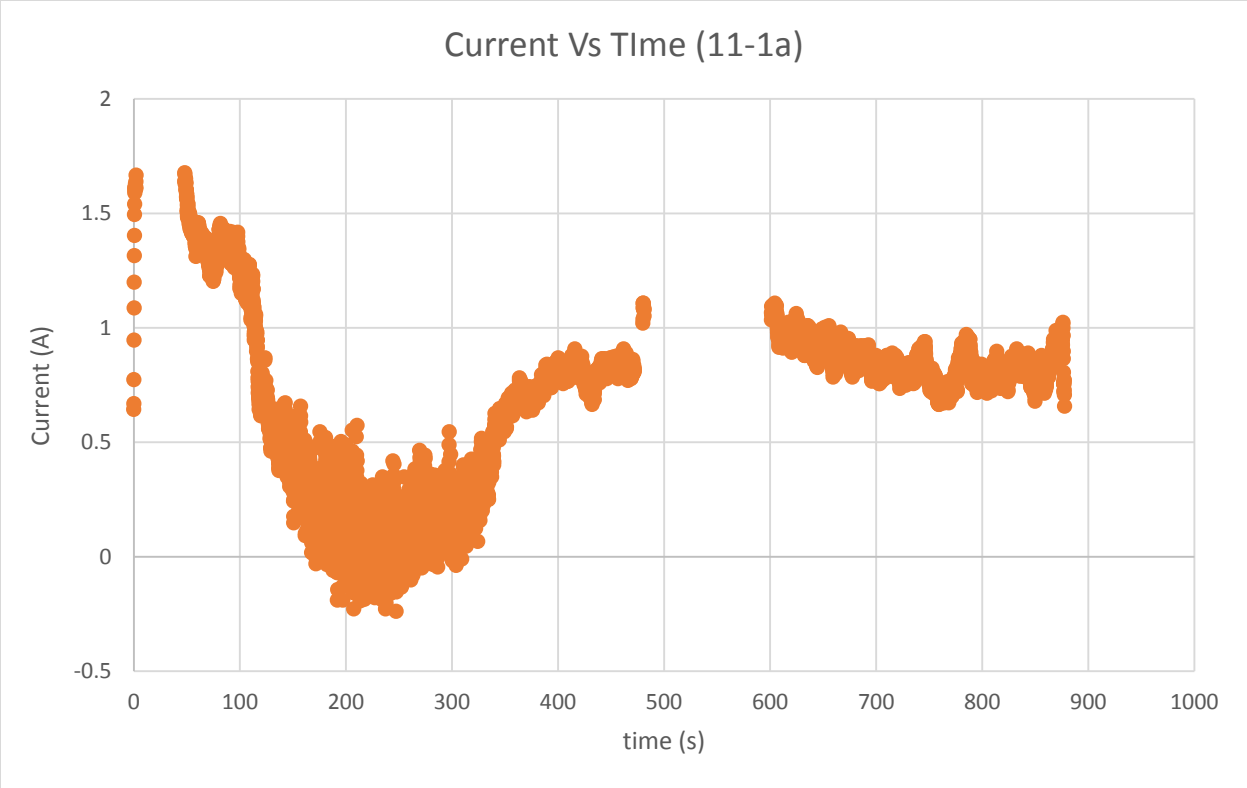

Figure E-25: Core 11-1a current vs time plot

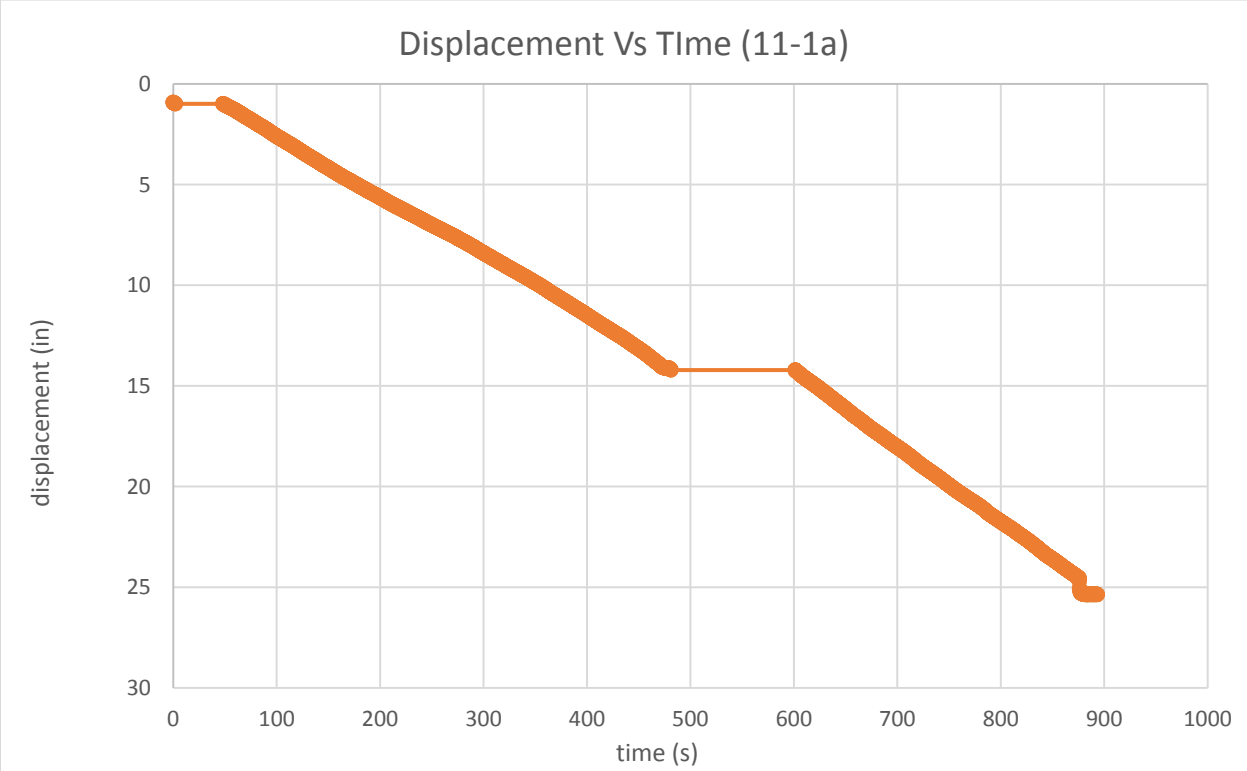

Figure E-26: Core 11-1a displacement vs time plot

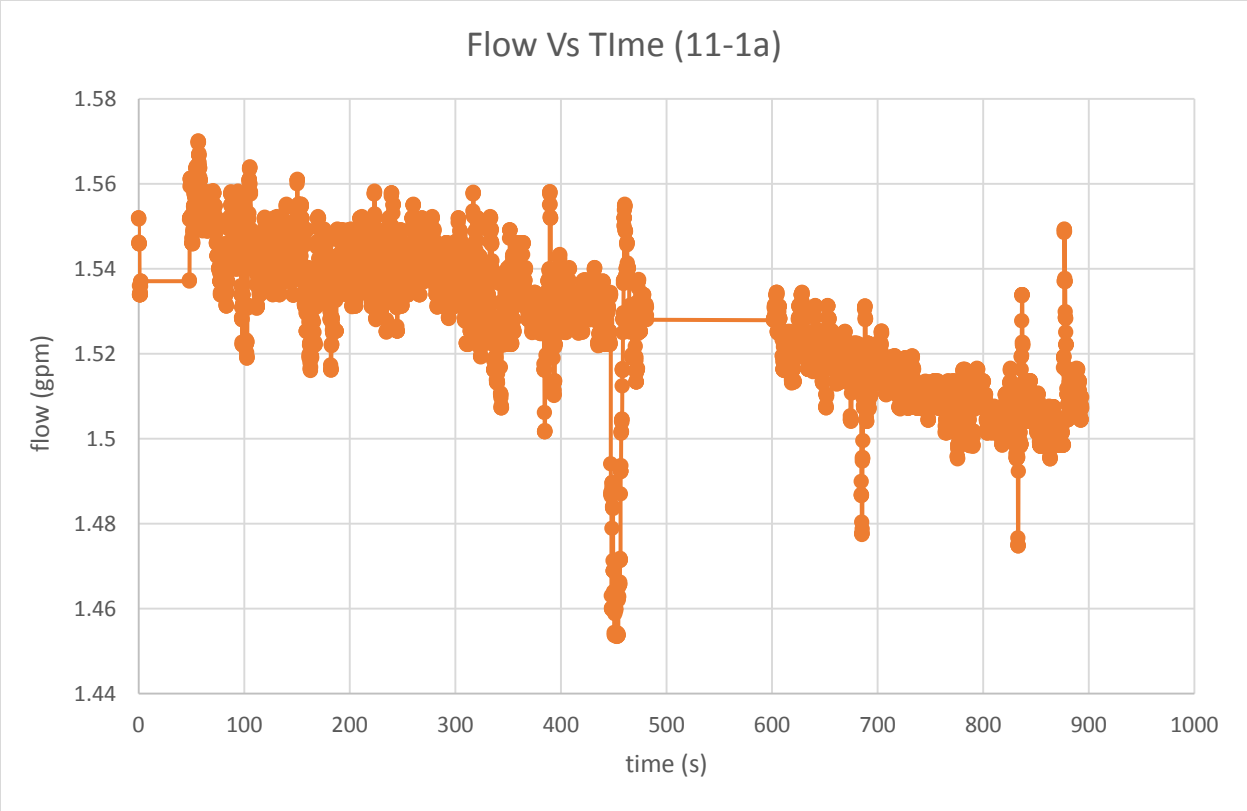

Figure E-27: Core 11-1a flow vs time plot

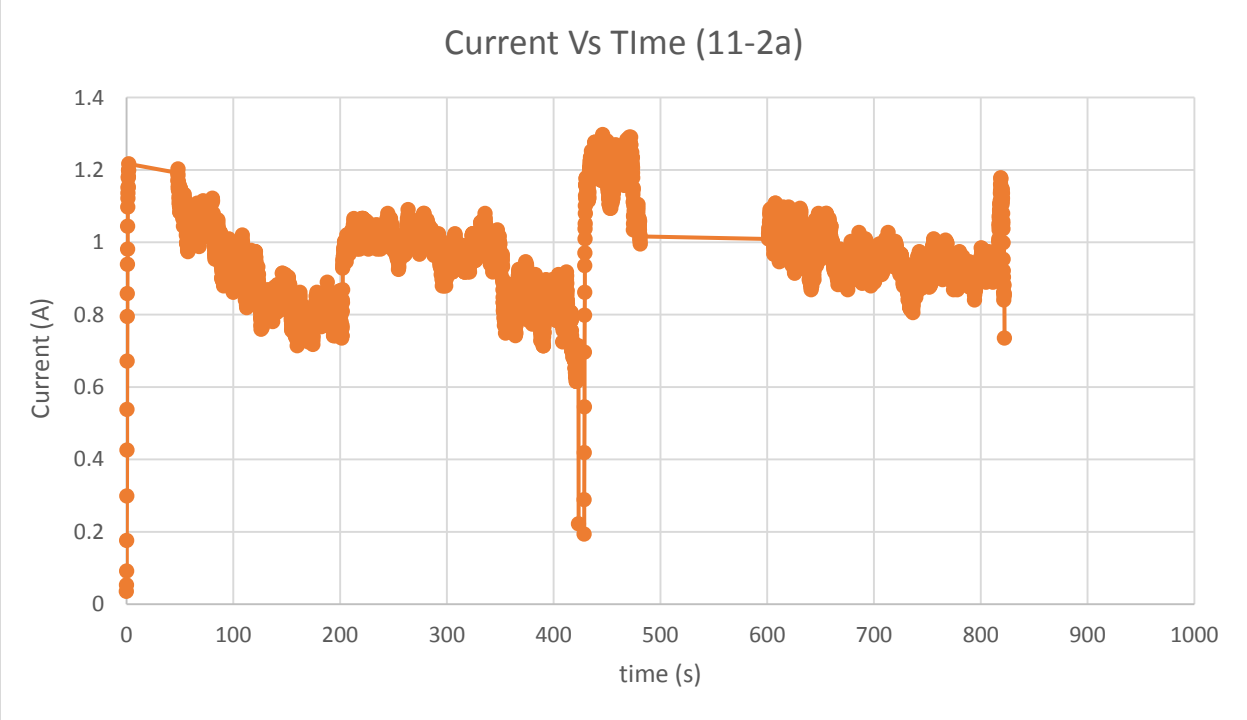

Figure E-28: Core 11-2a flow vs time plot

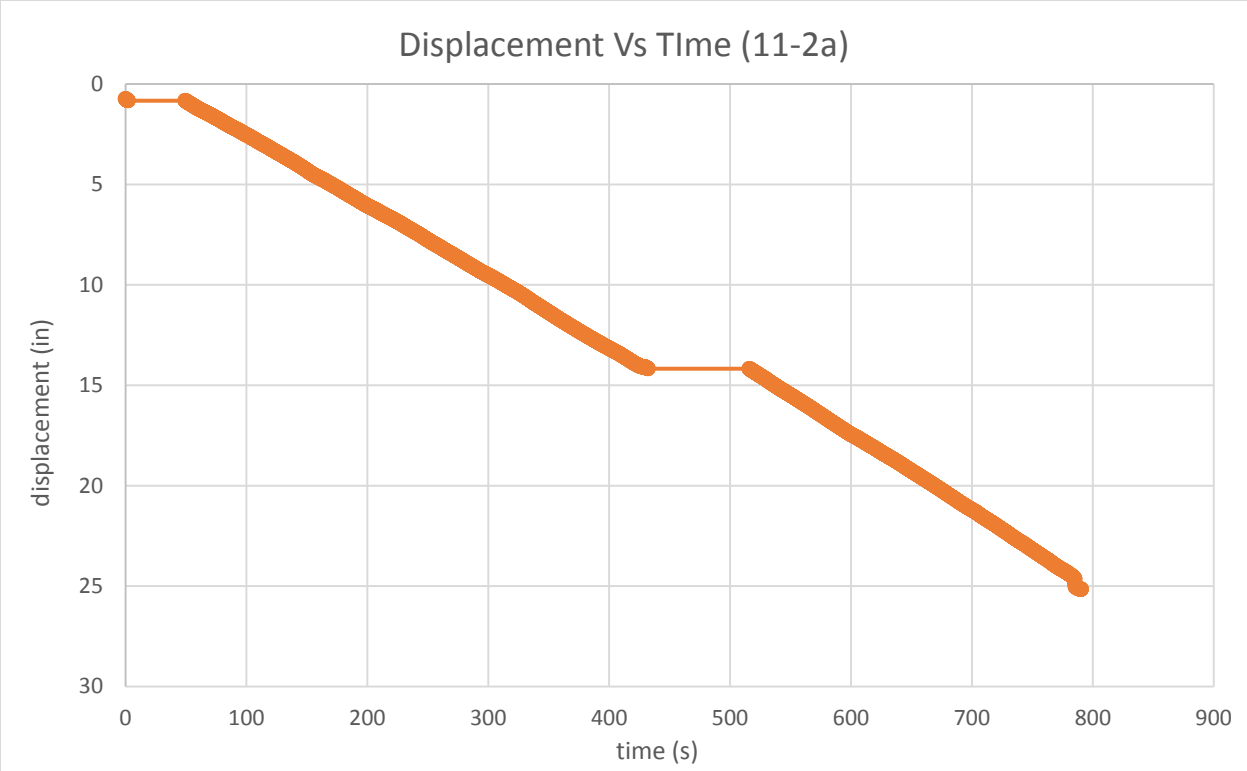

Figure E-29: Core 11-2a displacement vs time plot

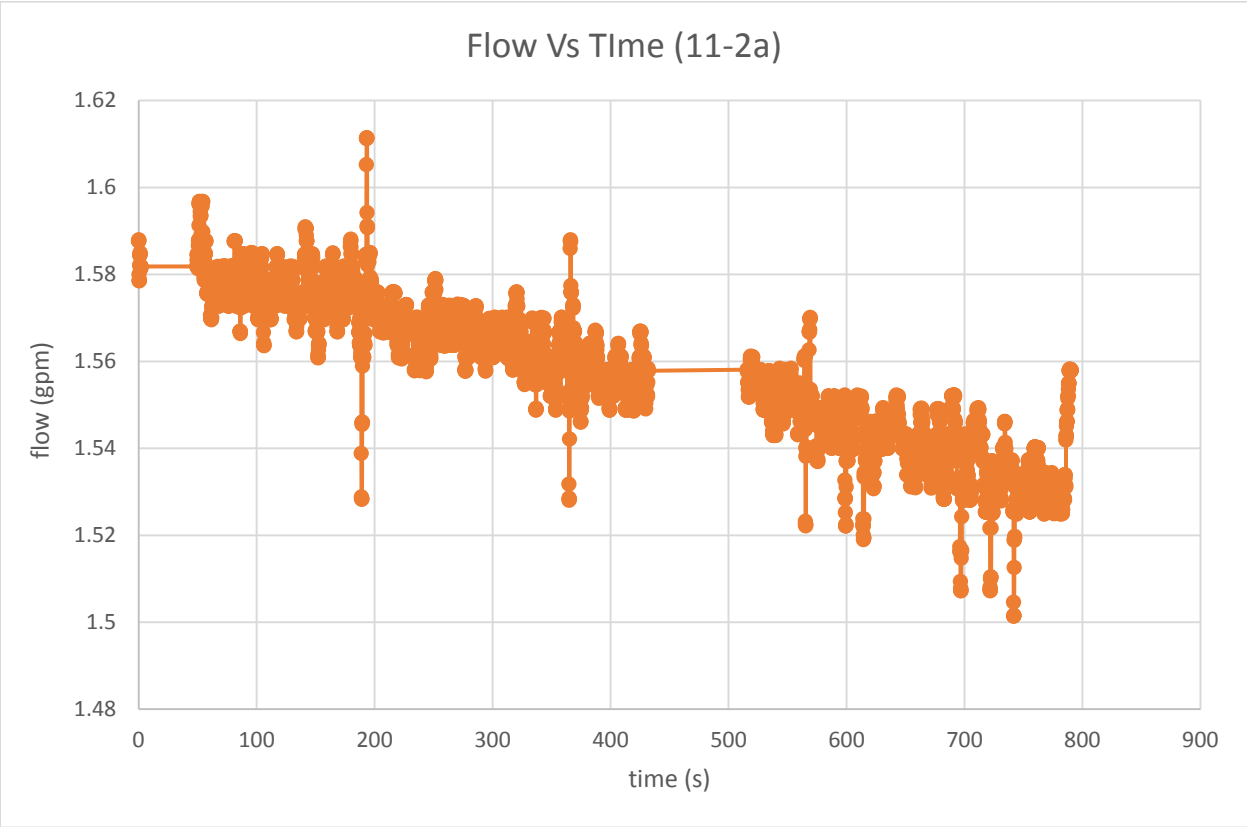

Figure E-30: Core 11-2a flow vs time plot

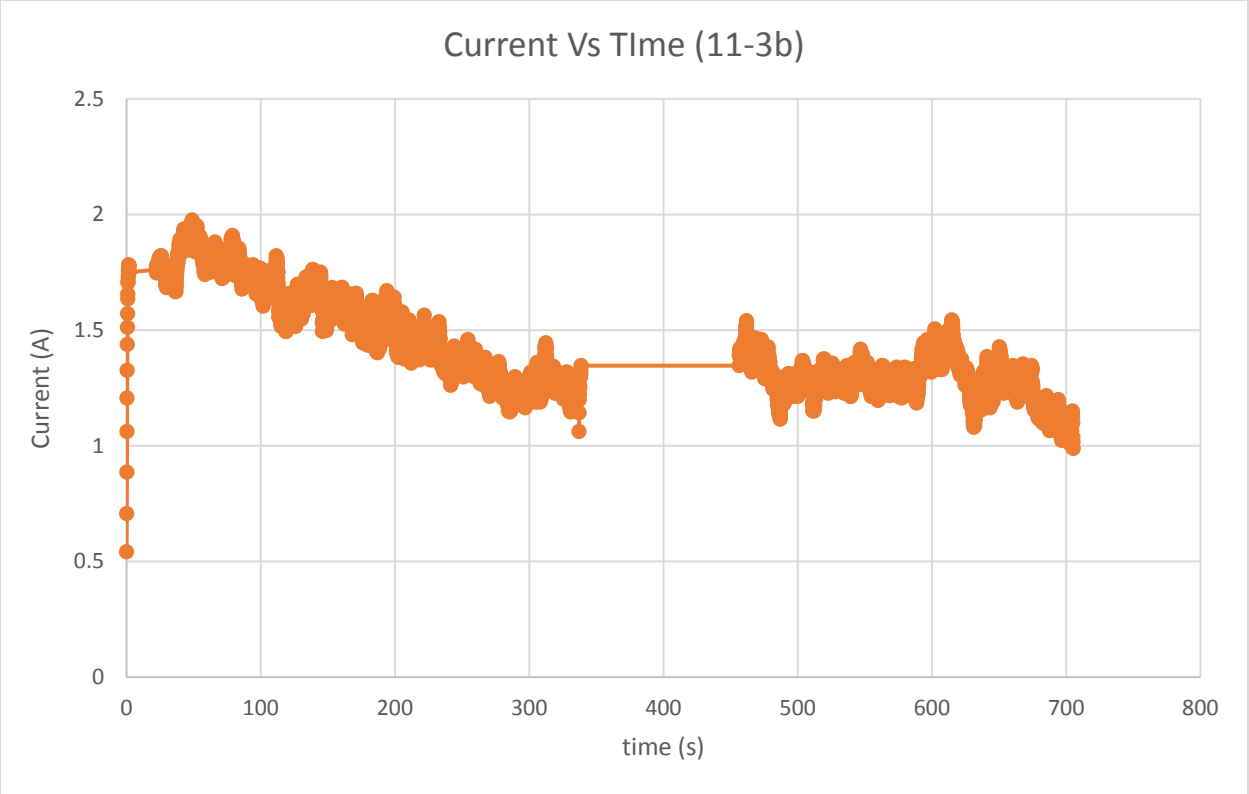

Figure E-31: Core 11-3b current vs time plot

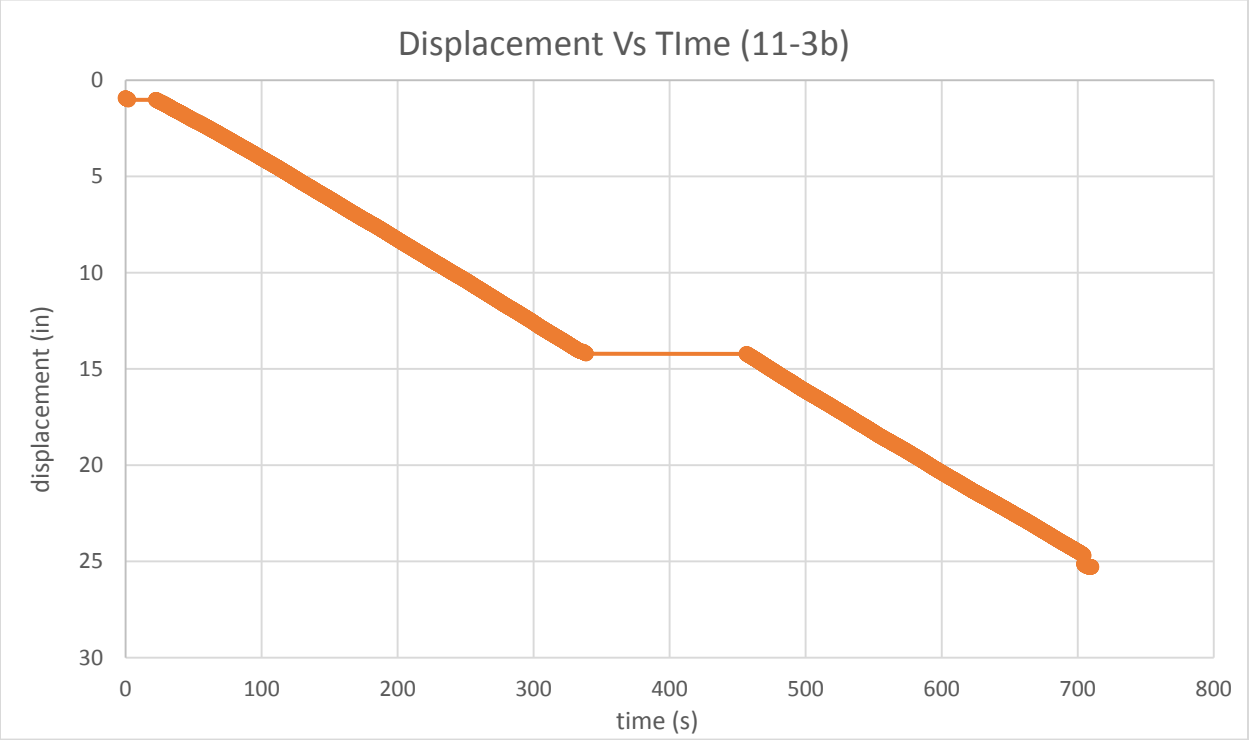

Figure E-32: Core 11-3b displacement vs time plot

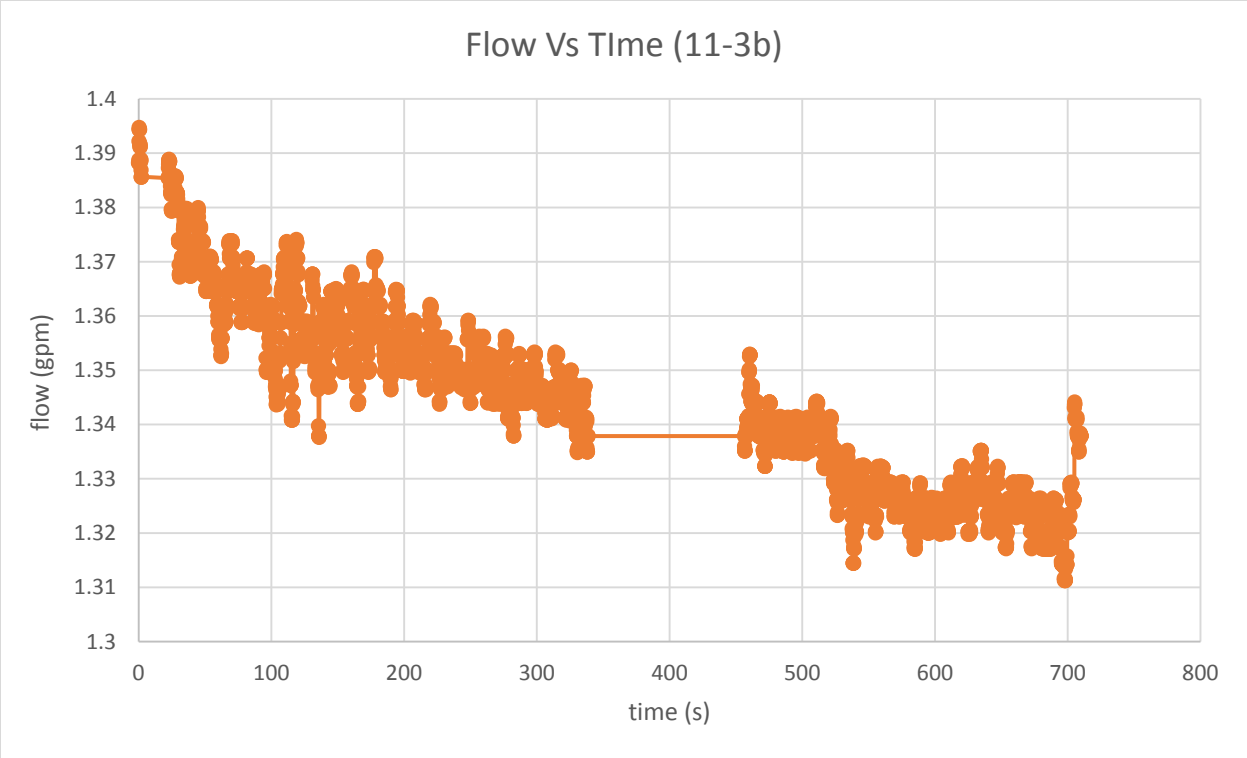

Figure E-33: Core 11-3b flow vs time plot

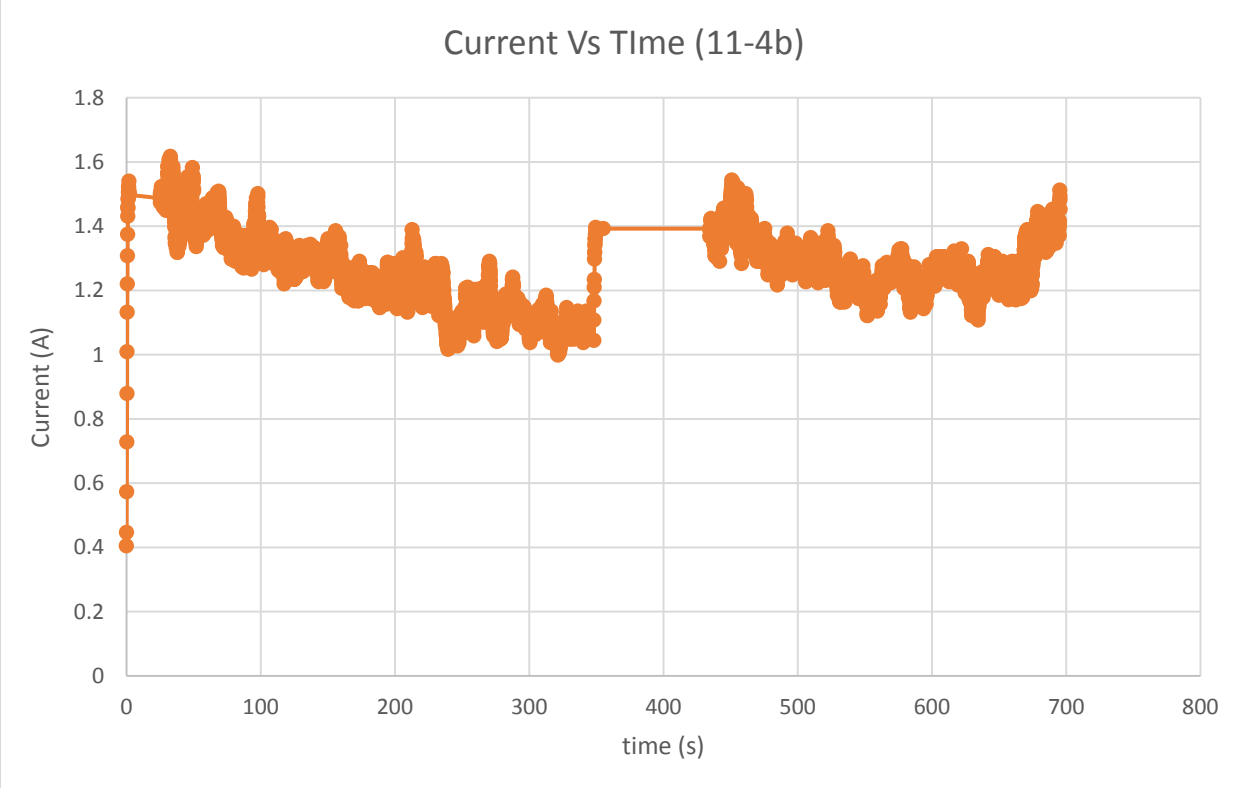

Figure E-34: Core 11-4b current vs time

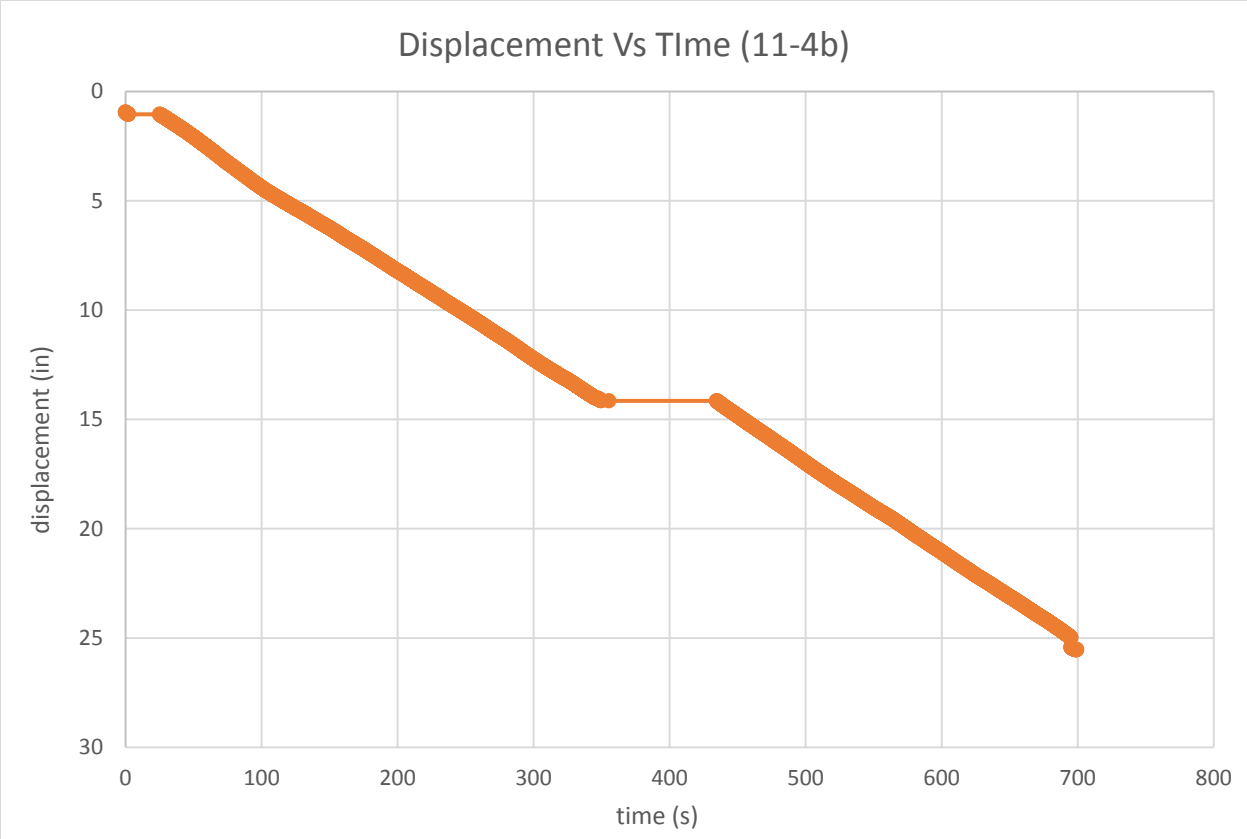

Figure E-35: Core 11-4b displacement vs time plot

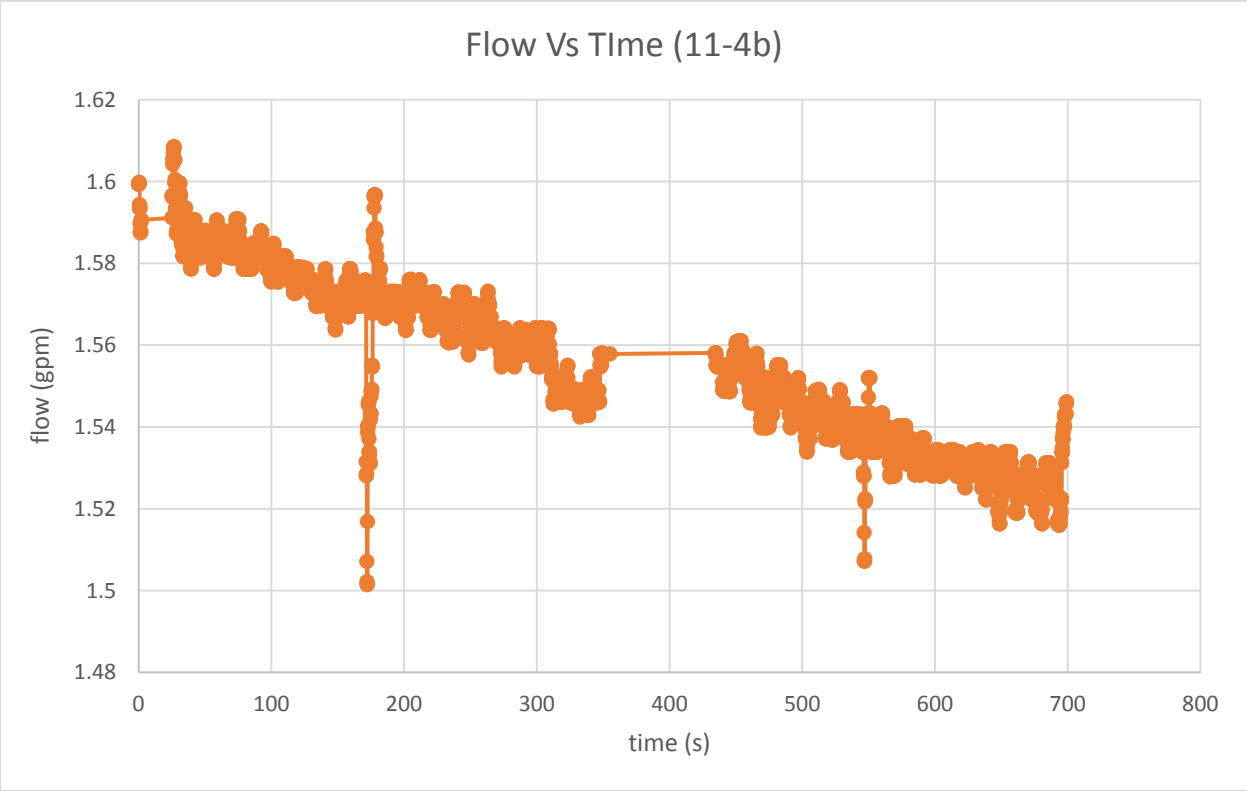

Figure E-36: Core 11-4b flow vs time plot

APPENDIX F
CORE COMPRESSIVE STRENGTH PROFILE DATA

Table F-1: Core 6-2a compressive strength profile data

CORE ID	Depth to sample (in)	Break Load (kips)	Strength (psi)
6-2a(1)1	1	4.996	6361.104765
6-2a(1)2	3	6.976	8882.119064
6-2a(1)3	5	5.345	6805.465367
6-2a(1)4	7	3.021	3846.456665
6-2a(1)5	9	6.289	8007.403497
6-2a(1)6	11	6.278	7993.397862
6-2a(1)7	13	5.482	6979.899184
6-2a(1)8	15	6.152	7832.969679
6-2a(3)1	21	1.467	1867.842412

Table F-2: Core 6-4b compressive strength profile data

CORE ID	Depth to sample (in)	Break Load (kips)	Strength (psi)
6-4b(2)1	2	5.039	6415.854066
6-4b(3)1	6.25	4.718	6007.144172
6-4b(3)2	8.5	4.435	5646.817381
6-4b(3)3	10.5	5.018	6389.116035
6-4b(3)4	13	4.272	5439.279335
6-4b(4)1	16.25	5.916	7532.485147
6-4b(4)2	18.25	6.013	7655.989382
6-4b(4)3	20	5.767	7342.772454
6-4b(4)4	22.25	8.505	10828.90233

Table F-3: Core 9-2a compressive strength profile data

CORE ID	Depth to sample (in)	Break Load (kips)	Strength (psi)
9-2a(1)1	0.5	3.703	4714.806034
9-2a(1)2	2.5	7.74	9854.874076
9-2a(4)1	8	3.2	4074.366543
9-2a(4)3	12.25	3.11	3959.774984
9-2a(4)4	14.5	2.715	3456.845364
9-2a(5)1	17.75	6.356	8092.710546
9-2a(7)1	22.25	4.804	6116.642773

Table F-4: Core 11-2a compressive strength profile data

CORE ID	Depth to sample (in)	Break Load (kips)	Strength (psi)
11-2a(1)1	1	5.59	7117.409055
11-2a(2)1	6	7.84	9982.198031
11-2a(2)2	8	7.758	9877.792388
11-2a(3)1	11	4.749	6046.614598
11-2a(4)1	15.25	6.421	8175.471117
11-2a(4)2	17.25	6.56	8352.451413
11-2a(4)3	19.25	7.203	9171.144441
11-2a(4)4	21.5	7.19	9154.592327

Table F-5: Core 11-4b compressive strength profile data

CORE ID	Depth to sample (in)	Break Load (kips)	Strength (psi)
11-4b(1)1	1	5.026	6399.301952
11-4b(1)2	3	6.932	8826.096524
11-4b(1)3	5	7.067	8997.983863
11-4b(1)4	7	5.16	6569.916051
11-4b(1)5	9	7.052	8978.885269
11-4b(1)6	11	5.05	6429.859701
11-4b(1)7	13	6.555	8346.085216
11-4b(1)8	15	5.299	6746.896348
11-4b(1)10	19	6.86	8734.423277
11-4b(1)11	21	6.229	7931.009124